U.PORTO

Universidade do Porto
FEUP Faculdade de Engenharia

Lifetime dynamic behavior of a Force-Sensing System for an automotive display:

Study of influences in the system's operation

André Carreiro Pacheco

Dissertation submitted to
Faculdade de Engenharia da Universidade do Porto
for the degree of:

Integrated Master in Mechanical Engineering

Advisor at FEUP:
Prof. João Manuel R. S. Tavares
(Full Professor)

Company's Advisor:
Eng. José André Alves Sousa

Departamento de Engenharia Mecânica
Faculdade de Engenharia da Universidade do Porto

Porto, 2021

The work presented in this dissertation was performed at
Bosch Car Multimedia, S.A.
Braga, Portugal.

André Carreiro Pacheco
E-mail: up201603587@fe.up.pt

Faculdade de Engenharia da Universidade do Porto
Departamento de Engenharia Mecânica
Porto, Portugal

Abstract

The automotive industry is undergoing one of the most significant changes in history, as driven by electrification, connectivity, autonomous driving, and shared mobility. With this change, new cockpit concepts are emerging to try to respond to new needs. An essential ingredient in these concepts is the number, shape, and appearance of in-vehicle displays. As their importance increases, new opportunities for expanding functionalities or increase safety are appearing. The measurement of the applied force on the screen is one such example.

The following dissertation was carried out during an internship in a mechanical development team at Bosch. The study aims to point out some possible limitations related to the operation of a new force-sensing system, namely changes due to temperature and air currents or after artificial aging.

Due to the fact that it is a new technology, there was no information about previous works. That allied with equipment restrictions and other limitations meant that creativity was tested to find ways to study the system. Therefore, this project is mainly considered experimental.

Parts were produced by 3D printing and CNC machining to make it possible to carry out experiments on the tensile machine. In addition, a bending apparatus with weights and mechanical stops was developed for testing inside a thermal chamber.

The assembly process and calibration of the system was studied, in particular, the influence of different screwing sequences and specification limits. Finally, the sequences were ranked from best to worst, and new specification limits were calculated and proposed.

In the end, it was concluded that the operation of the system is influenced by temperature, air flow and aging. However, the development of correct software can minimize the influence of these effects.

Keywords: Force-Sensing System, Automotive Display, Printed Circuit Board, PCB, Thermal Aging, Strain Gauge, Process Capability

Resumo

A indústria automóvel está a passar por uma das maiores mudanças na história, impulsionada pela eletrificação, conectividade, condução autónoma e mobilidade partilhada. Com esta mudança, surgem novos conceitos de interior automóvel que tentam responder a novas necessidades. Um ingrediente essencial nesses conceitos é o número, a forma e a aparência dos displays no veículo. À medida que a importância dos displays num carro aumenta, novas oportunidades para expandir funcionalidades ou aumentar a segurança estão também a aparecer. A medição da força aplicada no display é um destes exemplos.

A seguinte disssertação foi realizada durante um estágio numa equipa de desenvolvimento mecânico da Bosch. O estudo pretende apontar alguns possíveis problemas relacionados com o funcionamento de um novo sistema de deteção de força, nomeadamente alterações devido a temperatura e correntes de ar ou após envelhecimento artificial.

Devido ao facto de ser uma nova tecnologia, não existia informação de trabalhos realizados. Isso, aliado às restrições de equipamento e a outras limitações, fez com que a creatividade fosse posta à prova para arranjar formas de estudo do sistema. Sendo assim, este projeto é maioritariamente considerado experimental.

Peças foram produzidas por impressão 3D e maquinação CNC de modo a possibilitar a realização de experiências na máquina de tração. Além disso, outro jig com pesos e batentes mecânicos foi desenvolvido para teste dentro duma máquina térmica.

Foi estudada a influência do processo de montagem na calibração do sistema, em particular, a influência de diferentes sequências de aparafusamento e limites de especificação. Finalmente, as sequências foram classificadas da melhor para a pior, e novos limites de especificação foram calculados e propostos.

Por último, foi concluido que o funcionamento do sistema é influenciado pela temperatura, deslocamento de ar e envelhecimenento. No entanto, o desenvolvimento de um correto software pode minimizar a influência destes efeitos.

Keywords: Force-Sensing System, Automotive Display, Printed Circuit Board, PCB, Thermal Aging, Strain Gauge, Process Capability

Agradecimentos

Agradeço a todos os que contribuiram para a realização e apresentação deste trabalho:

Ao meu orientador na faculdade o Prof. Doutor João Tavares, pelo suporte e ajuda prestada e disponibilidade para me orientar.

Ao Eng. José Alves Sousa, meu orientador na Bosch, agradeço verdadeiramente toda a ajuda, constante disponibilidade, preocupação e motivação.

A toda a equipa que me acolheu da melhor maneira possível, num ambiente que fortaleceu a minha motivação, por toda a sabedoria e ajuda partilhada.

Ao Eng. Rui Alexandre Cardoso e Eng. João Rocha, agradeço por terem confiado em mim, no meu empenho e dedicação para este desafio.

Ao António Mota e Ricardo Milhazes pela companhia e amizade durante estes meses na empresa.

À Magda, pelo carinho, paciência e apoio.

À minha família, em especial aos meus pais, avó e tio, que sempre me apoiaram e fizeram tudo para que conseguisse atingir os meus objetivos.

Contents

1 Introduction **1**

1.1 Project Framework and Motivation . . . 1

1.1.1 Force-Sensing Technology in Electronic Devices . . . 1

1.1.2 Force-sensing Technology in Automotive Displays . . . 3

1.2 Bosch Group . . . 3

Bosch Car Multimedia Portugal, S.A. . . . 4

1.3 Objectives . . . 5

1.4 Outline . . . 6

2 Theoretical Foundation **7**

2.1 Strain Gauges . . . 7

2.1.1 Operation Principals . . . 7

2.1.2 Wheatstone Bridge . . . 8

2.2 Fixed beam with sinking support . . . 8

2.3 Screwing Process . . . 9

2.3.1 Basics . . . 10

2.3.2 Differential Torque Method (DTM) . . . 10

2.4 Process capability . . . 11

2.5 Summary . . . 12

3 Product and Concept Analysis **13**

3.1 Display 1 . . . 13

3.1.1 Carrier . . . 14

3.1.2 Display Housing (DH) . . . 14

3.1.3 Force-Sensing Elements . . . 14

3.1.4 Operation . . . 15

3.1.5 Strain Gauge . . . 16

3.1.6 Alignment . . . 17

3.2 Display 2 . . . 17

Force-Sensing Elements . . . 18

3.3 Sensor Data Processing . . . 18

3.3.1 Force Calculation . . . 18

3.3.2 Strain Gauge Output Readouts . . . 18

3.4 Available Material . . . 19

3.5 Summary . . . 20

4 Testing Development **21**
4.1 Experimental Design . . . 21
4.1.1 Aging Influence . . . 21
4.1.2 Temperature and Air Flow Influence . . . 22
4.1.3 Screwing Sequence Influence . . . 22
4.2 Tensile Machine Testing . . . 22
4.2.1 Setup Development . . . 23
4.2.2 Data Processing and Setups Preparation . . . 27
4.2.3 Studies and Expectations . . . 30
4.3 Developed Bending Apparatus . . . 33
4.3.1 Apparatus Development . . . 34
4.3.2 Studies and Expectations . . . 39
4.4 Assembly Testing . . . 41
4.4.1 Setup . . . 41
4.4.2 Studies and Expectations . . . 42
4.5 Calibration . . . 43
4.5.1 Screwing Influence . . . 44
4.5.2 Studies and Expectations . . . 45
4.6 Summary . . . 46

5 Results and Analysis **47**
5.1 Tensile Machine Testing . . . 47
5.1.1 Studies' Results . . . 47
5.1.2 Possible Reasons for Output Variation . . . 52
5.2 Developed Bending Apparatus . . . 59
5.2.1 Studies' Results . . . 59
5.2.2 Possible Reasons for Output Variation . . . 61
5.3 Assembly Testing . . . 62
Studies' Results . . . 62
5.4 Calibration . . . 68
Studies' Results . . . 68
5.5 Summary . . . 76

6 Conclusions and Future Works **77**
6.1 Final Conclusions . . . 77
6.2 Future Working Perspectives . . . 78

References **79**

A Developed Bending Apparatus **81**
A.1 Exploded View . . . 81

A.2 Results of FSE 6 and 9 tested with Developed Bending Apparatus 83
A.3 Output Measurement Methods 84

B Assembly **87**
B.1 Time Schedule of the Experiments with the Assembly 87
B.2 Test with weights 88
B.3 Test with weights - Complete results 89
B.4 Thermocouples temperature 91
B.5 Output variation during experiments 92
B.6 Output variation in each sensor 95

C Screwing **99**
C.1 Screwing Sequences 99
C.2 Screwing Results 100

Acronyms

S.A. - Sociedade Anónima

OEM - Original Equipment Manufacturer

D1 - Display 1

D2 - Display 2

SBTi - Science Based Targets initiative

PCB - Printed Circuit Board

GF - Gauges Factor

DH - Display Housing

FSE - Force Sensing Elements

CS - Carrier Screws

DHS - Display Housing Screw

SMT - Surface-Mounting Technology

ADC - Analog to Digital Converter

IDE - Integrated Development Environment

EI - Flexural Rigidity

CTE - Coefficient of Thermal Expansion

List of Figures

1.1 iPhone 3D Touch 2
1.2 Force-sensing Trackpad 2
1.3 Display trends: Increasingly larger displays [10] 4
1.4 Bosch's facilities in Braga 5

2.1 Wheatstone bridge: (a) basic configuration, (b) quarter bridge, (c) half-bridge, and (d) full-bridge configurations. 8
2.2 Fixed beam with a sinking support [17] 9
2.3 Main steps of screwing [18] 10
2.4 Total torque used in DTM with different core diameters [18] 11

3.1 Key elements of the D1's force-sensing system 13
3.2 Carrier and DH 14
3.3 FSE from D1 (with sensor notation) 15
3.4 Key elements of the force-sensing system 15
3.5 Maximize deformation of the strain gauge 16
3.6 Strain gauge of D1 and D2 16
3.7 Pin and Wheatstone bridge configuration 17
3.8 FSE from D1 (with sensor notation) 18
3.9 Custom made Arduino board 19

4.1 Scheme of the procedure to study the aging influence 21
4.2 The tensile machine used in the experiments 23
4.3 First approach in the tensile machine 23
4.4 Compression tools used 24
4.5 3D printed parts 24
4.6 Setup with printed parts 25
4.7 Relaxation phenomenon 25
4.8 Relaxation of the printed parts 26
4.9 Testing with metallic parts 26
4.10 Example of data after synchronisation 27
4.11 Tried interpolations 28
4.12 Example of Output/Force relation obtained through graph 28
4.13 The torque screwdriver used - wiha 30
4.14 Tensile machine programs used in experiments TM2 31
4.15 Tensile machine programs used in experiments TM4 and TM5 32

4.16 Types of stepper motors . . . 34
4.17 Load cell for this type of applications . . . 35
4.18 Bending apparatus for individual testing . . . 36
4.19 Selected bearing . . . 36
4.20 Bending apparatus inside thermal chamber . . . 37
4.21 Shaft during testing . . . 38
4.22 Force PCB to bend or to stay flat . . . 40
4.23 Assembly testing . . . 41
4.24 Scheme of the assembly test over time . . . 42
4.25 Calibration Setup . . . 44
4.26 Calibration positions . . . 44

5.1 Display housing loading results and positions . . . 47
5.2 An increase in the mechanical hysteresis did not imply an increase in the hysteresis of output graph . . . 48
5.3 Difference in stiffness and Output/Input relation between before and after cutting the FSE . . . 49
5.4 Percent variation between before and after cutting the FSE . . . 49
5.5 Hypothesis: The higher the hysteresis loop area is, the lower the output . . . 50
5.6 Difference between disassembly and not the FSEs . . . 50
5.7 Stiffness before and after aging . . . 51
5.8 Output before and after aging . . . 51
5.9 Relation between hysteresis and output of the homologous chart . . . 52
5.10 Representation of l_1 and l_2 . . . 53
5.11 Distance between screws in the tensile machine . . . 54
5.12 Distance between screws in the real case . . . 55
5.13 Two different positions of the strain gauge . . . 56
5.14 Confirm the warpage of the parts . . . 58
5.15 Belly over the spring . . . 58
5.16 Comparison of the values obtained with the developed bending apparatus and with the tensile machine . . . 59
5.17 Experiments with FSE out of the camber . . . 59
5.18 One test with feeler gauge to force the PCB to bent . . . 60
5.19 Two tests with clips to force the PFB to stay flat . . . 60
5.20 ΔOut_{02} at different temperatures . . . 61
5.21 Last part of experiment BA1 . . . 62
5.22 Output decrease during force readings . . . 63
5.23 Thermocouples' temperature during BA2 . . . 64
5.24 Air flow in BA2 . . . 65
5.25 Assembly setp vs Developed bending apparatus . . . 65

5.26 Average output variation in the first experiment before aging (BA1) 66
5.27 Average output variation in the second experiment before aging (BA2) . . . 66
5.28 Average output variation in the experiment after aging (AA) 67
5.29 Difference in output between the inside and outer positions 69
5.30 Inside position plots 70
5.31 Inside position: process capability report 72
5.32 Outer positions plots 73
5.33 Ppk values and calculation 74
5.34 Coverage limits using Weibull 75
5.35 Definition of new process limits with Weibul distribution 76

A.1 Exploded view - part 1/2 81
A.2 Exploded view - part 2/2 82
A.3 FSE number 9, S1 83
A.4 FSE number 9, S3 83
A.5 FSE number 6, S1 83
A.6 FSE number 6, S3 84
A.7 DBA3: ΔOut_{12} 84
A.8 DBA3: ΔOut_{01} 84
A.9 DBA3: ΔOut_{02} 85

B.1 Example of the measurements in a random sensor 88
B.2 BA1 - All measurements 89
B.3 BA1 - Average 89
B.4 BA2 - All measurements 89
B.5 BA2 - Average 90
B.6 AA - All measurements 90
B.7 AA - Average 90
B.8 Output variation during experiment BA1 92
B.9 Output variation during experiment BA2 93
B.10 Output variation during experiment AA 94
B.11 Output variation in S1 95
B.12 Output variation in S2 96
B.13 Output variation in S3 97
B.14 Output variation in S4 98

C.1 Results of screwing sequence A 100
C.2 Results of screwing sequence C 100
C.3 Results of screwing sequence E 100
C.4 Results of screwing sequence F 100

List of Tables

3.1 List of the available material 20

4.1 Studies in the Tensile Machine 30
4.2 Expected displacements with the developed bending apparatus 37
4.3 Studies with Developed Bending Apparatus 39
4.4 Studies with the Assembly Setup 42
4.5 Studies during Calibration 45

5.1 Distances between matrices with the Average output for each sensor and temperature 67
5.2 Distances between the matrices with the last measurement for each sensor and temperature 68
5.3 Ranking of the screwing sequences 69
5.4 Process performance in percent 71

B.1 Test with weights schedule 88

Chapter 1

Introduction

The first chapter of this written work intends to explain the circumstances in which this work was developed and the motivation for this project. Additionally, Bosch Car Multimedia Portugal, S.A., where the internship was performed, is described. In the end, the reader is able to know about the study objectives and the outline.

1.1 Project Framework and Motivation

This internship was realized in the mechanical development team XC/CI2-ECM2 from February to September 2021. The projects of this team focus on the development and support of the production of automotive central displays and instrument clusters for leading automotive companies (OEMs).

The team has been working on an innovative touch screen display that, during this work, will be called display one (D1). The project also includes another display with different geometry and larger dimensions, display two (D2). At the current date, both displays are approximately at the middle stage of the development phase and follow the haptic technology. This means that to provide maximum touching experience, actuators were added. They allow the creation of different vibrating patterns that can be felt differently at our fingertip. Furthermore, to increase user experience, a pressure-sensitive system has been developed, which is where this work is focused.

1.1.1 Force-Sensing Technology in Electronic Devices

Capacitive technology is one of the most common technologies to produce touch screens. Shortly, it uses transparent layers of electrodes in between the outer glass and the display. These layers will interact with other electrical conductor, such as our fingerprint or a stylus, changing its capacitance. That's the reason why the touch of a standard glove on our mobile phone is usually not recognized. Nowadays, the vast majority of capacitive displays are projected capacitive. On pro-cap displays, a single touch is stored as an event. Its position is determined by arranging two layers of electrodes in rows and columns, responsible for storing the X and Y coordinates, respectively. Another way to determine the touch position is, for example, the so-called surface capacitive. Apart from the electromagnetically actuated seen so far, there are also resistive displays, which are mechanically actuated, optical displays, and acoustic displays [1][2][3][4].

All these types of displays have in common that none of them, per se, is able to measure how hard the screen is being pressed. Although it might not sound like a signifi-

cant improvement, obtaining information about the touching pressure can change how we interact with our device, adding functionalities such as accessing shortcuts, previewing details and drawing art. That's why some manufactures patented new ways of implementing pressure sensitivity on their devices.

One of the pioneers of this type of technology is Apple. The company introduced pressure sensing technology on its watches, modern MacBooks, and Magic Trackpad 2. They call it Force Touch. This technology was also adapted for mobile phones and introduced in iPhone 6S and 6S Plus entitled 3D touch, as shown in Fig 1.1. The sensing construction on the iPhone 6s is much different from the Apple Watch, but both use capacitive sensing (i.e., detecting minute changes in capacitance due to change in distance) as the basis to detect the level of applied pressure [5][6].

Figure 1.1: iPhone 3D Touch

As the name suggests, 3D Touch intends to detect three pressure levels: the first is simple touch; the second is a slightly stronger pressure; the third is to keep pressing while applying more force to the iPhone screen. From the iPhone 11 line onwards, Apple decided to end the force sensitivity applications on iPhones and started the Haptic Touch, maintaining the linear actuator for vibrating feedback. Mac Trackpads use four sensing strain gauges, one on each edge of the pad, as Fig 1.2 suggests [5][6].

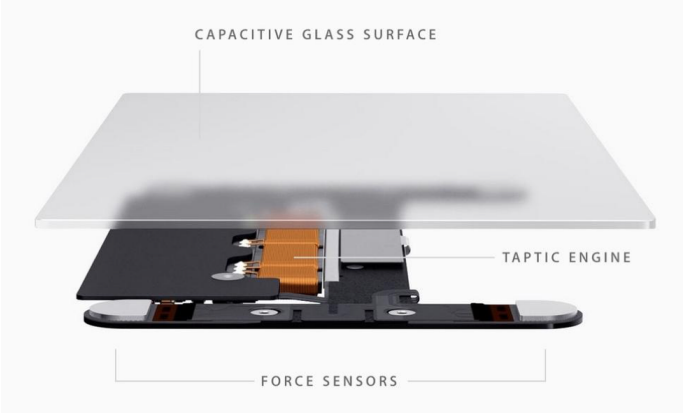

Figure 1.2: Force-sensing Trackpad

These are just some examples of the application of force-sensing technology. Nowadays, multiple and diversified ways to implement this technology in electronic devices can be found. Different industry requirements can lead to other solutions. Moreover, the implementation objectives of this technology can vary slightly from application to application. The automotive industry is an example of how this technology can be helpful apart from extending functionalities.

1.1.2 Force-sensing Technology in Automotive Displays

Traditionally, the driver's control of vehicle functions, apart from the actual driving task, has been carried out using various physical buttons and dials. With the increased number of functionalities, it is no longer possible to have one physical button or dial for each function. Instead, the user interface must adapt to the particular driving situation at each moment in time, leading to the development of touch interfaces such as touchscreens. For this reason, the number of displays in automobiles has increased significantly in the past decade. As the result, not only the number of in-vehicle displays has grown over this period, but also the display size has grown, as Fig 1.3 exemplifies [7].

A capacitive touchscreen is susceptible to false triggers when users come close to the screen with their finger or accidentally brushes the screen. In automotive applications, false triggers can be dangerous since nowadays, several car settings are adjusted in the central display. In this case, force-sensing can be employed to avoid false positives apart from expanding on input possibilities such as coupling with menu selections. If there is no defined pressure, no function is triggered. Consequently, just touching the device would not trigger an action by mistake. This is especially important at night when errant touches could result in relatively bright, distracting screens even with an ambient light sensor [8].

In the future, with an increasing maturity level in autonomous driving and electric vehicles, automotive displays are expected to acquire a more important role in a car. For example, the "driver" may want to be relaxed during autonomous driving, and one display can be used as an infotainment display as well as an indicator [9].

1.2 Bosch Group

The company where the internship was carried out, Bosch Group, was founded in 1886 when Robert Bosch opened the "Workshop for Precision Mechanics and Electrical Engineering", located in Stuttgart, Germany.

Nowadays, Bosch Group is a leading global supplier of technology and services. It employs roughly 394,500 associates worldwide (as of December 31, 2020). Accordingly to the company's website, the company generated sales of 71.5 billion euros in 2020 [11].

The company works in entirely different areas. Whether for the products that are supplied for the most prominent world manufacturers or the products sold directly by Bosch, it is understandable the importance that the development teams have in each business sector the company is divided: mobility solutions; industrial technology; energy

Figure 1.3: Display trends: Increasingly larger displays [10]

and building technology; consumer Goods.

Relatively to environmental questions and the big companies' responsibility on it, Bosch seems to be aware of its role. The company releases every year a sustainability report everyone can access easily. There, it is possible to check what are the concrete actions the company has been taking. On the website it is acclaimed that, since 2020, climate-neutral had been reached with more than 400 locations worldwide. This fact was officially confirmed by an independent auditing company. Finally, for the future, Bosch set itself climate action targets across the entire value chain and have had these confirmed externally by the Science Based Targets initiative (SBTi) [11][12][13].

Bosch Car Multimedia Portugal, S.A.

More precisely, the internship was performed at the Bosch facilities of Braga, visualized in Fig 1.4. The history of this unit begins with the opening of the Blaupunkt factory in 1990. At this time, the unit was dedicated to the production of car radios.

With the evolution of the automotive market demands, in 2009, the brand was sold. It became Bosch Car Multimedia Portugal, S.A., dedicated to developing and producing infotainment, instrumentation, and sensor systems for the automotive industry.

Accordingly to Bosch's site, the company doubled its turnover in the last 4 years and surpassed the billion euros mark in total sales, winning a place among the 4 largest exporters in Portugal in 2018 [11].

Figure 1.4: Bosch's facilities in Braga

Currently, more than 330 engineers develop solutions that contribute to safer and more comfortable mobility. This unit, which has 3280 employees, is also one of the most significant contributors to the results recorded by Bosch in Portugal, having reached 1000 million euros in sales in 2017, thanks to the more than 50 car manufacturers that turn to Bosch Car Multimedia for the supply of the most varied components. The products that leave this facility are supplied to customers, namely in Europe [11].

1.3 Objectives

The proposed objectives for this work are the study of influences in the force-sensing operation, manly:

1. Artificial aging;
2. Temperature and air flow;
3. Screwing sequence.

Since the investigation was not made with final series parts and the available material was limited, there was no primary concern in presenting exact values. Instead, the study intends to outline major mechanical limitations and fundamental concept flaws of the force-sensing system.

Efforts were made to design tests to reach the presented objectives. However, those tests had to be, on many occasions, adapted due to material and time restrictions. This process is explained in Chapter 4.

1.4 Outline

In this Section, the contents of the remaining Chapters of this document are summarised.

- **Chapter 2** - Theoretical foundation is presented. It will support some choices and conclusions of this work.
- **Chapter 3** - Intends to present some key parts of the displays that this work relies on as well as some relevant operational aspects.
- **Chapter 4** - Aims to explain which type of experiments were chosen and why. These experiments were divided into categories. Furthermore, each study inside one category is given a code. This code is the key connection of this document between Chapters 4 and 5.
- **Chapter 5** - The results are presented and analyzed, always using the experimental categories and studies' code assigned in Chapter 4.
- **Chapter 6** - At the end of this written document, some conclusions and considerations about possible future works are provided.

Chapter 2

Theoretical Foundation

This Chapter provides a better understanding of some theoretical foundations that will support the work performed. The Chapter starts with an overview of strain gauges. After, it is explained how to calculate forces in a fixed beam with sinking support. This structural mechanics theme will be relevant to analytical calculations. A section about screwing comes ahead. Finally, a section regarding process capability is provided.

2.1 Strain Gauges

A strain gauge is a device used to measure strain on an object. This technology is valuable for innumerable operations across many industries.

2.1.1 Operation Principals

Strain gauges are usually made of a thin wafer conductor that is placed on a carrier foil. A copper-nickel alloy is often used for the conductor due to its high-temperature stability. Compression and elongation of the workpiece cause a proportional change in the resistance value of the strain gauge.

The resistance change in function of length change (the sensitivity of the strain gauge) is called the gauge factor, and it is given by:

$$GF = \frac{\Delta R/R}{\Delta L/L} = \frac{\Delta R/R}{\epsilon_a}$$

Where GF stands for gauges factor (values are typically around 2), R is resistance, L is the wire's length, ϵ_a strain in the gauge.

The conductor shouldn't deform permanently. For that reason, in its turn, the maximum strain is near the yield strain of the wire. For example, for a 0,01 mm/mm yield strain and a $GF = 2$, we would get a $\Delta R/R = 0,002$. A 100 Ω would rise to 100.2 Ω, or drop to 99.8 Ω [14].

The problem with strain gauges is that, usually, resistance changes are small. To solve this problem a Wheatstone bridge can be used to convert small changes in resistance into measurable voltage changes [15].

2.1.2 Wheatstone Bridge

When working with strain gauges, it is common to have one, two, or three different gauges placed in a Wheatstone bridge. The names quarter, half, and full-bridge are the most common bridges layouts. The nominal resistance of each gauge is usually the same. The full bridge has the highest sensitivity; 4 times when compared to the quarter bridge, and 2 times when compared to half bridge.

Observing Fig 2.1, namely the notation presented in for the basic configuration, a Wheatstone bridge is balanced when V_2 is equal to V_3. When this situation is confirmed, since $\Delta V = 0$, there won't be any current flowing between these points. For example, if we want to determine the impedance of an additional resistance R1' positioned in the same branch as R1, we need to vary R4 until V_2 equals V_3. In many cases, R3 is a potentiometer, and between V_2 e V_3 a galvanometer is installed to detect no current. Once this state is reached, the additional resistance of R1' has the same value as the potentiometer variation [16].

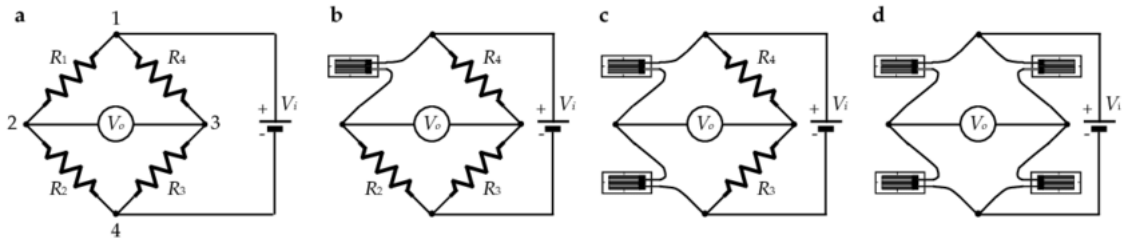

Figure 2.1: Wheatstone bridge: (a) basic configuration, (b) quarter bridge, (c) half-bridge, and (d) full-bridge configurations.

2.2 Fixed beam with sinking support

The presented case happens when the ends of a fixed beam don't remain perfectly aligned. Since the ends of such a beam are prevented from rotating, a deflection of one end of the beam relative to the other induces fixed-end moments as shown in Fig 2.2. In the same sense and for the relative displacement shown, a total anticlockwise moment equal to $M_A + M_B$ on the beam is produced. This moment is balanced by a clockwise couple formed by the force reactions at the supports. The resultant bending moment diagram is displayed in Fig 2.2.

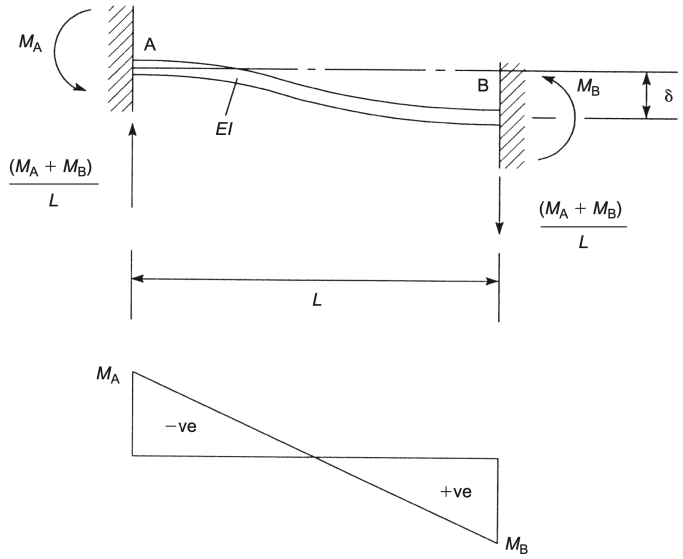

Figure 2.2: Fixed beam with a sinking support [17]

The theoretical moment is given by:

$$M_A = M_B = \frac{6EI\delta}{l^2}$$

The force is given by:

$$F_A = F_B = \frac{12EI\delta}{l^3}$$

Hence, the stiffness is:

$$K = \frac{dF}{d\delta} = \frac{12EI}{l^3}$$

Where M stands for moment, F force, E flexural modulus, I second moment of area, l horizontal distance between A and B, and δ vertical distance between supports.

2.3 Screwing Process

Screwing technology continues to be a key field for many varied assembly tasks. Screw connections are desirable due to their resilience, reusability of components, and the option of disassembling the connection at any time without destroying the parts. As a result, screws are the most frequently used mechanical elements that are both standardized and available in a wide range of designs.

2.3.1 Basics

The main screwing steps are explained in Fig 2.3 and are:

1. The screw is run down until the screw head touches the workpiece at the seating point (A).
2. The screw is then tightened until the final torque (C) is reached. This is often also the peak torque (B), but the final torque is lower in some cases.
3. The clamp angle (D) and clamp torque (E) are measured between the seating point and the peak torque.

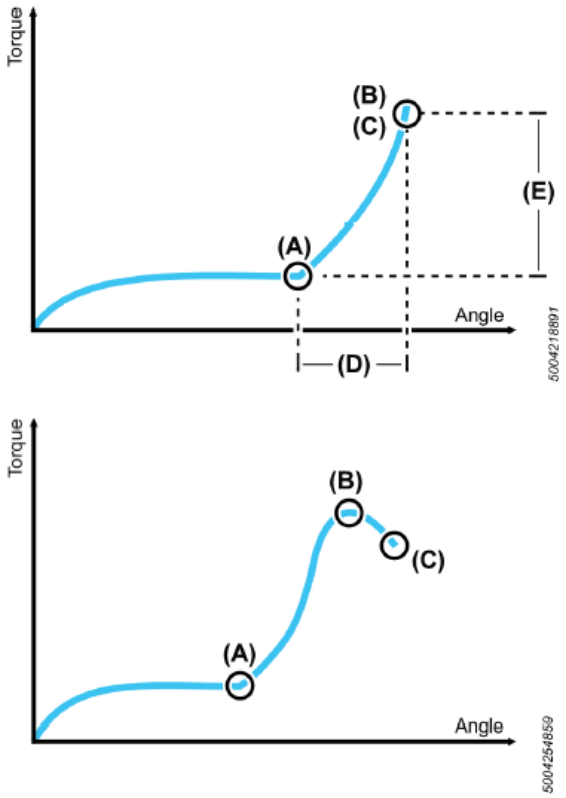

A	Seating point
B	Peak torque
C	Final torque
D	Clamp angle

Figure 2.3: Main steps of screwing [18]

2.3.2 Differential Torque Method (DTM)

The differential torque method is essentially a way to detect the seating point and apply the required offset torque. This detection is made with controllers, which monitor

the gradient of the torque over angle. The main goal of this strategy is to eliminate floating screws and apply the same preload force to all joints, independently from the joint's geometry variation. The total tightening torque (tapping torque plus offset torque) may differ from tightening operation to tightening operation. However, the same amount of torque (offset torque) will be applied to compress the joint, as shown in Fig 2.4 [18].

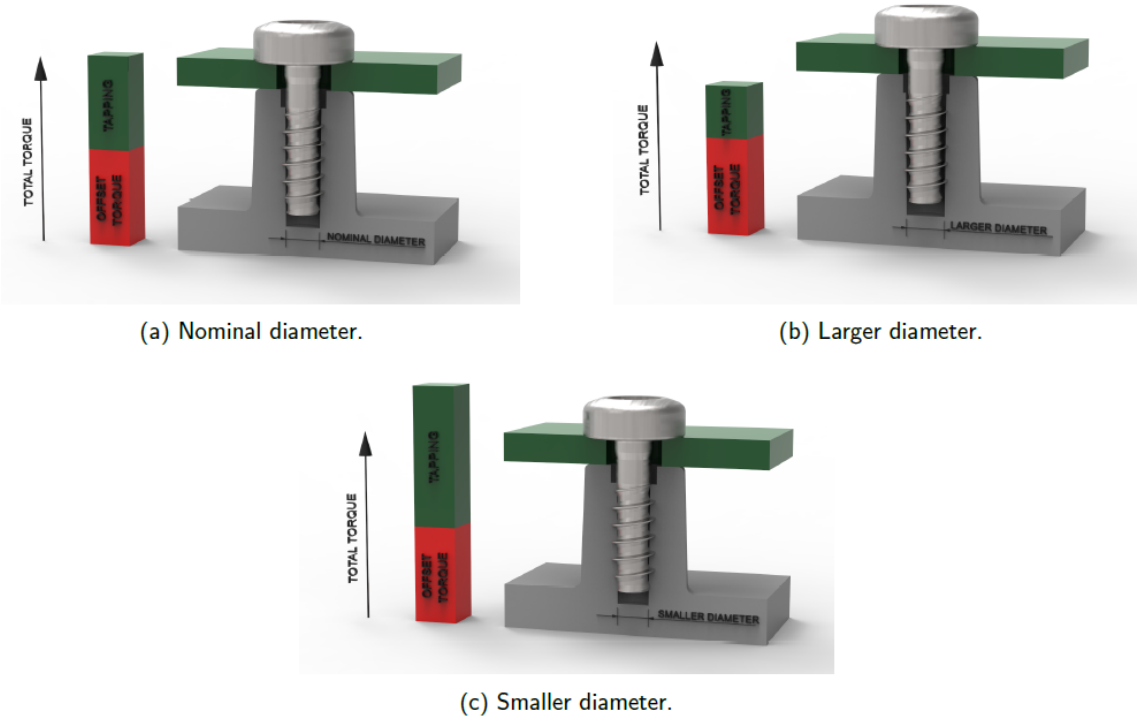

(a) Nominal diameter.

(b) Larger diameter.

(c) Smaller diameter.

Figure 2.4: Total torque used in DTM with different core diameters [18]

2.4 Process capability

In the automotive industry, considerable time and effort are spent designing parts and manufacturing processes. In order to ensure that the processes are capable and ready to production, a performance index is needed. The process performance index is the statistical calculation that manufacturing engineers employ to assess the statistical capability of the manufacturing process to produce high-quality products that stay within the specification limits.

One of the primary tools used to establish process capability is the Ppk calculation. It is a measurement of how close a production process is to its target values. The key to this calculation is that it takes into account both variation and distance from the mean in assessing capability, which is essential because if the mean is shifted significantly, there is the chance that the process will go out of control if the variation changes.

While Pp calculation accesses the performance potential (it assumes the process is centered), PpU and PpL measure the overall capability of the process based on its upper and lower specification limits, respectively. Finally, Ppk is given by the minimum of these

two indexes, where values of 1,33 and 1,67 are used as reference on the automotive industry [19].

Formulas:

$$\mathrm{P_p} = \frac{(\mathrm{USL} - (\mathrm{USL})}{6\sigma}$$
$$\mathrm{PpU} = \frac{(\mathrm{USL} - \overline{\mathbf{X}})}{3\sigma}$$
$$\mathrm{PpL} = \frac{(\overline{\mathbf{X}} - \mathrm{LSL})}{3\sigma}$$
$$\mathrm{Ppk} = Min(\mathrm{PpU}, \mathrm{PpL})$$

2.5 Summary

In this Chapter, information about some theoretical fundamentals is provided. This given information will help the understanding of some posterior aspects. Starting with strain gauges and then with a fixed beam with sinking support. A section about screwing comes ahead. Finally, a section regarding process capability is provided.

Chapter 3

Product and Concept Analysis

As already explained in chapter 1, display 1 (D1) and display 2 (D2) are two different devices that belong to the same project. This work is mainly focused on the development of D1. Nevertheless, both displays were developed under the same force-sensing concept, and to take advantage of all the material available, some components of the force-sensing system from D2 were also studied. In this Chapter, some key parts of both displays are presented as well as some relevant operational aspects. All the presented parts are still prototypes, therefore susceptible to changes.

3.1 Display 1

In Fig 3.1, a simplified modulation of the main components of D1's force-sensing system is presented.

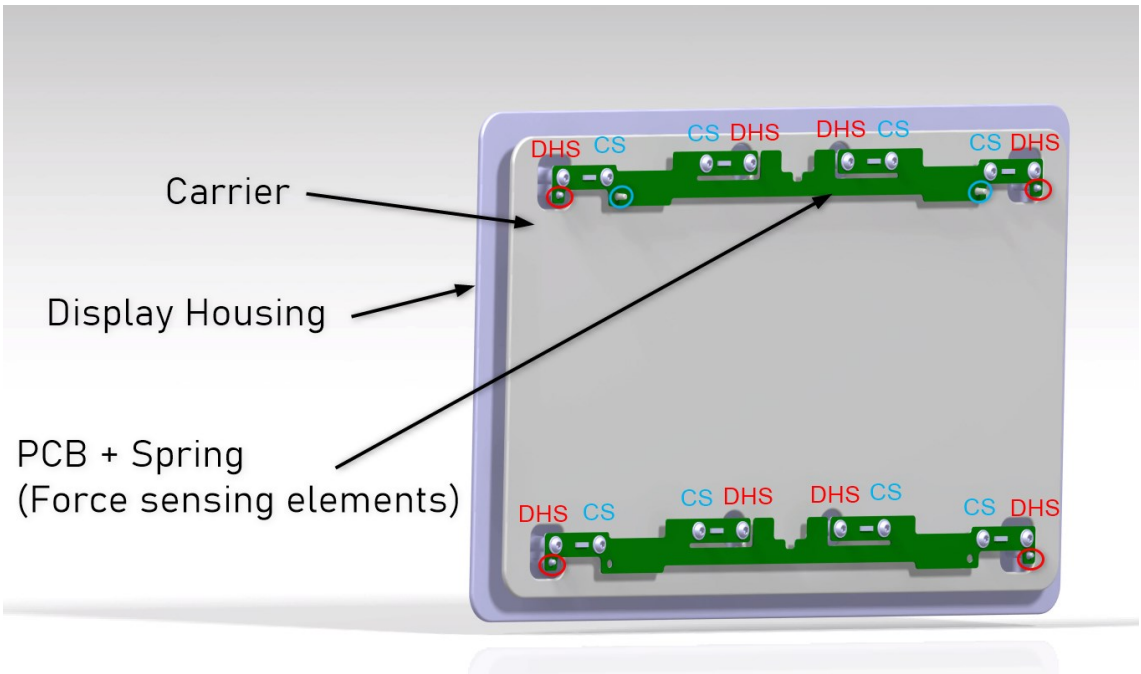

Figure 3.1: Key elements of the D1's force-sensing system

3.1.1 Carrier

Starting with the carrier, presented in Fig 3.2a, this component is responsible for connecting the display to the car frame.

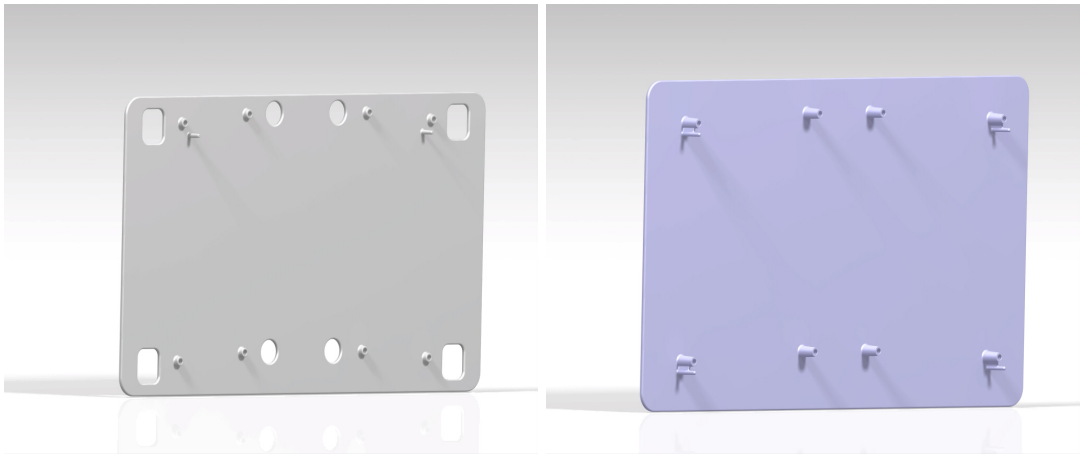

(a) Carrier (b) Display housing (DH)

Figure 3.2: Carrier and DH

3.1.2 Display Housing (DH)

In Fig 3.2b the display housing (DH) is visualized. As the name suggests, on the back of this component is fixed the display.

3.1.3 Force-Sensing Elements

Some of the main components of the force-sensing system are 2 pairs per display of a printed circuit board (PCB) overlapping 2 steel springs with approximately the same geometry, presented in Fig 3.3. During this work, one combination spring + PCB will be referred to as a force-sensing element, or simply FSE.

As visible in Fig 3.3, each spring and PCB has 4 tabs, named S1 to S4, where a strain gauge is placed. S3 and S4 are the inside tabs (In), and S1 and S2 are the outer tabs (Out). Also, to differentiate from the upper and lower FSE, an ”U” or an ”L” will be added before the sensor name. For example, US1 means sensor 1 from the upper spring.

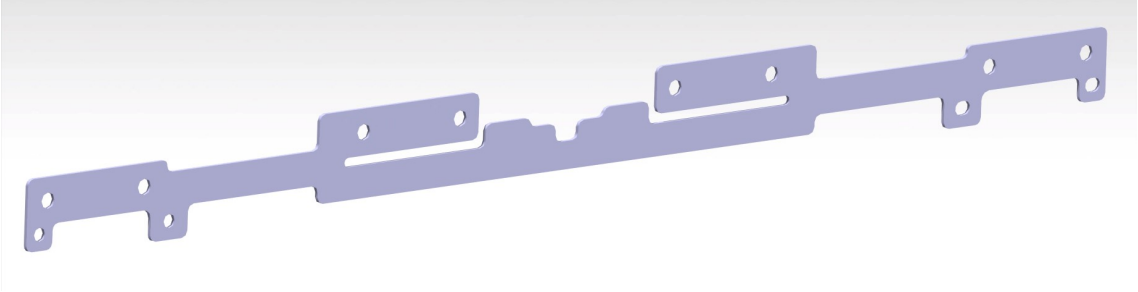

(a) Steel spring of D1

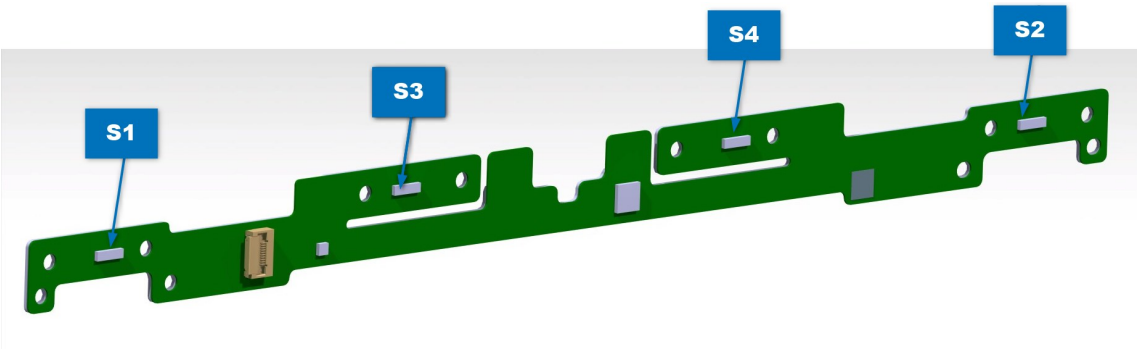

(b) Spring and PCB of D1

Figure 3.3: FSE from D1 (with sensor notation)

The FSE are installed on the carrier through 8 M3 self-tapping screws. The presented screws will be referred to as carrier's screws during this work since they connect to the carrier. The DH connects on the remaining holes of FSE, which will be called DH's screws (DHS). These screws can be visualized in Fig 3.1 and in Fig 3.4.

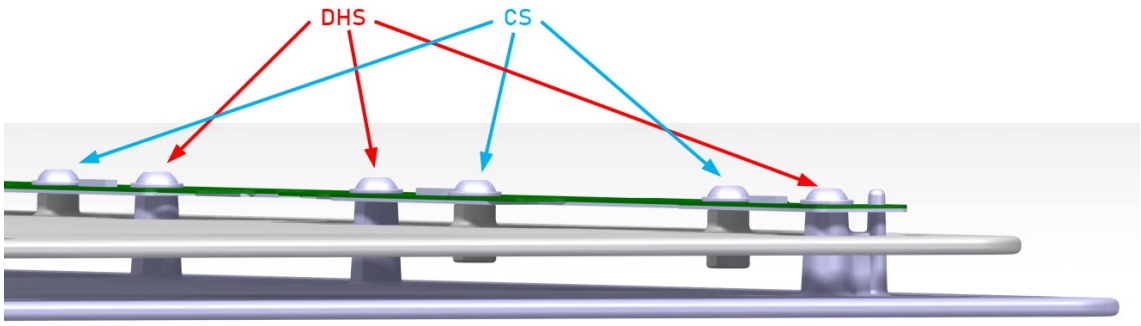

Figure 3.4: Key elements of the force-sensing system

3.1.4 Operation

With the carrier fixed to the car frame, when the screen is pressed, the display housing can move 1.5 mm before the DH hits the carrier's mechanical stoppers that prevent the FSE from being damage by permanent deformation. While the display housing moves, the FSE bend between each pair of screws. One is connecting to the DH and the other to

the carrier, as represented in Fig 3.5.

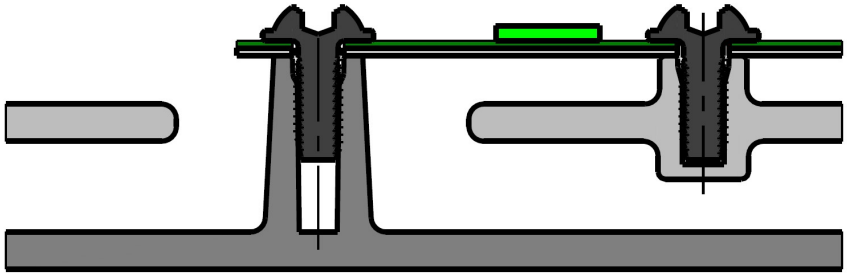

Figure 3.5: Maximize deformation of the strain gauge

Whether the DH is pressed or pulled, the FSEs bend with an S-shape, as Fig 3.6b represents. This case is comparable to a fixed beam with sinking support presented in Chapter 2.

3.1.5 Strain Gauge

Between each pair of screws, there is the strain gauge presented in Fig 3.6 responsible for measuring the deformation.

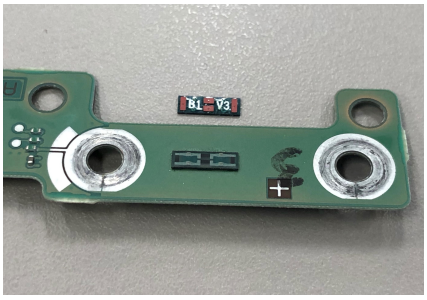

(a) Real image of the gauge

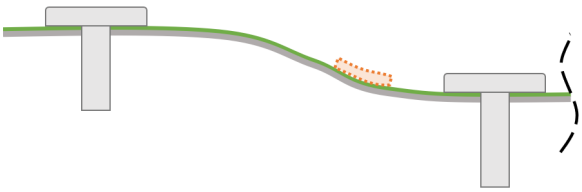

(b) Maximize deformation of the strain gauge

Figure 3.6: Strain gauge of D1 and D2

Observing Fig 3.6a, it is clearly visible that the gauge is not placed exactly in the middle of the screws. That is because if the FSE bends in an S-shape, the deformation in the middle is almost null. Previous studies placed the strain gauge in a position to boost output and consequently the sensitivity of the sensor and the resolution of the system.

The strain gauge used is advised for surface-mounting technology (SMT). Its pin configuration is presented in Fig 3.7a.

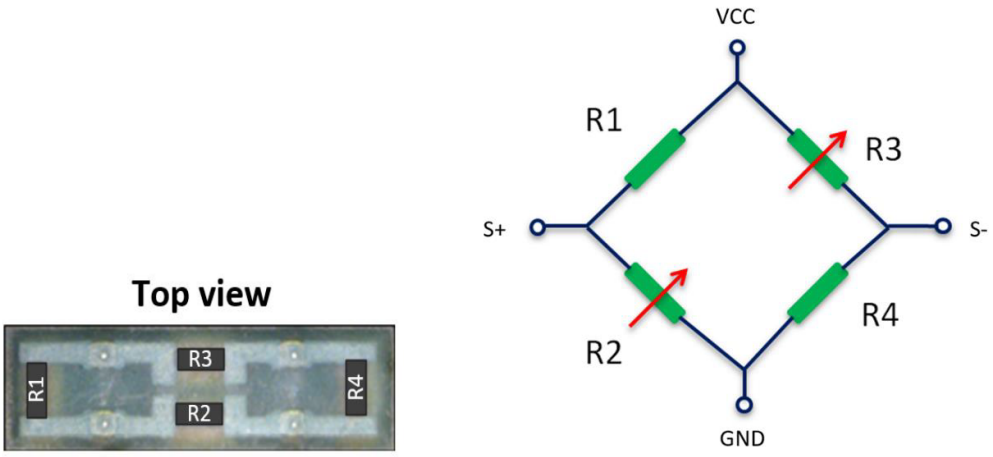

(a) (b)

Figure 3.7: Pin and Wheatstone bridge configuration

Resistances R1 and R3 are aligned with the spring. Its impedance increases when the strain gauge bends concavely down. When the strain gauge bends concavely up, the resistive element is compressed, and its length decreases. Hence, the voltage drops between its extremities.

In this product, an half-bridge configuration was used. It is presented in Fig 3.7b. Since R3 and R2 are both either in tension or compression, the voltage drop between S_- and S_+ will be amplified.

3.1.6 Alignment

Returning to Fig 3.1, the red circles point to the pins whose function is to align the force-sensing elements with the carrier. Two pins for each pair are enough to fix the parts in the x and y directions. In order to align the remaining part (the carrier), two pins are used in the upper side, circled blue in the same figure. With these pins, the carrier also stays aligned with the display housing in the x and y-direction. The screws are responsible for fixing the force-sensing elements to the carrier and DH in the z-direction.

3.2 Display 2

Display 2 is a display that works with the same force-sensing concept as D1, which means that the key components of this device are the same, even though the dimensions and geometries of its carrier and DH are different.

Force-Sensing Elements

The D2's FSEs have a similar geometry to the ones of D1. In fact, the holes are in the same positions, which eased the work of developing a testing machine to test both. Nevertheless, the D2's FSEs don't fit in the D1's carrier due to some constructive elements.

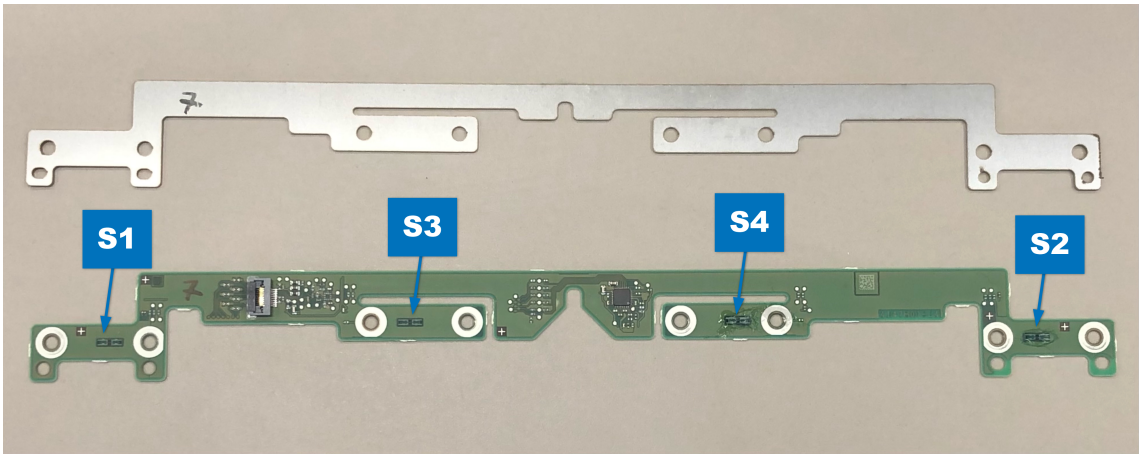

Figure 3.8: FSE from D1 (with sensor notation)

The force-sensing elements are also installed on the D2's carrier through 8 M3 self-tapping screws. Similar to D1, and as visible in Fig 3.8, each spring and PCB has 4 tabs, named S1 to S4, where a strain gauge is placed. S3 and S4 are the inside tabs (In Positions), and S1 and S2 are the outer tabs (Out Positions).

3.3 Sensor Data Processing

3.3.1 Force Calculation

Compared with the free state output, the strain gauges may present a positive output when bending concavely down and a positive value when bending in the opposite direction. While the screen is being pressed, depending on the position, there might be strain gauges bending in both directions, i.e., there might be positive and negative output values. The algorithm that is being developed intends to use the information from the 8 strain gauges as well as the information from the touch screen to calculate the final value.

3.3.2 Strain Gauge Output Readouts

In the real case, the analog output of the springs is sent to the main PCB that converts it to digital values to be processed. The values could be extracted easier from the springs while flashing with an Arduino. This microprocessor uses 24 bits for each sensor, so the free state output is around $\frac{2^{24}}{2} = 8388608$ steps. Then the value increases or decreases depending on which side is bending. The custom-made board presented in Fig 3.9 was

used for this purpose. It has two analog-to-digital converters (ADC), with two flat cables connectors, with 10 and 12 pins, respectively. Nevertheless, this only allowed reading one PCB at a time. Then, one 8-channel bi-directional logic level converter makes the connection between the ADC's and the Arduino Nano. This chip performs bidirectional level shifting from any voltage to any voltage and will auto-detect the direction. The Arduino Nano connects with the computer through the interface Arduino IDE.

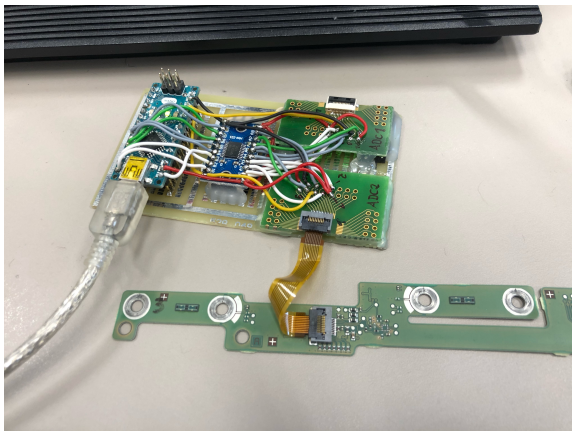

Figure 3.9: Custom made Arduino board

The results were directly copied from Arduino's serial monitor to Microsoft Excel. Some Arduino code alterations were often made to present the results with or without an offset. This offset allowed to do a reset on the values, and it was used for a calibration method before some experiments. The offset is initialized as soon as the Arduino button is pressed.

3.4 Available Material

The material that was available for testing is presented in Table 3.1:

Table 3.1: List of the available material

FSE No	Display	State	Sensors Not Working
1	D1	Climatic Chamber (Corrosion) and Acoustic Tests	1, 4
2	D2	New	-
3	D1	Climatic Chamber (Corrosion) and Acoustic Tests	3, 4
4	D1	Climatic Chamber (Corrosion) and Acoustic Tests	-
5	D1	Climatic Chamber (Corrosion) and Acoustic Tests	-
6	D2	New	-
7	D2	New	-
8	D2	New	-
9	D1	New	-
10	D1	”New” (One side slighty bent)	-
11	D1	New	-
12	D1	New	-

3.5 Summary

In this Chapter, display 1 (D1) and display 2 (D2) is presented. Apart from the key components, some important operational aspects are explained. One of these aspects is the deformation of the multi-material combination where the strain gauges are placed. Therefore, this Chapter precedes the explanation of the experiments performed, whose understanding requires knowledge about the product.

Chapter 4

Testing Development

A reasonable amount of time was committed to developing tests and setups to obtain conclusions about the proposed objectives. However, the task planning changed over time due to material and time restrictions, and while some findings were being drawn. Hence, Chapter 4 intends to present the decision process of the more appropriate experiments, setups, equipment, and, inevitably, some conclusions that changed the testing path.

4.1 Experimental Design

This section explains which type of experiments were designed to obtain a conclusion for each objective and how the experimental path to follow changed:

4.1.1 Aging Influence

Obtaining conclusions about the influence of aging implies studying the system before and after aging. After initial research, it was found that this type of bi-material stacks could present complex behaviors in temperature. Hence, it was decided to test the system in temperature step tests.

Figure 4.1: Scheme of the procedure to study the aging influence

Initially, a bending apparatus was developed to test the force-sensing elements (FSE) inside a thermal chamber. Because the chamber had small dimensions, the FSE had to be cut in half. The initial objective was to use the developed bending apparatus to test before and after aging. Tensile machine tests were selected also to obtain information about the mechanical behaviour of the FSE through the Force/Displacement curve. The chosen path for the first objective is depicted in Fig 4.1.

During the experiments with the developed bending apparatus, one thermal chamber with bigger dimensions became available. Several reasons lead to switch the setup and test the FSE assembled in the carrier and display housing (DH). In the end, the results from

the assembly testing are considered to be more reliable, for reasons presented in Chapter 5.

4.1.2 Temperature and Air Flow Influence

This objective was added because, during the first experiments, some unexpected behaviors were noticed. The purpose is to understand if the output variation initially seen was effectively related to temperature and wind and if that should or not become a concern for the following developments of the product. The experiments with the assembly initially developed to study the aging influence were adapted with the purpose of studying also these effects.

4.1.3 Screwing Sequence Influence

Some calibration trials were performed. During this process, the output of each sensor is measured. Due to the complex alignment between the components, it was expected that the screwing orders could influence the stresses in the FSE. In order to study this influence, some samples were screwed with different screwing orders. Then, the calibration process was performed to study its effect on the results.

To sum up, the experiments can be divided in four main categories:

- Tensile Machine Testing;
- Developed Bending Apparatus;
- Assembly Testing;
- Calibration.

During the following sections, each experiment category will be explained, as well as the experiments performed. The presentation is organized accordingly to the order that the tasks were performed. The data treatment had to be done, in many instances, some days after the respective experiment. This was needed to take advantage of the equipment availability and consequent completion of all tasks. Some conclusions didn't come out immediately after performing the tests, and some experiments had to be performed without being sure of their reliability.

4.2 Tensile Machine Testing

Several tests were performed in the tensile machine presented in Fig 4.2. The software allowed to obtain the data in f(Time, Force, Displacement), which would be later

synchronized with the output from the strain gauge, f(Time, Output Sensors), collected with the custom made Arduino board previously presented.

Figure 4.2: The tensile machine used in the experiments

4.2.1 Setup Development

First Approach

The first experiments in the tensile machine were done while loading the screw directly with a small compression punch in the four different positions of the spring, as exemplified in Fig 4.3. The screw could easily rotate, and the point of contact between the screw and the tool varied between each experiment. Therefore the stiffness values were expected to be lower than in the actual situation. In the end, this experiment allowed to have an idea about the values involved.

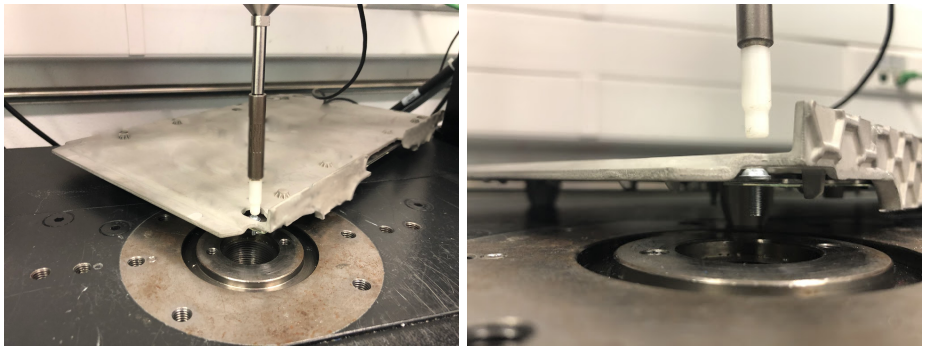

Figure 4.3: First approach in the tensile machine

Display Housing Loading

The most realistic way to study the behavior of the pressure sensing system is to load directly on the display housing, as exemplified in Fig 4.4. Some tests were performed to have reference values of the loads involved. Having these values would help to develop a setup to test the assembly inside a thermal chamber.

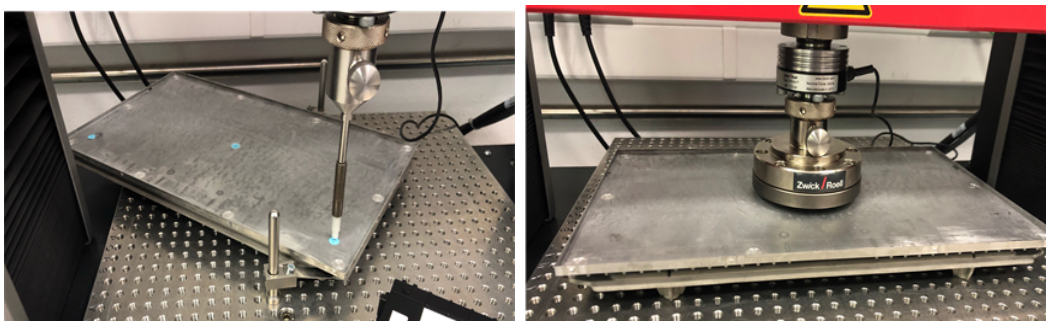

(a) (b)

Figure 4.4: Compression tools used

Setup with 3D Printed Parts

After deciding to study the FSEs individually, the parts of Fig 4.5 were printed with Polyjet 3D printer. The advantage of this setup is the possibility to test the force-sensing elements of D1 as well as the force-sensing elements of D2. That's because the D2's FSEs don't fit on the D1's carrier.

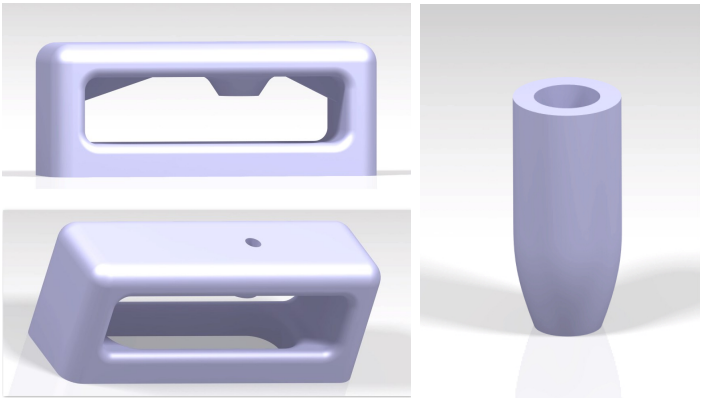

(a) Simulate Carrier (b) Simulate DH

Figure 4.5: 3D printed parts

The parts presented in Fig 4.5a were used to simulate the carrier while fixing the FSEs for testing. While connecting to the tensile machine tool, the printed adaptor in Fig 4.5b replicates the screw dome of the DH. Hence, the screw is not able to rotate as in the setup presented in the first approach. In Fig 4.6 the testing setup with printed parts is exhibited.

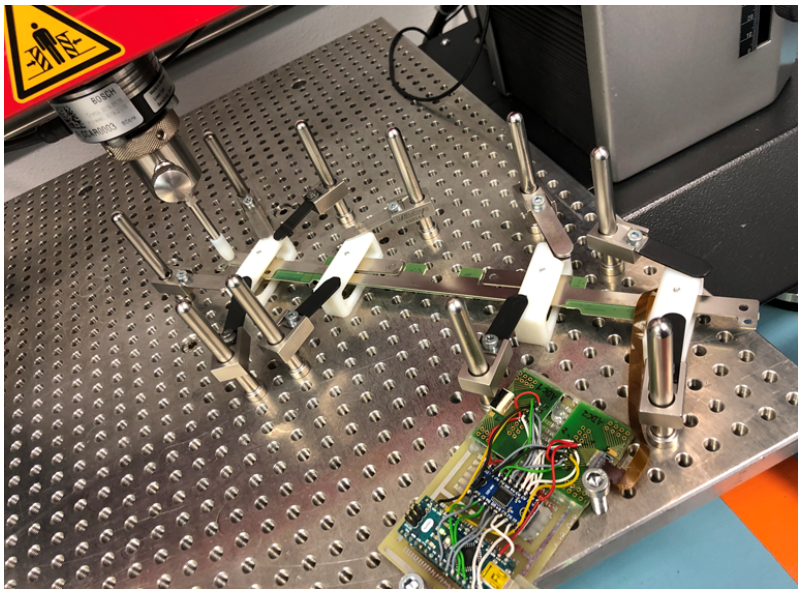

Figure 4.6: Setup with printed parts

After testing some FSEs, the relaxation phenomenon visible inside the circles of Fig 4.7 appeared. This relaxation was also visible in the Load/Displacement graph in the form of mechanical hysteresis.

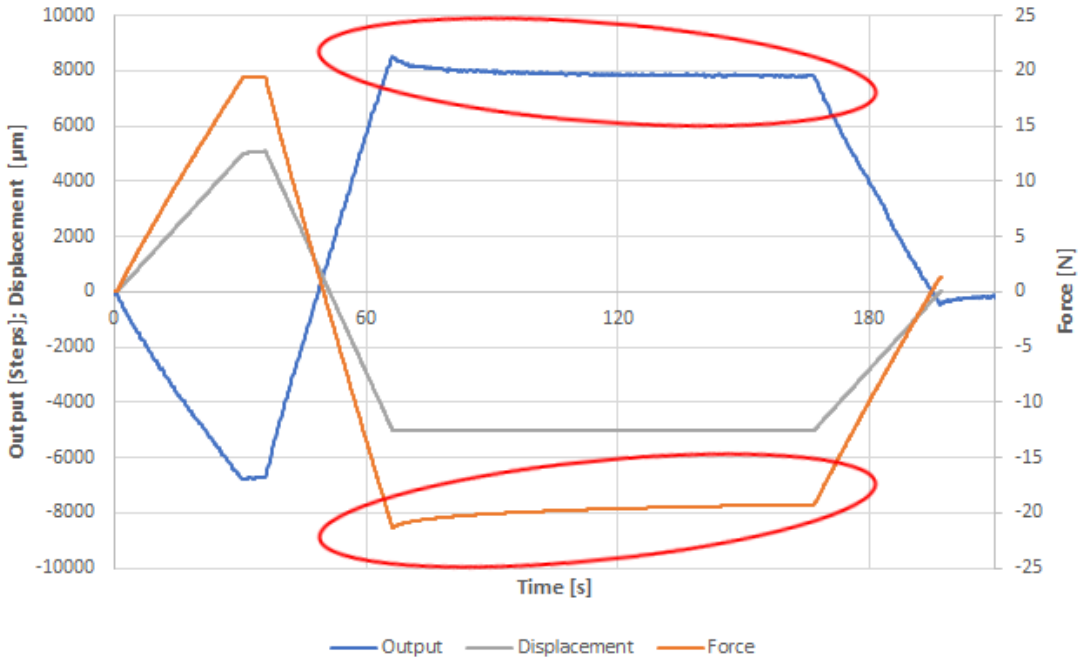

Figure 4.7: Relaxation phenomenon

This situation led to testing the printed parts individually, as Fig 4.8a presents, with the objective of understanding if this phenomenon was related to the FSE. However, the relaxation effect remained when testing only the printed parts, as shown in Fig 4.8b.

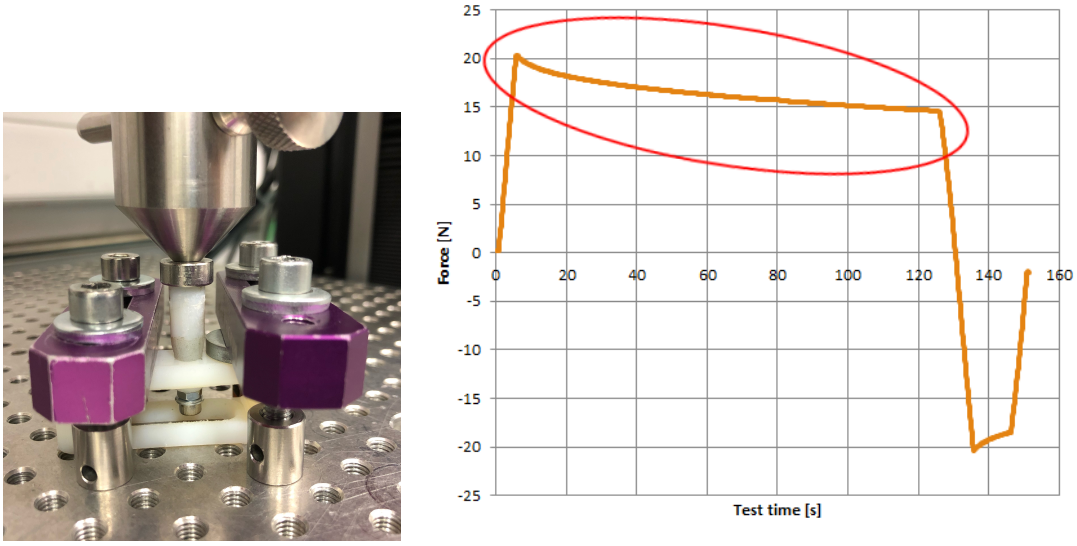

(a) Testing the setup (b) Result of testing the printed parts

Figure 4.8: Relaxation of the printed parts

Without knowing exactly how much this relaxation could influence the final results, it was decided to find another testing setup.

Final Setup

The full metallic setup with the carrier of D1, presented in Fig 4.9, was used in the end.

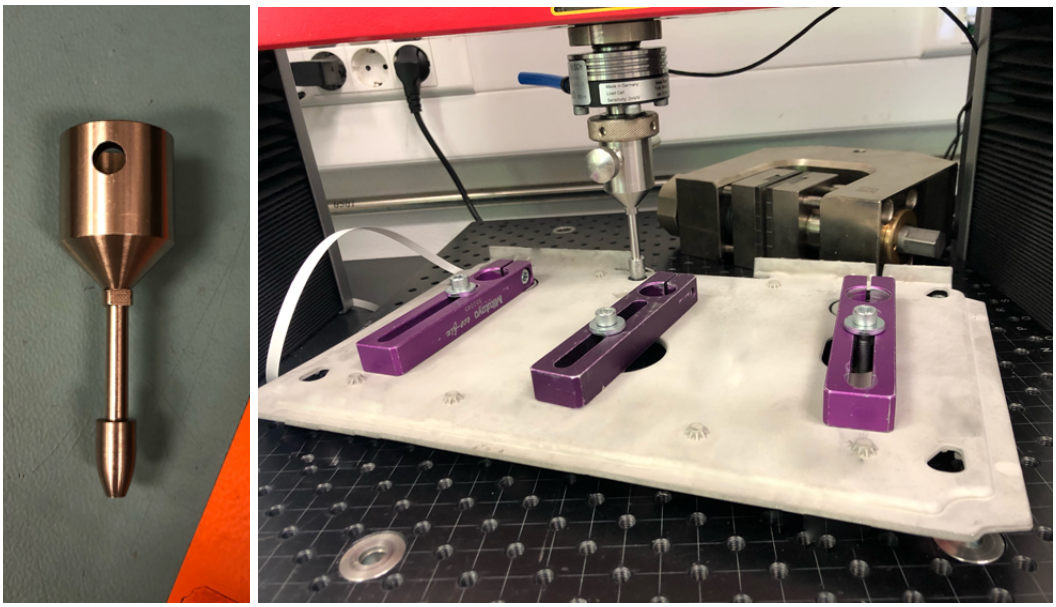

(a) Adaptor (b) Setup

Figure 4.9: Testing with metallic parts

This solution wasn't considered before because the FSE from D2 didn't fit in the D1's carrier. Although the holes of the FSE from both displays were in the same positions, the FSE of display 2 overlaps some screw domes. To solve this question, some elements of the component had to be machined. One of these elements were the alignment pins circled in Fig 3.1.

Finally, the relaxation value was reduced to practically zero, and the force-sensing elements' stiffness increased slightly.

4.2.2 Data Processing and Setups Preparation

Data Synchronisation

To study the sensitivity of the system, in other words, the relation Output/Input (Strain gauge output/Applied Force), presented in Fig 4.12, the time variable from both data sources had to be synchronized. This was achieved using Microsoft Excel, where the point of maximum displacement and force was aligned with the point of maximum sensor output, as represented in Fig 4.10.

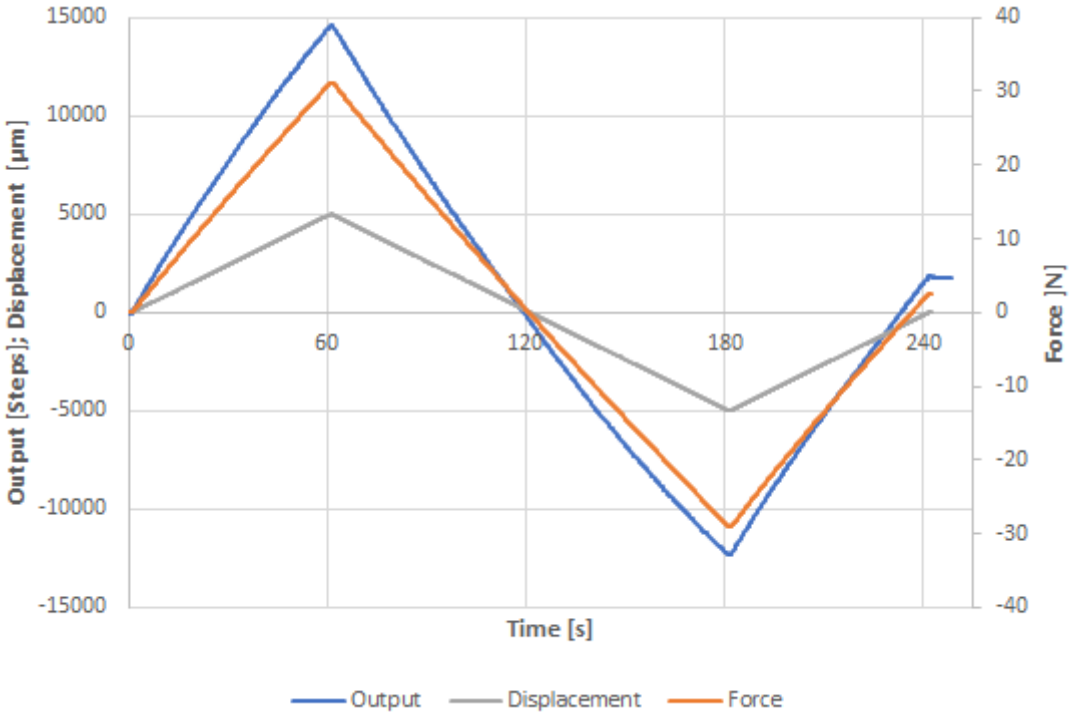

Figure 4.10: Example of data after synchronisation

Nevertheless, it was still necessary to obtain the Output=f(Force).

With the value of 2 Hz, the lowest sample rate was more than enough to have credible data. Therefore, it was decided to perform downsampling over the tensile machine data. Since the Arduino sample rate is not strictly constant, an interpolation was needed. It was decided to perform an interpolation over the data from the tensile machine since it

has the highest sample rate (10 Hz).

The following interpolations of Fig 4.11 were tried.

Figure 4.11: Tried interpolations

Since the relation Output/Input results were considerably similar when calculated with both methods, a 1D nearest-neighbor was adopted for all the following experiments. This solution was chosen because it required less processing capacity.

After data processing, it was possible to obtain the graph Output/Input, as Fig 4.12 exemplifies. The value of the slope of the graph is considered to be the value of the relation.

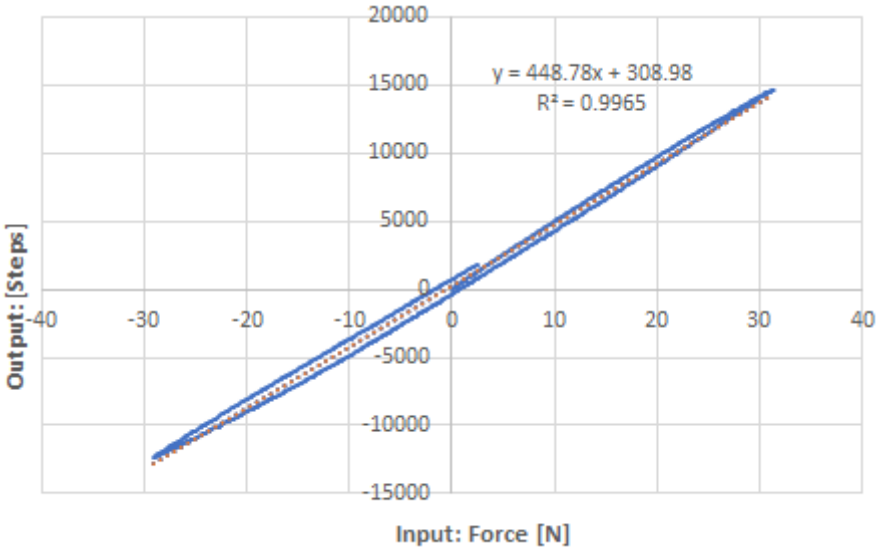

Figure 4.12: Example of Output/Force relation obtained through graph

Offset with Arduino/Force

As mentioned before, the programs started with the FSE horizontal (not pre-stressed), and for that it was used a zero offset. This procedure was essential to prevent over-bending and permanent deformation of the spring. The machine had to be lowered or raised manually with everything assembled until the FSE archived the most relaxed state. There were two ways of knowing when that position was obtained: Using the zero-force or the zero Arduino offset. Below, the main steps of these procedures are explained.

Arduino offset:

- Screw the adaptor in the FSE;
- Press the Arduino button to initialize the zero output offset;
- Screw the remaining stem;
- Lower the tensile machine plate carefully until the parts fit in;
- Insert the locking pin;
- Lower or raise the plate until the output sensor is null;
- During this process, pay attention to the sensor output, avoiding high values that could mean permanent deformation.

Force offset:

- Assembly all the metallic parts in the tensile machine;
- In the software, click on the button to initialize the zero-force offset;
- Unlock the pin and screw the stem and adaptors in the force-sensing element;
- Lower the tensile machine plate carefully until the parts fit in;
- Insert the locking pin;
- Lower or raise the plate until the force is null;
- During this process, pay attention to the load cell output, avoiding high values that could mean permanent deformation.

It was decided to use the Arduino offset, expecting that the final result would be the same. Nevertheless, in the end, some experiments found that the two methods did not lead to the same result. The initial position often differed by 0.2 to 0.8 mm between both methods. This fact could be related to small stress reliefs in the screwing of the PCB. In the end of this work it was realized that the most correct method should have been the force offset.

Screwing torque

The FSEs were screwed with the torque screwdriver presented in Fig 4.13. All experiments were screwed with the same torque values previously studied by Bosch (0.85N.cm).

Figure 4.13: The torque screwdriver used - wiha

4.2.3 Studies and Expectations

The main studies in the tensile machine, and whose results are presented in the Chapter 5, can be divided in the following categories:

Table 4.1: Studies in the Tensile Machine

Code	FSE No	Display	Aim	Setup
TM1	1, 3	D1	Study the behaviour of the assembly	DH Loading
TM2	1, 3, 4	D1	Study the behaviour of the FSE	Final Setup
TM3	5	D1	Study the influence of cutting the springs	Final Setup
TM4	2	D2	Study the influence of unscrew and screw the FSE again	Final Setup
TM5	2, 6, 8, 9, 10	D1, D2	Study the influence of aging and the possible correlation between hysteresis loop area and slope of the Output/Input chart	Final Setup

TM1

The goal of TM1 was to characterize the mechanical behavior of the system in terms of Force/Displacement. For this, a tensile machine program was used. It consisted of a list of events, as for example:

1. Lower down to coordinate -0.8 mm at 1 mm/min;
2. Wait 10 seconds maintaining the force constant;

3. Return to zero point with speed 1 mm/min.

This was precisely the program used during the display housing loading. These programs are easily visualized in a Displacement/Time chart as they will be presented from now on.

When loading the DH, the stiffness of the system was expected to vary from inward to outward.

TM2

This was the first experiment with the final setup, so several tensile machine programs were tried out. As the system consists of mechanical and electronic components, the objective was to verify how the FSE behaves through the Force/Displacement and Output/Input charts. For example, since the FSEs are composed of a bi-material stack-up, it was expected that the FSEs could have different mechanical behaviors when bending up or down. The gauges' output is directly proportional to the deformation of the gauge. Deformation of the gauge is related to the displacement. Then, once the Force/Displacement relation changes, the Output/Force relation should also vary.

TM3

As mentioned before, the dimensions of the climatic chamber did not allow to test of a complete FSE. Therefore, they would need to be cut in half. In order to test the influence of cutting the springs and PCBs, 3 programs represented in Fig 4.14 were chosen. Program 1 was repeated so results are the average of 4 values. Programs should start with the force-sensing element horizontally. The FSE number 5 was tested before and after being cut. For cutting the FSE, the setup was disassembled.

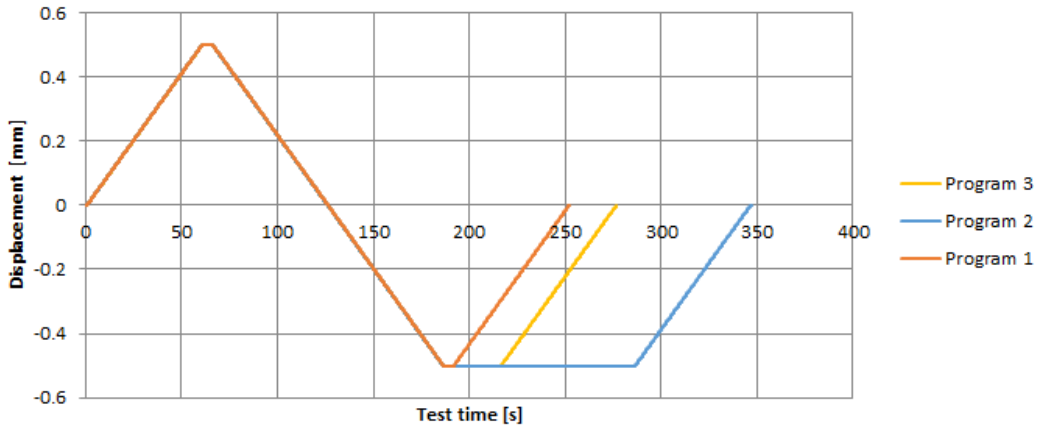

Figure 4.14: Tensile machine programs used in experiments TM2

Previous simulations proved that differences in the screw domes' heights of the carrier would not influence the overall stiffness by a significant value, which means that this

characteristic depends mainly on the FSE S-shaped bending area. Therefore, from the mechanical point of view, it was not expected any difference in the behavior after cutting the FSEs in half.

Regarding the electronics, since the main components of the PCB, including 2 strain gauges and the FPC connector, are on the same half, it was not expected any influence on the output of the sensors.

This was also the first time that several positions were tested with the same setup and program, which allowed to observe other phenomena. The inside positions were expected to have slightly different stiffness than the ones in the outside. Less stiffness means that, for the same force, the deformation of the FSE is higher, as well as the output of the respective strain gauge. Hence, it was predicted that in the positions with lower stiffness, the output would be higher.

After these experiments, the FSEs were cut. One half of the spring was assigned to experiments in the tensile machine, and the other experiments with the developed bending machine.

TM4

Experiments TM4 aimed to test the effect of disassembling and reassembling the setup. For that, it was decided to test the same spring 8 times. Half of the tests would be performed without touching the setup. For the others, everything was disassembled and mounted again between each test.

Now with more trials, it was decided to use merely 2 tensile machine programs. Not using the events where the force or displacement is constant eased the data synchronization. That's because the peaks in the output and load or displacement charts were more clearly visible. The final programs also started with the force-sensing element horizontally. Then the FSE would bend 0.5mm to each side and return to 0, completing a full cycle. The first program would start by going up and the second by going down. Both programs are represented in the Fig 4.15

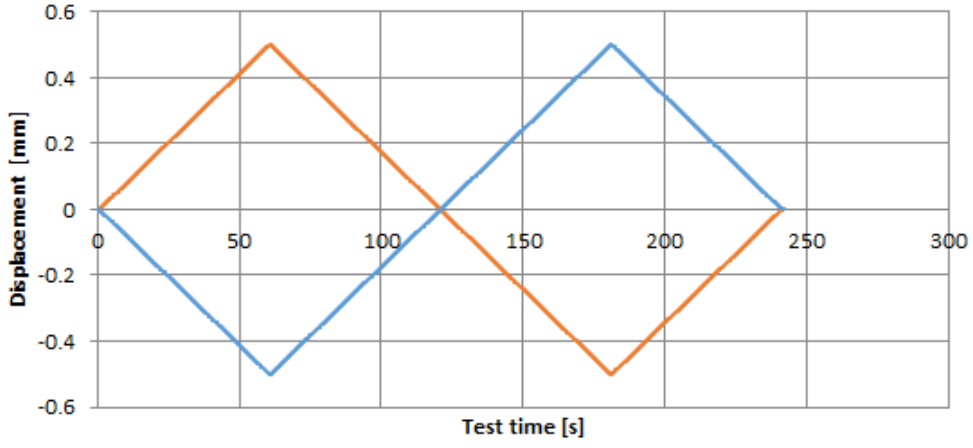

Figure 4.15: Tensile machine programs used in experiments TM4 and TM5

The variation of the stiffness and the Output/Input relation was usually minimal between the two programs. Nevertheless, running two programs was not much longer than running just one, considering that preparing the experiment took more time than the experiments itself. In point of fact, running one cycle took 3 minutes while, on the other hand, preparing the setup and executing the zero offset usually took more than 15 min.

During the result presentation, only one value is presented. That value is the average from both programs.

TM5

The influence of aging was tested in the experiments TM5. The same tensile machine programs as in the experiments TM4 were used, and the FSE had to be disassembled to bring to the thermal chamber for aging.

The FSEs were aged inside a thermal chamber for 750 h at a constant temperature of 85ºC, usually the maximum operating temperature for interior components in the automotive industry.

During experiments TM3, it arouses doubt that a correlation could exist between the Output/Input slope and hysteresis loop area of the homologous chart. In the end, the TM5 data was used to study this possibility. To calculate the area, the trapezoidal rule was used. This rule approximates the finite integral of a function dividing the spacing into trapezoids. Using Equation 4.1, the areas under the upward and downward curves of all experiments were calculated and then subtracted to obtain the area between them [20].

$$\int_a^b f(x)\,dx \approx \sum_{k=1}^{N-1} \frac{f(x_k) + f(x_{k+1})}{2}(x_{k+1} - x_k) \tag{4.1}$$

4.3 Developed Bending Apparatus

One of the objectives was to test the force-sensing system at different temperatures. For that, a bending apparatus should simulate the most authentic case possible and enable the gathering of the Output/Input relation: the input being the force applied on the display that has an intensity, position, and direction, and the output as being the values of the sensors in steps after the ADC.

In the perfect case, a robot inside the thermal chamber would press on several points before aging and on the same points after the aging. Then, the results could be compared. But unfortunately, this type of equipment was not available, and the thermal chamber available for testing had relatively small dimensions, so another solution had to be found.

4.3.1 Apparatus Development

The following aspects presented are some of the requirements and biggest limitations for the apparatus development:

- Only one small thermal chamber (290×235×290 mm) was available. The carrier and display housing didn't fit horizontally, and the springs had to be cut;
- Opening the door of the thermal chamber at high/low temperatures resulted in a quick thermal variation. Therefore, the experiments had to be performed with the chamber closed;
- The system should be able to read a load with precision at temperatures from -40 to 85ºC;
- The capacity to read displacement was not required but was an advantage.

Motors and Load Cells

The idea of using a precision motor and a load cell came out. Due to the small increments that would be needed, stepper motors were the first choice. With the growing demand in areas such as 3D printing, it is easy to find a wide variety of equipment at low prices. Additionally, they can usually be controlled with simple microprocessors like Arduino. Several software examples of controlling them are available on online forums.

In this case, a linear stepper motor would be required since the necessary movement is along an axis and not around it. There are two types of linear stepper motors: non-captive (Fig 4.16a) and captive (Fig 4.16b) .

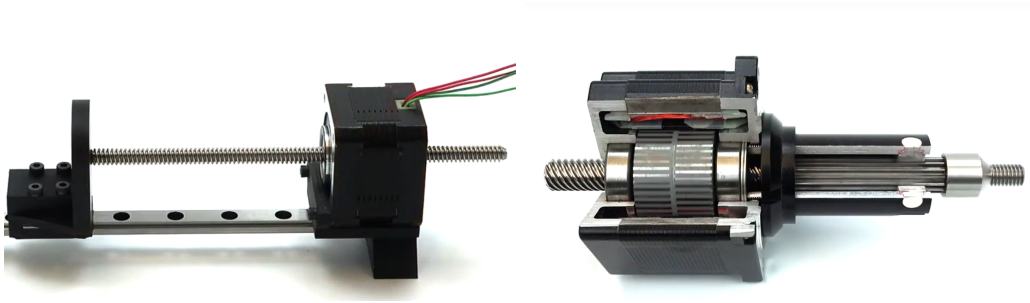

(a) Non-captive stepper (b) Captive stepper

Figure 4.16: Types of stepper motors

The captive actuator has a built in anti-rotation mechanism through the use of a splined output shaft that allows it to extend and retract as a unit with no requirements for additional anti-rotation. The captive actuator is designed for shorter strokes. The Non-captive actuator has a leadscrew going through the motor and has no reasonable

stroke limits but must be attached to an assembly that will not rotate. This will then allow the leadscrew to extend and retract without rotating [21].

Therefore, an captive stepper, would be preferred for this application.

About the load cells, it was regarded the usage of:

- S shape load cells (Fig 4.17a);
- tension/compression load cells (Fig 4.17b);
- single point load cells (Fig 4.17c);
- shear beam and bending beam load cells (Fig 4.17d).

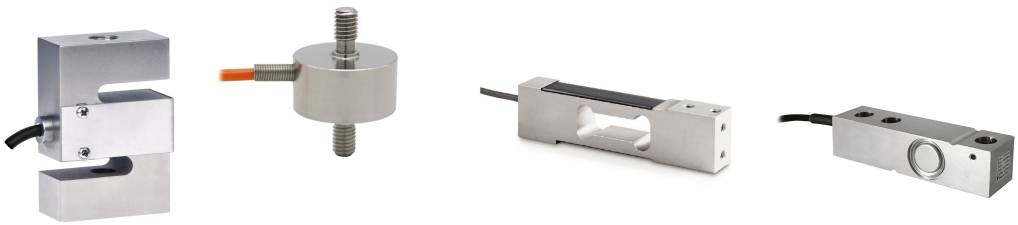

(a) (b) (c) (d)

Figure 4.17: Load cell for this type of applications

The tension/compression load cells (Fig 4.17b) were especially explored for their small dimensions and simple integration into a apparatus.

At the end of this research, it was not easy to find equipment that could guarantee the precision, mainly at -40^{o}C and at the same time being supplied by a certified Bosch company. Hence, it was decided to develop a apparatus without electronic components.

Final Setup

In the end, because electronic components were not an option, they were substituted by weights and mechanical stoppers. Therefore, the final setup uses a system with weights to impose 3 different load levels and stopper bolts that can be used to impose a displacement. Nevertheless, it was not possible to obtain the values Force=f(Displacement). Two pulleys were used to lift and lower the weights without opening the door while using a fishing line. Also, it was decided to cut the FSEs in halves. Since the springs were symmetric, it was decided to use one half for the tensile machine tests and the other for the thermal chamber tests. After the modulation of the apparatus in Fig 4.18a, the equipment went to manufacturing, and the final result is presented in Fig 4.18b.

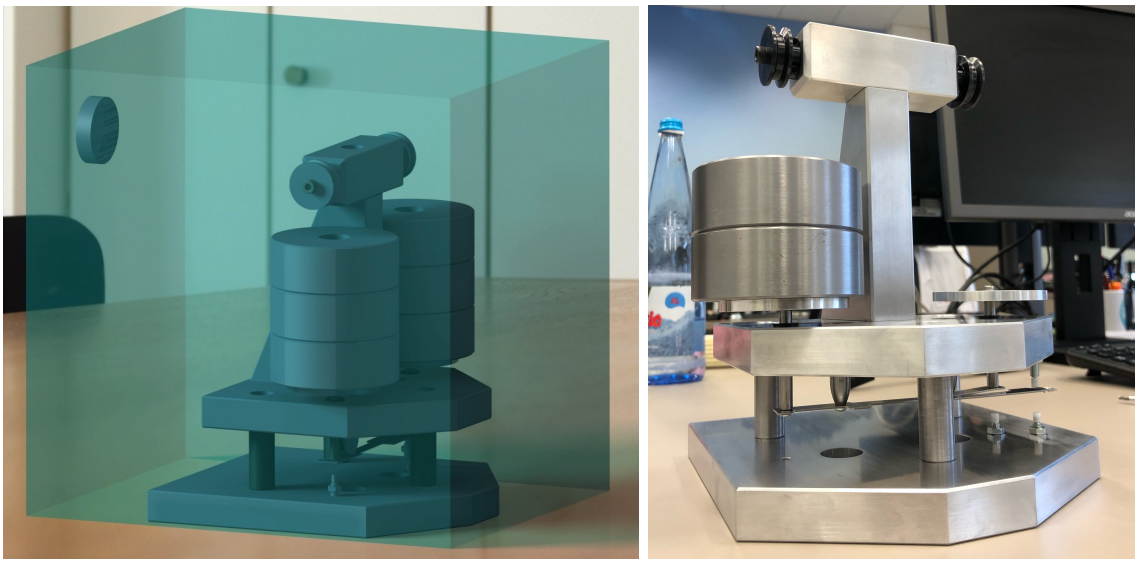

(a) Modulation of the bending apparatus inside thermal chamber

(b) Bending apparatus after manufacturing

Figure 4.18: Bending apparatus for individual testing

The bearings, presented in Fig 4.19, were selected carefully. Since the upper plate was in aluminum (high coefficient of thermal expansion) to reduce costs, the bearing should have high compressing strength. The shaft was recommended for the bearing, and the pair is advised for uses where low friction at a vast range of temperatures is needed.

Figure 4.19: Selected bearing

The weights were made of steel and weighed approximately 1.05 kg each. Since the FSE stiffness values are between 40 to 70 N/mm, the resulting displacements are expected to be roughly the presented values of Table 4.2.

Table 4.2: Expected displacements with the developed bending apparatus

Number of weights	Displacement
1	≈ (0.15-0.26) mm
2	≈ (0.29-0.52) mm
3	≈ (0.44-0.77) mm

It was already verified in previous experiments that the FSEs didn't enter the permanent deformation region with this range of displacements. Still, it was decided not to load the FSEs with 3 weights, at least without any stopper to limit the displacement.

In Fig 4.20 it is possible to observe how two fishing lines were attached to the weights inside the thermal chamber. Outside the chamber, it was possible to lift each weight individually. Additionally, a multimeter that was used to verify the temperature near the strain gauge can be visualized.

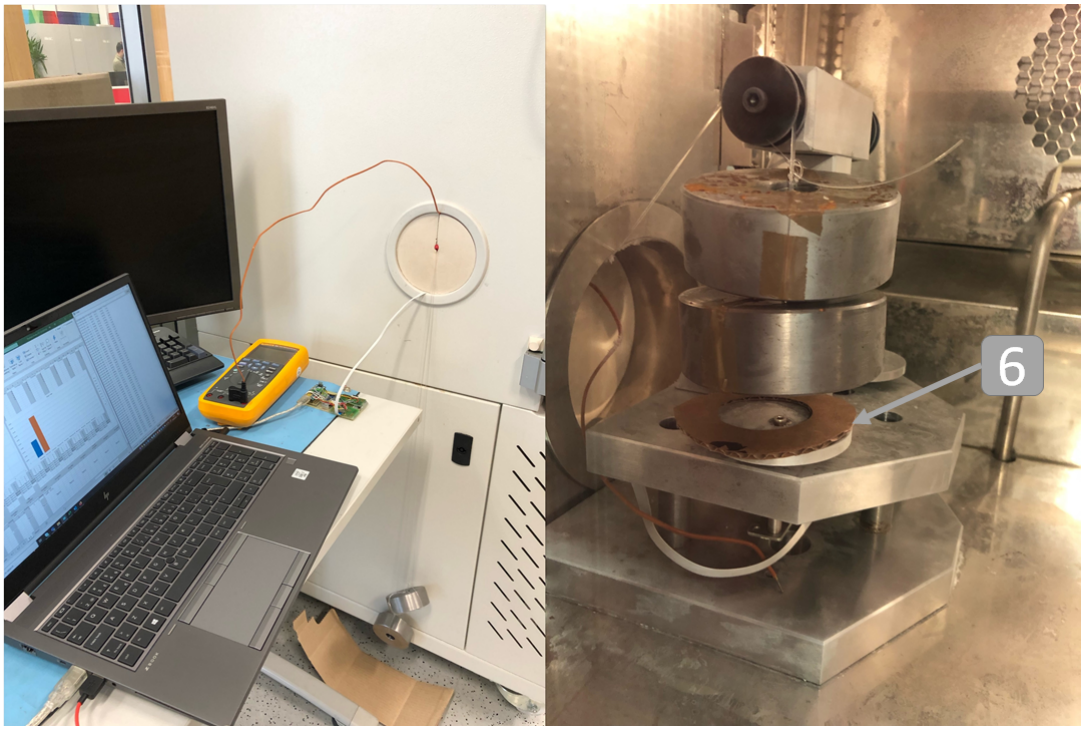

Figure 4.20: Bending apparatus inside thermal chamber

For a better understanding of the developed bending apparatus, 2D drawings are presented in Appendix A.1.

Final Bending Apparatus Operation

A brief explanation of the apparatus operation and other relevant related factors is presented. When one weight is placed on the support plate, numbered 6 in Fig 4.20, the weight, plate, and shaft move down. Therefore, the FSE bends.

When the FSE bends, the friction between the bearing and the shaft increases. This happens because the FSE pushes the shaft progressively against the bearing wall, as Fig 4.21 exemplifies.

However, the objective of this bending apparatus was only to understand if there was any change in the FSE operation before and after aging. Therefore, that friction is not relevant if it stays constant before and after aging. In Fig 4.21b, the FSE is bending excessively to explain the effect better. The expected displacements are much smaller, as presented in Table 4.2.

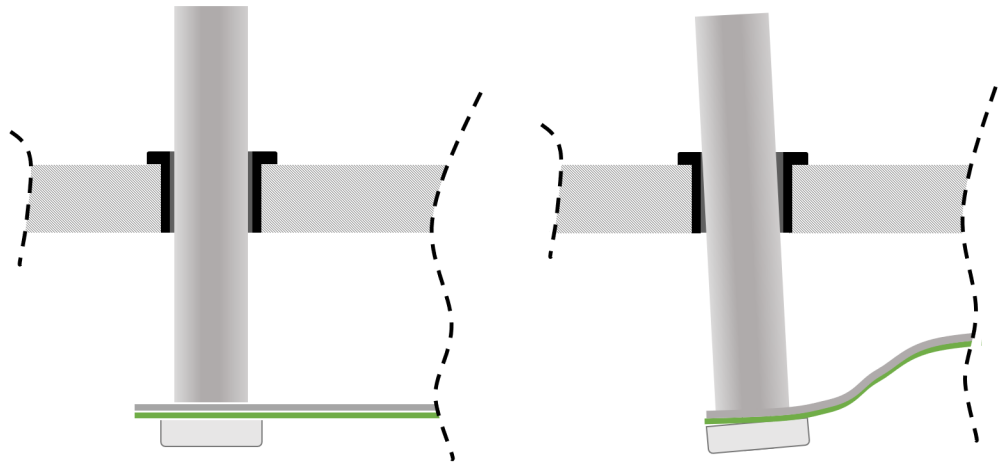

(a) Shaft when FSE is horizontal (b) Shaft when the FSE starts to bend

Figure 4.21: Shaft during testing

The friction value can also vary slightly at different temperatures since the upper plate, and the FSE have different expansion coefficients. Once again, the objective was to compare each temperature before aging with the values at the same temperature after aging. If the friction coefficient stays similar for every temperature before and after aging, in other words, if when tested at 3 different temperatures (T_1, T_2 and T_3) the condition of Equation 4.2 is verified, there shouldn't be any problem. The index of Equation 4.2 μ' represents the values after aging.

$$\begin{aligned} \mu_{T1} &\approx \mu_{T1}{}' \\ \mu_{T2} &\approx \mu_{T2}{}' \\ \mu_{T3} &\approx \mu_{T3}{}' \end{aligned} \tag{4.2}$$

During these experiments, the torque screwdriver presented in Fig 4.13 was used to screw the bolts. The screws of the carrier were screwed firstly to relieve the bending from inside to outside.

4.3.2 Studies and Expectations

The primary study categories with the developed bending apparatus, and whose results are presented in Chapter 5, are shown in Table 4.3.

Table 4.3: Studies with Developed Bending Apparatus

Code	FSE No	Display	Aim
DBA1	2, 6, 8, 9, 10	D1, D2	Study the setup repeatability, and compare results with tensile machine
DBA2	5	D1, D2	Study the influence of the PCB's warpping
DBA3	6, 9	D1, D2	2 step temperature tests with bending apparatus

DBA1

Since it was decided not to load with 3 weights, there were 3 different ways to quantify the output values:

$$\Delta Out_{12} = Out_2 - Out_1$$

$$\Delta Out_{01} = Out_1 - Out_0$$

$$\Delta Out_{02} = Out_2 - Out_0$$

Where Out_2 is the output with two weights and Out_1 is the output with one weight, and Out_0 is the output with zero weights.

If the ΔOut divided by the weight were compared, then it was expected that the values varied slightly due to the friction increase. In theory, the values should vary accordingly to:

$$\frac{\Delta Out_{01}}{1 \times Weight} > \frac{\Delta Out_{02}}{2 \times Weight} > \frac{\Delta Out_{12}}{1 \times Weight}$$

Equation 4.3 helps to understand the previous order.

$$\frac{\Delta Out_{02}}{2 \times Weight} = \frac{\Delta Out_{01} + \Delta Out_{12}}{2 \times Weight} \tag{4.3}$$

Initially, the relation Output/Input calculated with ΔOut_{12} appeared to vary slightly less than the others. Without time to further study these possibilities or recording more values for all the FSEs, it was decided to use ΔOut_{12}. In the beginning, several tests were performed with the developed bending apparatus before putting it into the thermal

chamber. DBA1' objective was to understand how the output values vary and compare them with the tensile machine results.

DBA2

During the experiments in the tensile machine, it was thought that the bending of the PCB over the spring could be one of the cause of the disparity in the output values. That's because it seemed by eye that sometimes the PCB was not doing fully contact with the spring. The experiments DBA2 intended to study this factor.

By using a feeler gauge, the PCB was forced to bend 0.4 mm over the spring, as Fig 4.22a exemplifies. Then, in other FSE, it a clip was used to force the PCB to stay flat and have complete contact with the spring, as Fig 4.22b exemplifies.

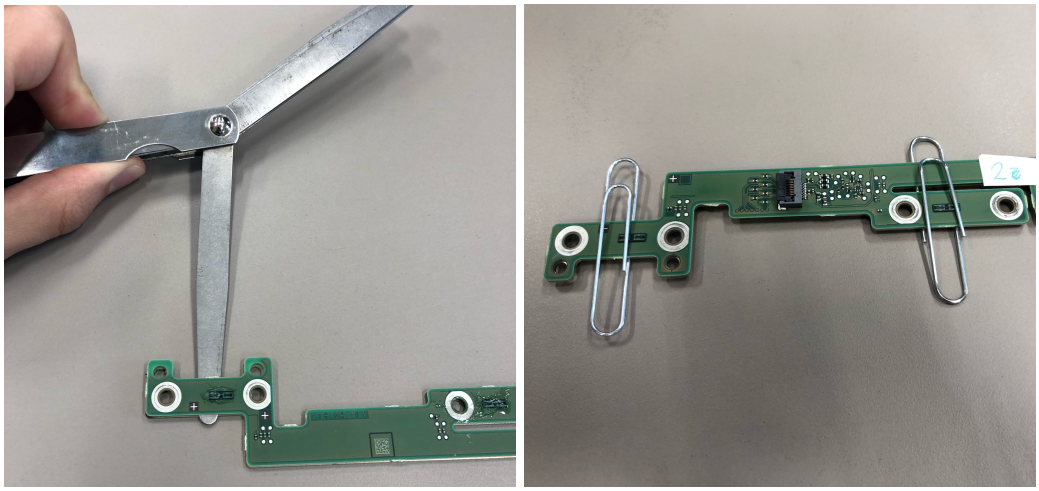

(a) Feeler gauge used to bend the PCB (b) Clip used to force the PCB to stay flat

Figure 4.22: Force PCB to bend or to stay flat

DBA3

Although the initial objective was to test the FSE before and after aging, only the pre-aging tests were performed in the end. That's because, to age the FSEs, they would need to be disassembled. By this time, it was concluded that loose the screws and tight back again was leading to a significant error. However, this error appeared to be smaller with the developed bending apparatus when compared with the tensile machine experiments. The initial objective was mainly discarded because it arose the possibility of developing a setup where the aging could be studied without disassembling anything.

Therefore, DBA3 aims only to compare the output values at different temperatures before aging. As explained previously, a hardly quantified error was expected. Unlike the previous experiments, the output value without any weight was recorded due to the more reduced amount of tests. This allowed to calculate the values ΔOut_{02}, ΔOut_{12} and ΔOut_{01}.

4.4 Assembly Testing

Once a thermal chamber with more significant dimensions became available, it was possible to test the assembly. At that time, it was already known that the reassembly of the parts was influencing the sensors' output. Hence, the objective was to maintain the parts screwed during all the experiments and the aging process. Once again, to perform the experiments without opening the door of the thermal chamber, the pulleys of the last bending apparatus were re-adapted. With that allied to the fishing line, it was possible to lower and raise the weights as exemplified in Fig 4.23a. Also, it was doubtful the direct influence of the temperature in the output of the gauges. Hence, some thermocouples were placed in key points, as Fig 4.23b exemplifies.

4.4.1 Setup

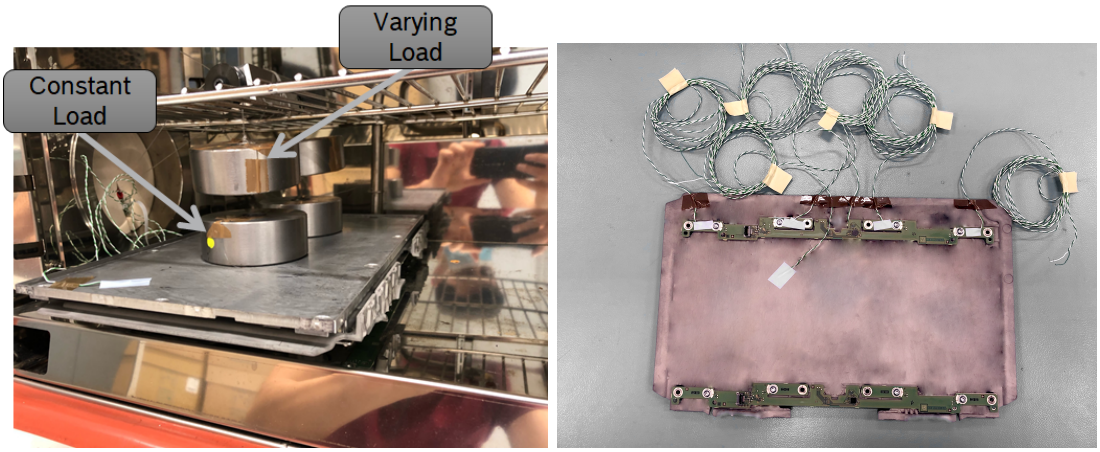

(a) Setup inside thermal chamber (b) Thermocouples instalation

Figure 4.23: Assembly testing

As visible in Fig 4.23a, it was decided to impose 2 weights of constant load, and a varying load of 2 weights as well.

The maximum force would be approximately 41,2 N applied near the center of the DH. In the experiments TM1, it was already verified that the FSE is far beyond its elastic region's limits when this value of force is applied.

The thermocouples were placed in:

- Four strain gauges of the PCB whose output is being measured;
- Spring that overlaps the PCB;
- Carrier
- Display Housing

The goal of monitoring the temperature was to understand if there was any correlation between the temperature and output variation.

Just one PCB was able to be measured, and that was, of course, the one where the thermocouples were placed.

The assembly was, once again, screwed with the torque screwdriver presented in Fig 4.13 and the screwing sequence was random.

4.4.2 Studies and Expectations

The main studies with the assembly setup, and whose results are presented in the Chapter 5, are:

Table 4.4: Studies with the Assembly Setup

Code	FSE No	Display	Aim
A1	11, 12	D1	Study the effect of temperature and air flow and compare the assembly setup with the developed bending apparatus
A2	11, 12	D1	Study the aging effect

A1

With this setup, 3 experiments were performed. Two of them before aging (to test the repeatability), named BA1 and BA2, and one after aging (AA). All experiments were performed with the same parameters and consisted of the step temperature test represented in Fig 4.24. Two characteristics of the system were studied, the absolute output value and the sensitivity to measure force. To test the last one, during the last 5 minutes of each constant temperature level, a test with weights was carried out. After 4 hours and 20 minutes, the door of the chamber was opened, and air was forced to flow to test the effect of air flow.

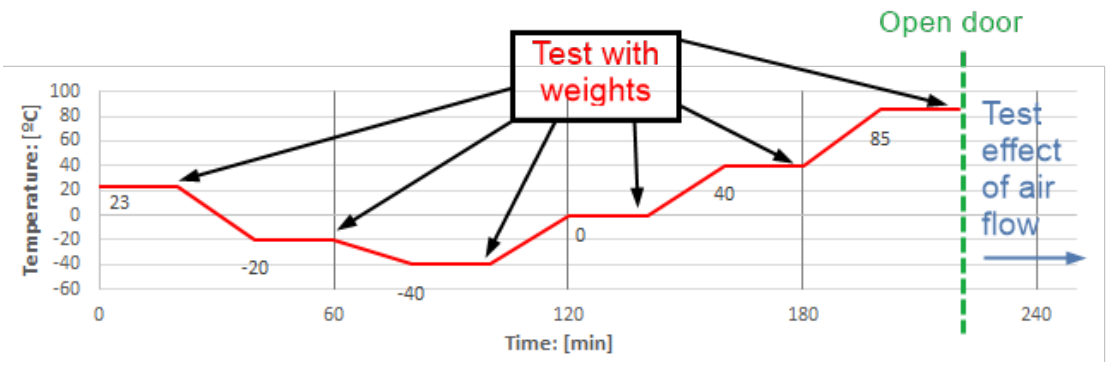

Figure 4.24: Scheme of the assembly test over time

The thermal chamber software controlled the imposed temperature. As a result, every experiment would have the same temperature.

The temperature acquisition with thermocouples failed in the first and in the last experiments because the sample rate was set too high. Nevertheless, the temperatures are expected to be very similar in each experiment since both were performed with the same thermal chamber program, and the components were placed precisely in the same position inside the chamber.

During the test with weights, 3 weights were placed over the DH, and the average was calculated. The final value was named *Average* Δ*Output*. In the beginning, it was decided to place the weights in 3 different ways. The first 2 placements would consist in placing the weights in sequential order, simulating the case where the user is keeping the pressure while applying more force (similar to the third pressure level of 3D touch technology presented in Chapter 1). In the third and last placement, both weights would be lowered at a time. For a better understanding of the tests with weights, a time schedule and an output representative chart with the measurements are presented in Appendix B.2. Additionally, a complete time schedule of the experiment is presented in appendix B.1.

A1's main objective is to observe the results from all experiments and analyze the FSE behavior and the influences of some external factors, such as air flow and temperature. During previous trials, it was noticed that air flowing through the FSE provoked an output variation. However, it was not precise if this was caused by the cooling of the sensor or by some possible vibrations induced in the FSE. Additionally, a comparison between the assembly setup and the developed bending apparatus is made.

While temperature varies, the strain gauges are constantly measuring the force applied by the constant load. Nevertheless, the output is expected to vary as temperature changes because of the tensions associated with the coefficient of thermal expansion (CTE) mismatch and to the change in sensitivity of the strain gauge.

A2

The assembly aged in the thermal chamber for 750 h at a constant temperature of 85^{o}C. Once again following the standards for the automobile industry. During the aging, any bolt was screwed or unscrewed.

A2 intends to compare the results between the experiments before aging and the experiments after aging.

4.5 Calibration

The calibration process of D1 was previously set by Bosch and consisted of placing a 500g weight on the display using the setup presented in Fig 4.25.

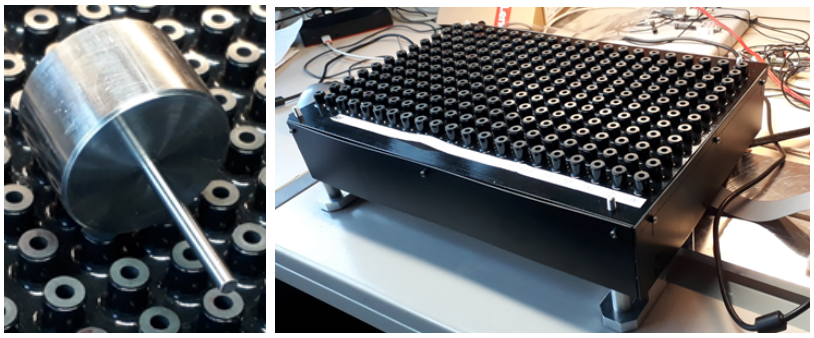

(a) Weight (b) Grid with weight positions

Figure 4.25: Calibration Setup

During the calibration, the weight is placed on the positions numbered in Fig 4.26. Then, for each position, the output variation on the respective strain gauge is analyzed. For example, for strain gauge US1 it is confirmed if the output variation when the weight is placed on hole 1, is between some predefined values.

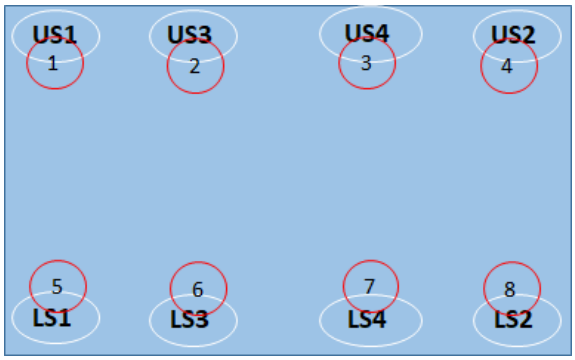

Figure 4.26: Calibration positions

The calibration process was investigated because the values were often out of the limits. On some occasions, when placing the weight in some positions, the variation of respective strain gauge was negative, as if the PCB was bending the opposite side it was suppose to. It was thought that the only reason that could lead to negative values was the improper tightening of the screws. Also, it was unknown if different screwing sequences could lead to less disperse output values while controlling the warpage of the PCB.

4.5.1 Screwing Influence

The screwing sequence was expected to be relevant to release the curvature of the PCB. It was also expected that to accomplish a lower curvature of the PCB, the screws of the carrier should be tight first.

Only the upper FSE is aligned by pins in the carrier, so only this spring and PCB could be assembled without the display housing aligning the parts (pre-screwing of the force-sensing system in the carrier).

When the carrier is placed over the display housing, the screw domes are uneven 4

mm vertically. The screwing in place means that the carrier is lifted 4 mm, and the FSE is bent concave down in the carrier screw, provoking tensions, mainly in the first screws.

4.5.2 Studies and Expectations

During calibration, the main studies performed, and whose results are presented in the Chapter 5, are:

Table 4.5: Studies during Calibration

Code	Aim
C1	Rank the screwing sequences
C2	Define new limits

C1

In Appendix C.1 it is possible to visualize the screwing orders examined. In fact, each chosen sequence has a motive behind:

- Sequences A) and D) intend to fix firstly the FSE that does the alignment with both carrier and DH. Nevertheless, to perform the screwing of the lower FSE, the carrier tilts and tensions around the upper FSE's screws appear;
- In sequence D), the pre-screwing of the upper FSE in the carrier aims to avoid the bending of the upper FSE;
- For sequence B), spacers were printed. They were intended to be placed between the carrier and the display housing to fix the components in the final position during the screwing process;
- Sequences C), E), and F) present a more balanced way to lift the carrier;
- Sequence C) intends to lift the carrier completely by tightening all its screws. Just then, the DH is fixed, starting by the upper FSE that aligns both carrier and DH;
- In sequence E) and F), the carrier is already in place after tightening the first 4 screws.

Once there were only 16 displays available to study, it was decided to assemble 4 displays with 4 screwing orders.

Sequences B) and D) were discarded because of the more challenging implementation in the line. Therefore, sequences A), C), E), and F) were tested.

To order from best to worst, the sequences were evaluated through the following factors:

1. Average of the dispersion of the output values in all sensors evaluated by the standard deviation (σ);
2. Average output values (Out).

More precisely, low dispersion of output values provides more similarities in the operation of the different displays that are produced. That reduces the dependence on software calibration. On the other hand, high output values lead to a better sensitivity and provides a better resolution to the system.

It was decided that these factors should have the same weight in the decision of the best sequence. The score would be given by Equation 4.4, where:

$$\text{Final Score} = \hat{Out} - \hat{\sigma} \tag{4.4}$$

The normalization was performed with the maximum of the set, as Equation 4.5 exemplifies:

$$\hat{Out}_x = \frac{\text{Out}_x}{\text{Max}_{\text{Out}}} \tag{4.5}$$

Where x is the sequence, and Max_{Out} is the maximum average output value for one sequence.

C2

Study C2 focused on the calculation o new specification limits using process capability presented in Chapter 2.

4.6 Summary

The process of deciding the best procedures, setups, and equipment to use as well as the exact studies performed are presented in this Chapter. To each study, a code is associated. This code is repeated during the result presentation, in Chapter 5. Hence, these two Chapters appear in the more obvious sequence where the two complement each other.

Chapter 5

Results and Analysis

This Chapter explores the results obtained from the various performed experiments. Beginning with the tensile machine testing, then with the developed bending apparatus, assembly testing, and calibration, the results are present and analyzed. The testing categories and investigations are the same and presented in the same order as in Chapter 4.

5.1 Tensile Machine Testing

5.1.1 Studies' Results

TM1

While loading in the display housing with the same compression tool previously presented in Fig 4.4a, the stiffness values varied from 70 to 100 N/mm. The maximum value was in the center of the display. As visible in Fig 5.1, as soon as the loading point moves away horizontally or vertically from the center, the display housing offers less resistance. Therefore, the results reflected the expectation.

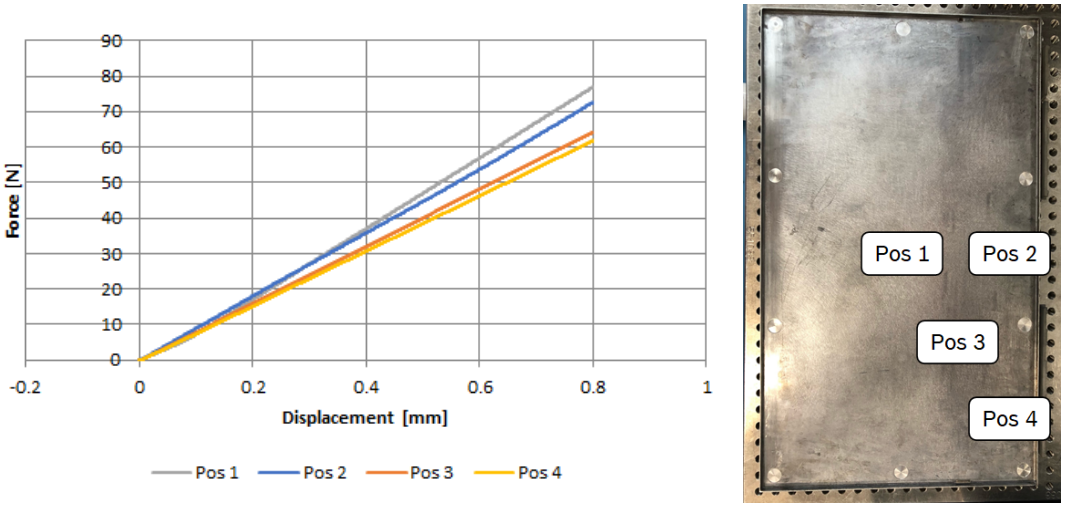

Figure 5.1: Display housing loading results and positions

Afterward, the obtained values were essential to prove that the experiments with the assembly wouldn't provoke permanent deformation in the FSE.

TM2

During the first experiments, the expectation that the force-sensing elements (FSEs) have different mechanical behaviors when bending up or down didn't verify. The Force/Displacement charts didn't present a clear point where the slope is changed. The same conclusion was taken with the Output/Input charts.

Both graphs presented hysteresis, but it was more evident in the Output/Input chart. Nevertheless, it was verified that an increase in the mechanical hysteresis did not imply an increase in the hysteresis of the output graph, as exemplified in Fig 5.2 where two experiences are presented.

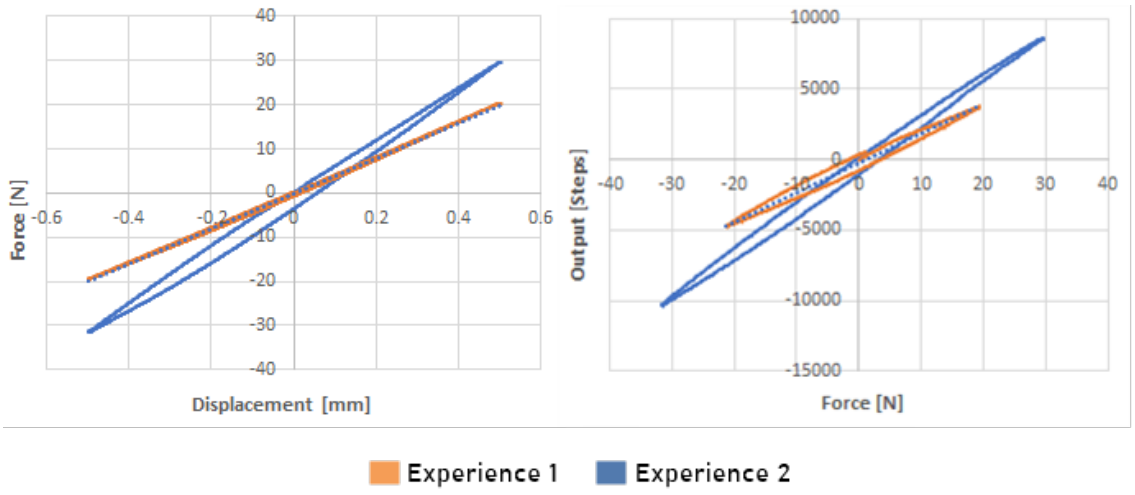

Figure 5.2: An increase in the mechanical hysteresis did not imply an increase in the hysteresis of output graph

TM3

With the results of Fig 5.3 that present the effect of cutting the FSEs in half, it is observed that the stiffness values had minimal variations when compared with the output values. This observation is supported by the chart presented in Fig 5.4. It gives the percent variation of stiffness and output of the strain gauges before and after being cut.

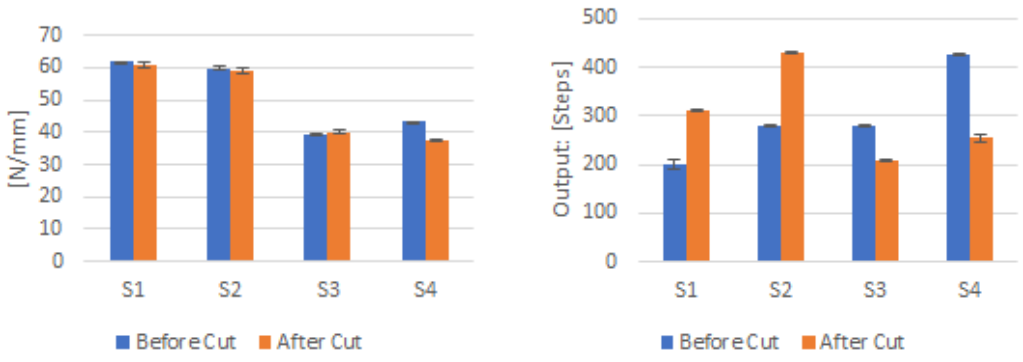

Figure 5.3: Difference in stiffness and Output/Input relation between before and after cutting the FSE

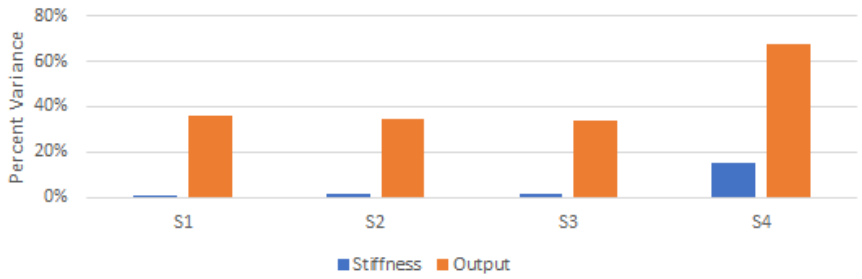

Figure 5.4: Percent variation between before and after cutting the FSE

In Fig 5.3, it is also noticed that the stiffness values of the outside sensors are higher, as forecast. Hence, the output in the same positions was expected to be lower. However, that is only verified in the experiments before cutting the FSEs, and not clearly and convincingly since S2 and S3 have approximately the same value. In fact, the Output/Input relation created the impression that they vary randomly.

While analyzing the Output/Input charts by eye, the idea that the hysteresis and sensitivity were correlated arose. In other words, it seemed that when the hysteresis loop area was superior, the slope of the relation Output/Input was lower. Therefore, a possible link between these two variables seemed to be possible. Fig 5.5 exemplifies one of the experiments where this phenomenon is observed. Unfortunately, until that moment, the number of experiments did not allow to make any conclusions.

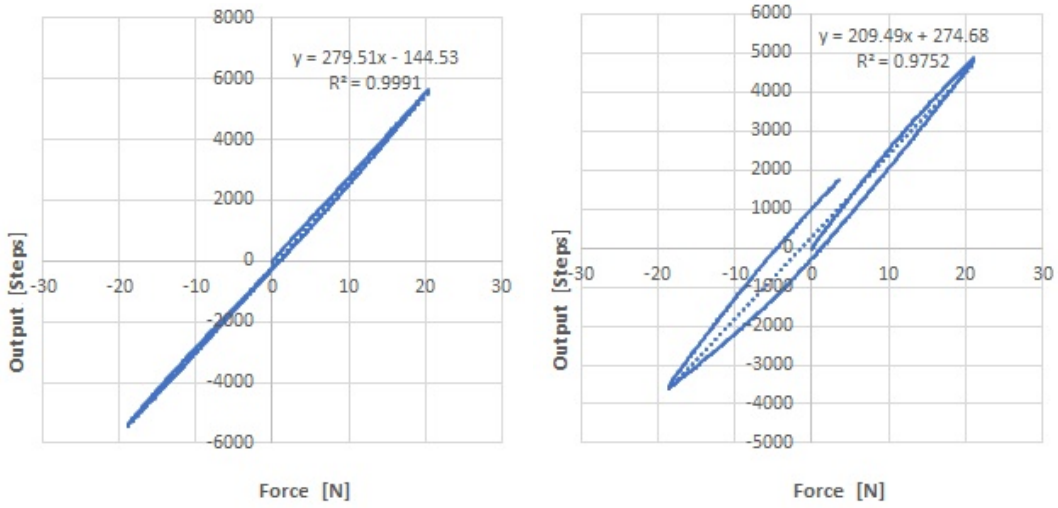

Figure 5.5: Hypothesis: The higher the hysteresis loop area is, the lower the output

By this time, it was thought that the output variation could be related to the assembly rather than with cutting the springs. That's the reason why it was decided to perform TM4 experiments.

TM4

Investigation TM4 intends to study the effect of disassembling the setup between experiments. In Fig 5.6, grey and yellow lines present the results from 4 consecutive tests. The setup was not touched during these tests. It is possible to observe that, although the Output/Input relation decreases, both relations did not vary significantly.

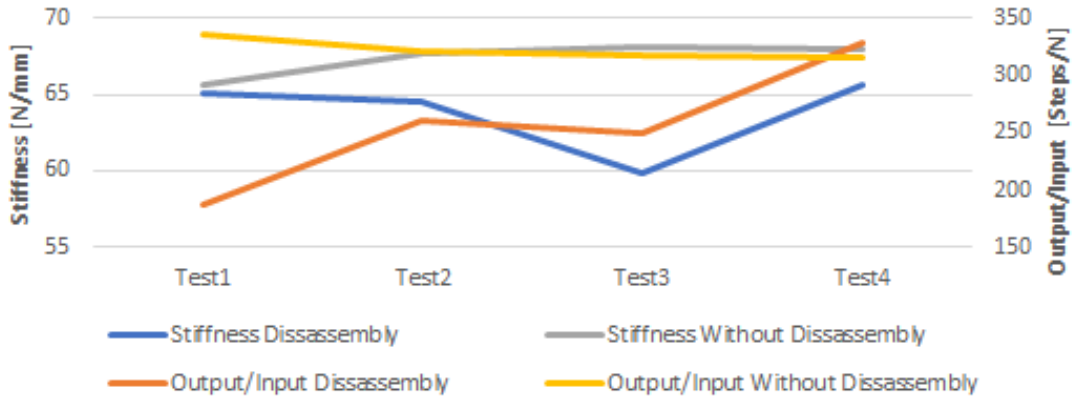

Figure 5.6: Difference between disassembly and not the FSEs

This was not verified in the situation where, after each test, the bolts of the FSE were loosened and tight back again. The blue and orange lines show that the mechanical properties changed more than in the previous example, and the Output/Input relation increased almost by 50%.

These results lead to some concerns about the study of the aging with the tensile machine and developed bending apparatus. The setup would need to be disassembled to bring the FSE to the thermal chamber. Despite knowing that there would be a relevant error mainly in the Output/Input values, it was decided to continue the testing plan.

TM5

For performing the experiments, TM5, 5 FSEs were used. They were the FSE number 9 and 10 from D1 and FSE number 2, 6, and 7 from D2. As it is possible to observe in Fig 5.7, the stiffness values increased after aging for both displays and for all positions. With Fig 5.8 it is possible to observe that, how it was expected, the Output/Input relation appears to vary randomly.

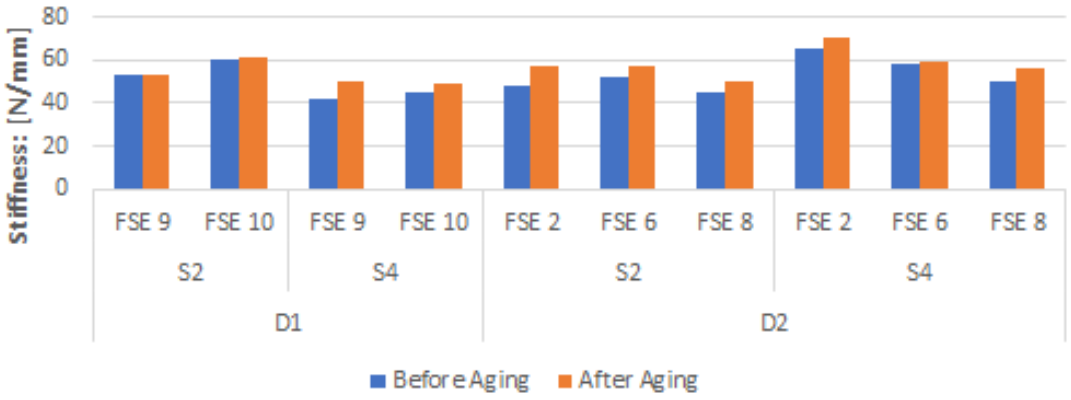

Figure 5.7: Stiffness before and after aging

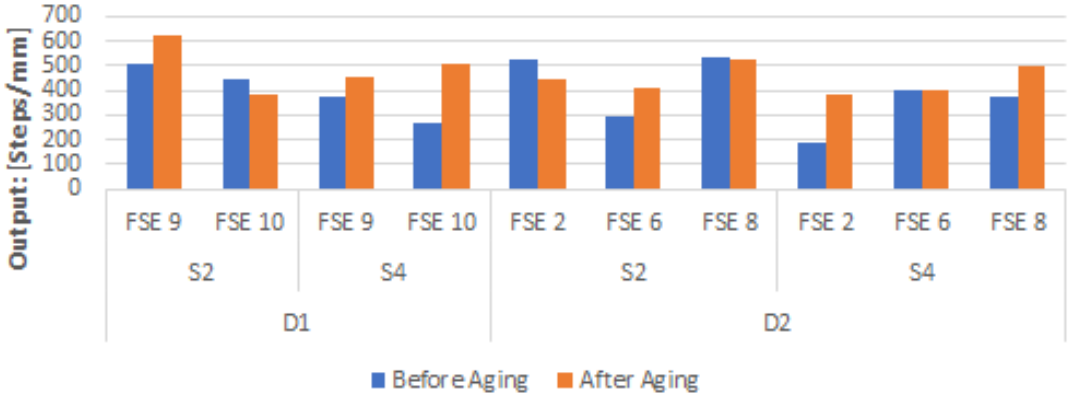

Figure 5.8: Output before and after aging

Using the data from experiments TM5, a possible link was studied between the Output/Input relation and the hysteresis loop area in the homologous chart. Results presented in Fig 5.9 were calculated through the trapezoid method, as illustrated in Chapter 4.

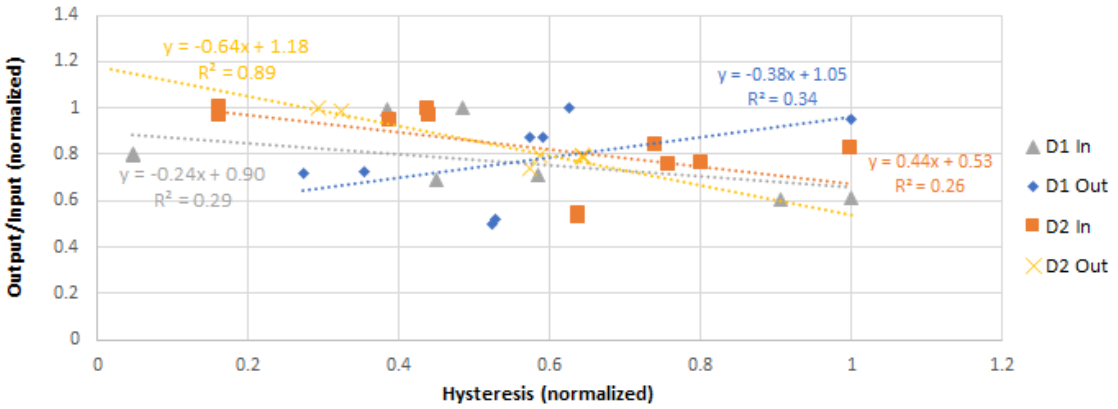

Figure 5.9: Relation between hysteresis and output of the homologous chart

Only outer positions of D2 presented a acceptable fitting in a linear function. Nevertheless, to conclude about a clear relation using the small amount of data available, the other positions would also be aligned with the tendency, and with higher coefficients of determination (R^2). When fitting other functions (i.e. exponential, logarithmic, power;...), the R^2 values were also low and not all functions had similar values.

5.1.2 Possible Reasons for Output Variation

As already presented, the Output/Input relation values varied significantly after unscrew and tight back everything. Here are given some possibilities of factors that may had contributed to this phenomenon. Some of these factors are exclusive of the developed testing setup, but others may remain in the assembly.

Tolerances on Distance Between Screws

It was realized that the component's manufacturing tolerances, per se, could lead to different stiffness values.

With the case seen in the chapter 2, the FSE bending is approximated by a theoretical model.

In this case and according to Fig 5.10, l can take a minimum value, l_1, or a maximum value, l_2. The theoretical beam fixture was defined as being the center of the screw.

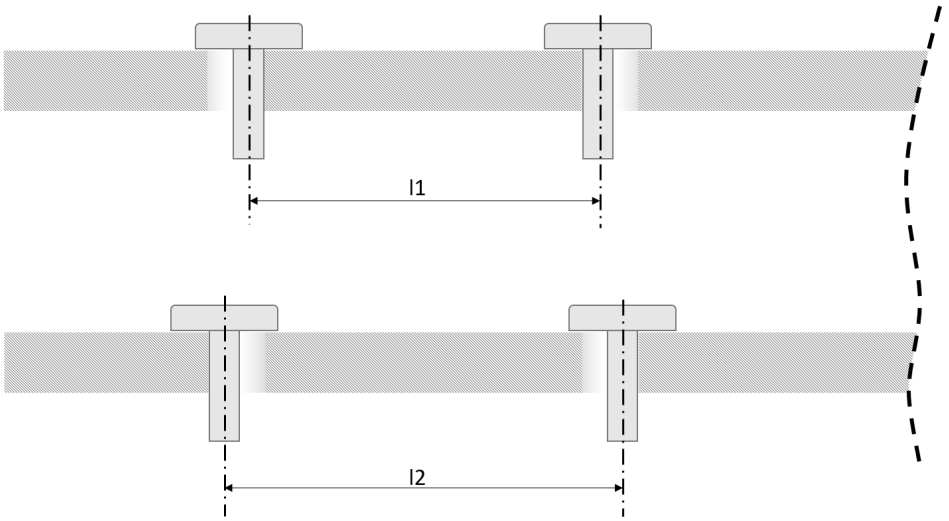

Figure 5.10: Representation of l_1 and l_2

From the Bosch's internal drawings, it is possible to observe that:

- Nominal distance between the carrier's hole and display housing's (DH) hole is 26mm;
- Both holes positioning tolerance is 0.2 mm;
- The display housing's hole is $4.7\varnothing \pm 0.1$ mm;
- The carrier's hole is $4\varnothing \pm 0.2$ mm;
- The diameter of the screw is $3\varnothing \pm 0.05$ mm;

Hence, l_1 and l_2 are respectively:

$$l_1 = (26 - 2 \times 0.1) - \frac{4.7 + 0.1}{2} - \frac{4 + 0.1}{2} + 2 \times \frac{3 - 0.05}{2} = 24.3$$

$$l_2 = (26 + 2 \times 0.1) + \frac{4.7 + 0.1}{2} + \frac{4 + 0.1}{2} - 2 \times \frac{3 - 0.05}{2} = 27.7$$

Since:

$$K_1 = \frac{12EI}{l_1^3} \qquad K_2 = \frac{12EI}{l_2^3} \tag{5.1}$$

In the worst case scenario, the difference between the stiffness values K_1 and K_2, calculated with the l_1 and l_2 respectively, is given by:

$$\frac{K_1}{K_2} = \frac{l_2^3}{l_1^3} = \frac{19.07^3}{15.97^3} = 1.48$$

The calculations show that the stiffness can increase up to 48% just due to component's tolerances. Observing Fig 5.11 it is visible that the distance between screws is controlled by two independent parts, the carrier and the adaptor that connect to the tensile machine. Therefore, it is not improbable that the screws are tight near the extreme right or left of the hole.

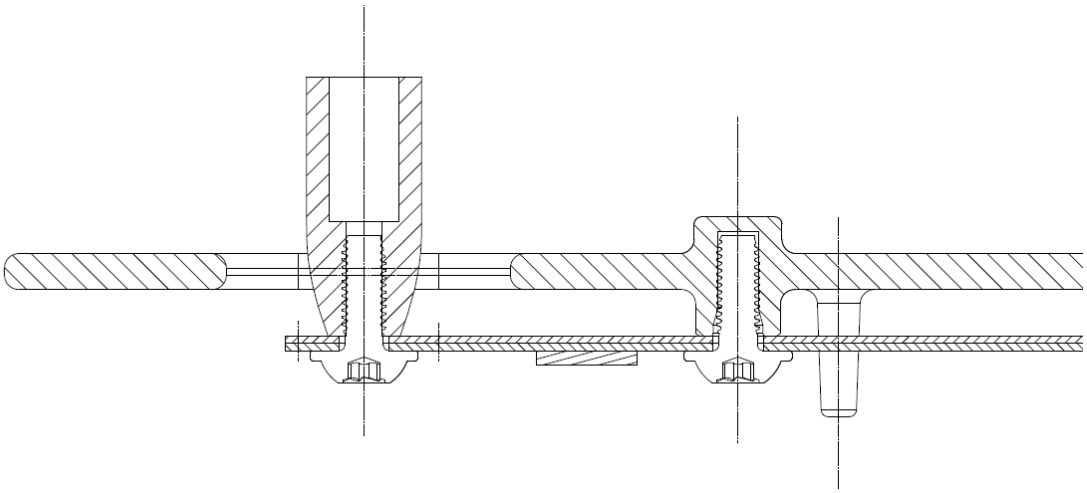

Figure 5.11: Distance between screws in the tensile machine

In the actual case, as visible in Fig 5.12, the distance between screws is imposed by the carrier's screw dome and the DH's screw dome. The alignment between the carrier, spring, and DH controls that distance.

The alignment pins and the DHS' screw dome are dimensioned from a datum A, presented in Fig 5.12.

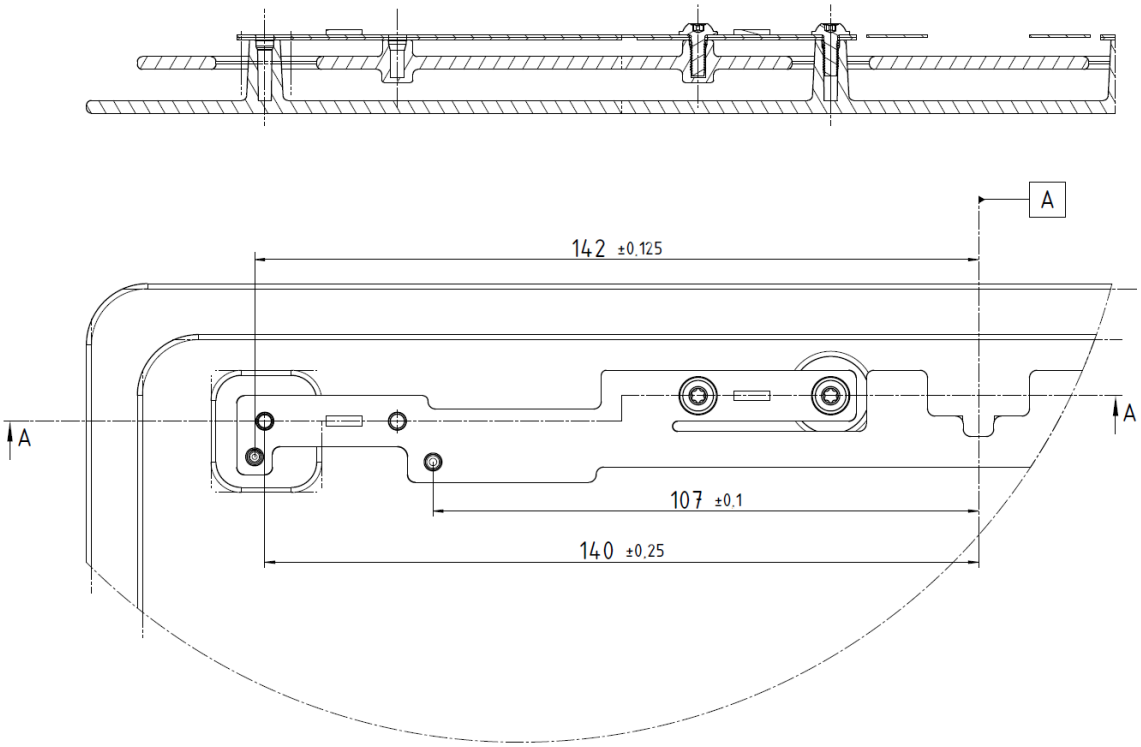

Figure 5.12: Distance between screws in the real case

To calculate the maximum and minimum distance between the screws for this assembly, a tolerance stack-up analysis must be performed. The following chain path was followed:

Center of the DH's screw dome ⇒ Datum A ⇒ Center of DH's alignment pin ⇒ DH's pin edge ⇒ Spring pin hole edge (left hole) ⇒ Center of spring pin hole (left hole) ⇒ Datum A ⇒ Spring pin hole center (right hole) ⇒ Spring pin hole edge (right hole) ⇒ Carrier's pin edge ⇒ Carrier's pin center ⇒ Center of the carrier's screw dome

After calculations, l_3 and l_4 (l_1 and l_2 of the real case, respectively) are:

$$l_3 = 25.27$$

$$l_4 = 26.63$$

Since:

$$K_3 = \frac{12EI}{l_3^3} \qquad K_4 = \frac{12EI}{l_4^3}$$

In the worst case scenario, the difference between the stiffness values K_3 and K_4,

calculated with l_3 and l_4 respectively, is:

$$\frac{K_3}{K_4} = \frac{l_4^3}{l_3^3} = \frac{26.16^3}{25.73^3} = 1.17$$

The difference from the previous case, apart from the final value of 17% increase in stiffness, is the probability of this event, or situations near it, to happen.

In this case, for the worst-case scenario to happen, all the involved parts have to be supplied on their tolerance limits. Furthermore, the combination of components' dimensions and tolerances has to be perfect for this to happen. Considering that most of the manufacturing processes' natural tolerances follow a normal distribution, a more realistic approach for long tolerance chains is to consider that most parts are not supplied on their maximum or minimum material condition. Assuming that each dimension has a three-sigma variation and that their manufacturing processes are 1.33 Cpk capable, a Monte Carlo simulation can be used to perform statistical analysis. The results showed that 99,7% of the assemblies will have less than 3% of stiffness variation between them.

Tolerances on Strain Gauge Positioning

During the experiences in the tensile machine, because of the difference between the PCB's holes diameter and the screw diameter, the PCB can slide slightly when the screws are loosened. Once the PCB slides, the strain gauges also move to different positions. These different positions present other deformations, thus different output values. In Fig 5.13 this situation is exemplified with two places of the strain gauge painted blue and orange.

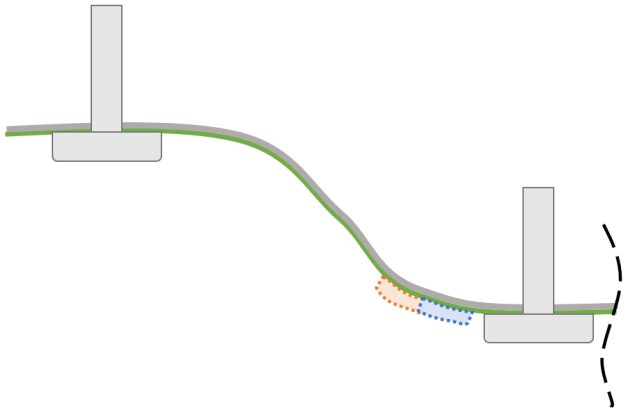

Figure 5.13: Two different positions of the strain gauge

From the drawings, it is possible to observe that:

- PCB's smallest hole holes is $4.3\varnothing + 0.1$ mm;
- Diameter of the screw is $3\varnothing \pm 0.05$ mm;

- Surface-mounting technology (SMT) positioning tolerance of the strain gauge is 0.1 mm.

With these, it is possible to compute the following:

$$\begin{aligned} 4.4 - 2.95 &= 1.45 \\ \frac{1.45}{2} &= 0.725 \\ 0.725 + 0.1 &= 0.825 \end{aligned}$$

During the experiments, the PCB was able to move 0.825 relatively to the screws.

This effect is minimized in the assembly since the PCB is aligned with the DH through one pin.

From the drawings, it is possible to observe that:

- Pins diameter is $2.85\varnothing + 0.05$ mm;
- PCB's alignment hole is $2.95\varnothing \pm 0.1$ mm;
- The SMT positioning tolerance of the strain gauge is 0.01 mm.

With these, it is possible to compute the following:

$$\begin{aligned} 3.05 - 2.8 &= 0.25 \\ \frac{0.25}{2} &= 0.125 \\ 0.125 + 0.1 &= 0.225 \end{aligned}$$

In the actual case, the PCB can move 0.225 mm relatively to the alignment pin.

It is difficult to determine the influence of the gauge positioning in the output of the gauge without FEM simulations. Further analysis would allow understanding if additional tolerance adjustments are beneficial for the sensitivity values dispersion.

Warpage of the Tensile Machine Parts

It was essential to guarantee that the lower face of the adaptor was horizontal when it was assembled in the tensile machine. On one occasion, some strange results were popping out, and the conclusion was that they were related with the warpage of the parts in Fig 4.9a. On that occasion, the components had to be re-machined, and special care was taken during the following experiments, as Fig 5.14 exemplifies.

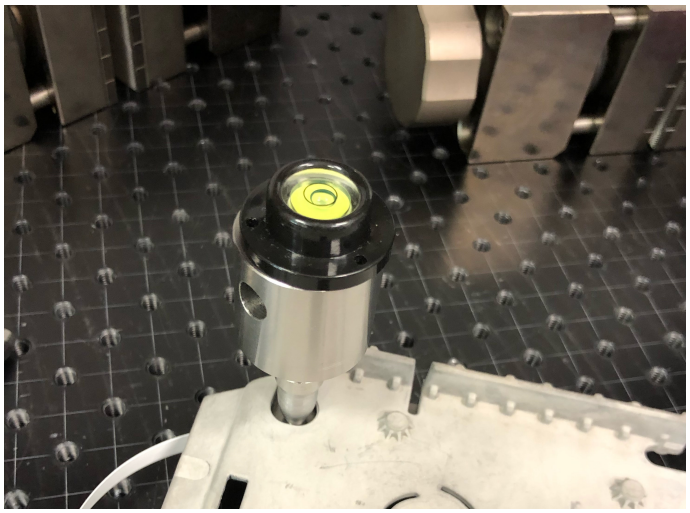

Figure 5.14: Confirm the warpage of the parts

Even with all the carefulness, it is possible that a small amount of error was related to this factor.

PCB's Warpage

Another possibility is that, in some experiments, the PCB could be creating a slight belly over the spring, as exemplified in Fig 5.15. This situation was visible in some experiments. With this belly, the PCB would bend with a different shape, modifying the sensitivity of the system.

Figure 5.15: Belly over the spring

Screw Domes Wear and Re-use

The carrier was changed after the aging. It is possible that the new screw domes increase the clamping force and then increasing the stiffness. This would explain the increase in stiffness during study TM5. The available time did not allow to further research about this topic.

5.2 Developed Bending Apparatus

5.2.1 Studies' Results

DBA1

Firstly, a comparison between the developed bending apparatus and tensile machine is performed. In Appendix A.2, that show some of the results obtained with the bending apparatus outside of the chamber, it is verified that the output values diverged less around the average than the results from the tensile machine.

Despite the repeatably problems mainly with the tensile machine it is observed in Fig 5.16, that represents the direct comparison between experiments that, except in the 3 tests circled red, the output values with the developed bending apparatus were slightly superior. This tendency was expected due to the friction between the bearing and the shaft.

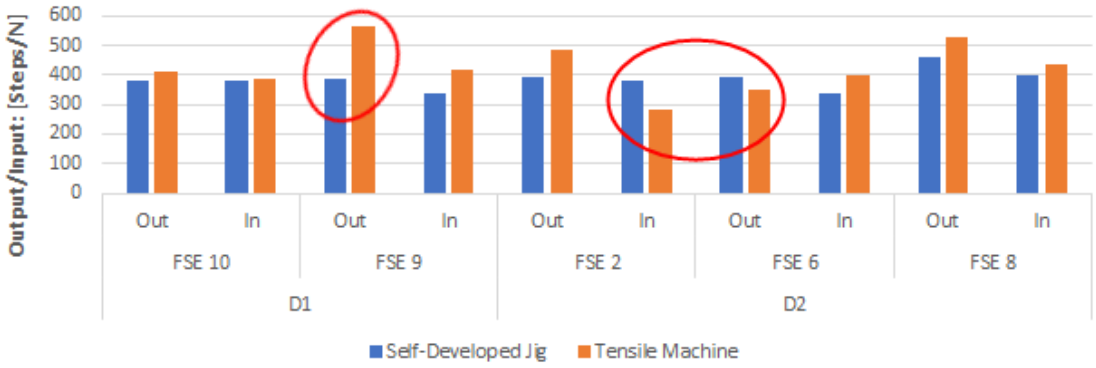

Figure 5.16: Comparison of the values obtained with the developed bending apparatus and with the tensile machine

In Fig 5.17, it is visualized that there was a slight tendency for position 1, the outside sensor, to have higher output.

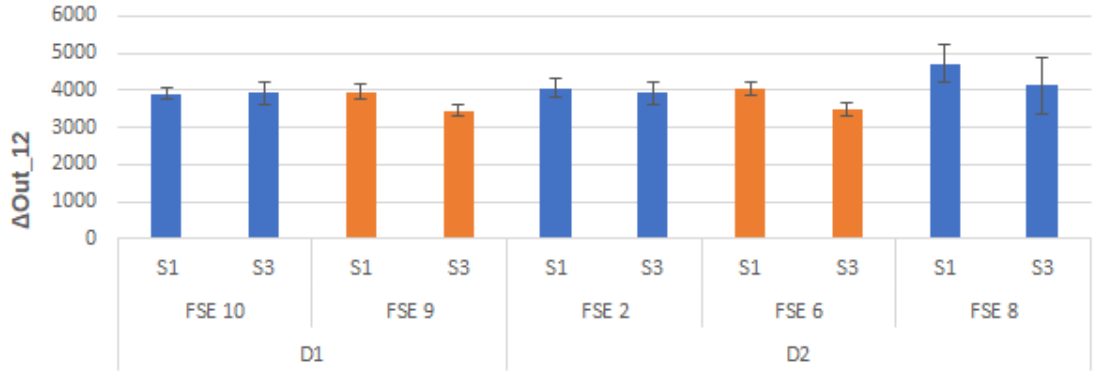

Figure 5.17: Experiments with FSE out of the camber

DBA2

As previously said, it is thought that one of the possible errors for the results in the tensile machine is the deflection of the PCB over the flat spring. To simulate this effect, a feeler gauge and a clip were used to force the PCB to stay concave and completely flat, respectively. With a feeler gauge forcing the PCB to bent just 0.4 mm, the output was the highest between 7 experiments, as visible in the chart of Fig 5.18

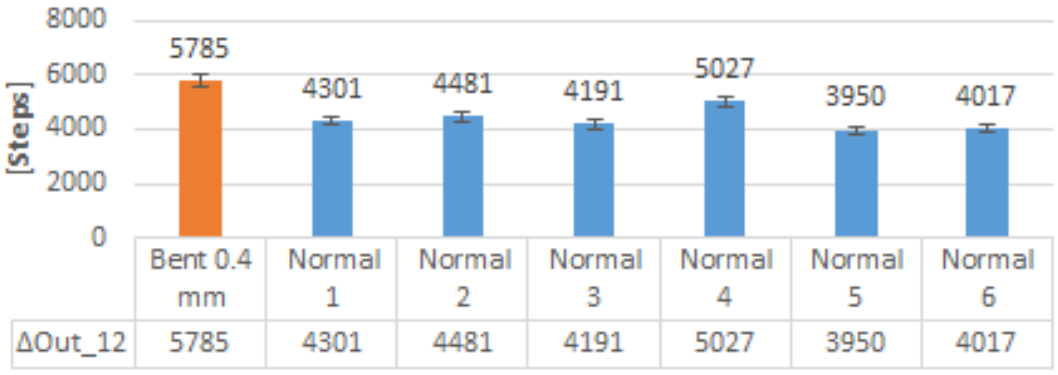

Figure 5.18: One test with feeler gauge to force the PCB to bent

With a clip forcing the PCB to stay flat, the output was below the average, but not always the lowest, as visible in the chart of Fig 5.19

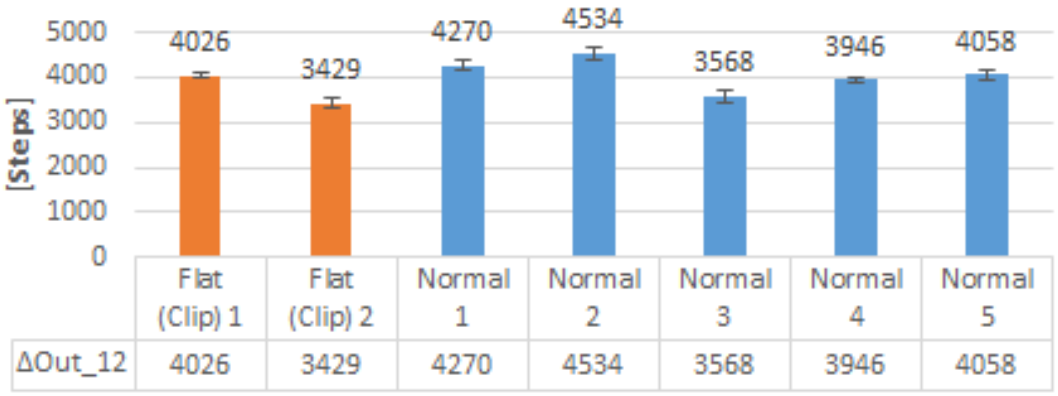

Figure 5.19: Two tests with clips to force the PFB to stay flat

The number of tests realized doesn't allow to make concrete conclusions about the effect of the PCB bending over the spring. The feller gauge seemed to increase slightly the output, but it is uncertain if 0.4 mm of PCB bending can happen in the actual case. Nevertheless, if there is an error associated with this factor, it seems that it is not the most relevant.

DBA3

The initial objective was to use the bending apparatus to test the FSEs before and after aging. However, that objective was mainly discarded because it arose the possibility of developing a setup where the aging could be studied without disassembling anything. Nevertheless, it was decided to use the developed bending apparatus to perform tests at 3 different temperatures before aging, knowing that the variation of the friction coefficient would induce an expected low error.

In Fig 5.20, the results of testing at 3 different temperatures, -27.5, 24 and 80^{o}C, are exhibited.

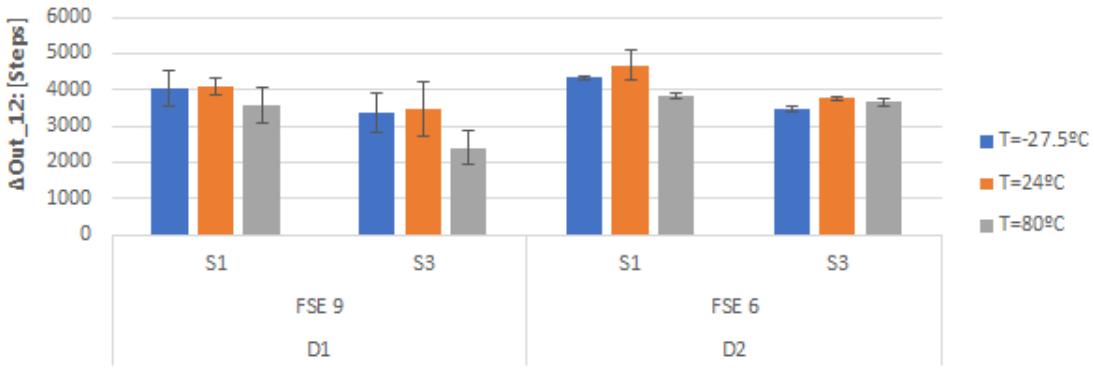

Figure 5.20: ΔOut_{02} at different temperatures

In these experiments, it was possible to gather also the "no weight output". With that value, the ΔOut_{02} and ΔOut_{01} were also calculated. As displayed in Appendix A.3, the tendencies are extremely similar. Furthermore, it is easily confirmed that Equation 4.3.2 was verified in the results.

5.2.2 Possible Reasons for Output Variation

As already explained, it was verified that the output values diverged less around the average than the results from the tensile machine. This can be because some possible errors were eliminated or minimized.

The two possible errors presented for the tensile machine that remained for the developed bending apparatus are the tolerances on strain gauge positioning and the PCB's warpage. On the other hand, the distance between the screws stays similar during each assembly. That's because with this setup, this distance is determined by the position of the shaft and part numbered 4, in the apparatus drawing in Appendix A.1. Thus, the distance between these components is practically steady. The screw domes' wear out influence also diminished because the equipment was produced in more rigid materials.

The biggest achievement of the first two experimental categories were mainly the understanding of how to minimize the dispersion of the sensibility values of the system, that is still a concern in the actual case.

5.3 Assembly Testing

During the result presentation, the two experiences before aging are called BA1 and BA2, according to the sequence they were performed. The experience performed after aging is named AA.

Studies' Results

A1

The output protuberances identified in Fig 5.21 are associated with the sensor response to place the weights (≈ 2.1 Kg) in the DH.

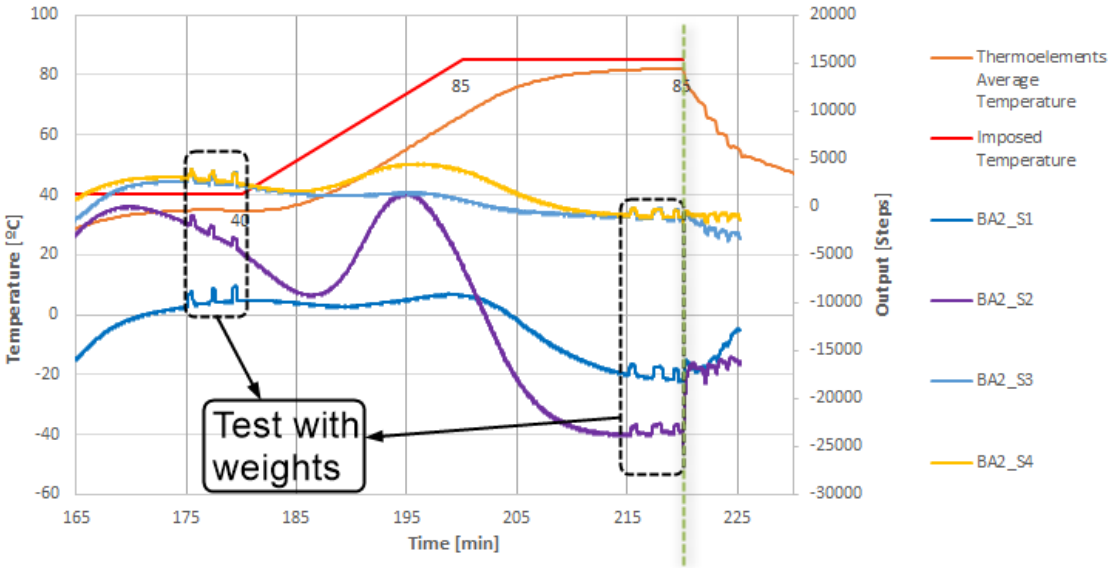

Figure 5.21: Last part of experiment BA1

Even when no weight is being placed, the absolute output is constantly varying due to tensions related to the coefficient of thermal expansion (CTE) mismatch and changes in the sensitivity of the sensors. It is visible that these fluctuations in output are largely superior to those caused by placing the weight. Its gradient of output increase or decrease, in its turn, is usually smaller. Nonetheless, when the weights are placed during high output variations, the induced error in the force measurement becomes significant. Apart from that, as Fig 5.22 exemplifies, the fastest the weights are placed, the smaller the error. Therefore, performing two measurements out of three while lowering the weights one at a time might not have been the best option if the objective is to compare experiments.

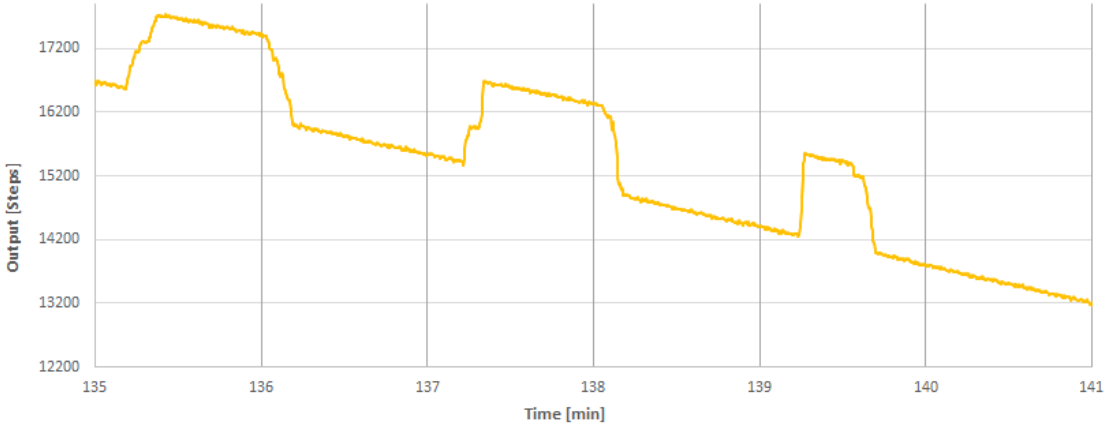

Figure 5.22: Output decrease during force readings

The case presented in Fig 5.22 was the case between all of the performed experiments where this situation was more critical. Output is decreasing at 577 steps per minute. If other factors did not influence the output, then the 3 displayed increases due to weights would have been 11.1, 5.6, and 1.8 % higher, ordered from left to right.

It is important to refer that the weight tests were always performed in points where the output gradient change was under 600 steps per minute. For example, in sensor number 3 during minute 193 of experience AA, the output gradient is 4900. The error will also increase when the applied load decreases. An the actual load will be generally lower.

The temperatures in the sensors measured with the thermocouples are presented in Fig 5.23. It is visible that the sensors near the door of the thermal chamber (S2 and S4) change their temperature more rapidly than the remaining, probably because of air currents generated. These were also the sensors nearest to the door of the thermal chamber. In fact, in minute 202, the temperature difference between S3 and S2 is 19^{o}C. The chart with all measured temperatures is presented in Appendix B.4.

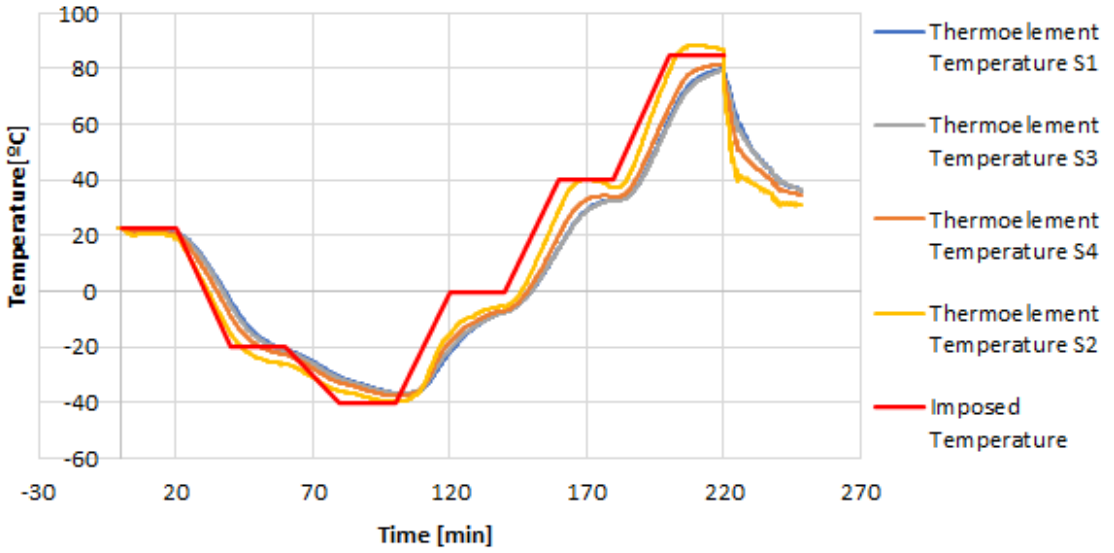

Figure 5.23: Thermocouples' temperature during BA2

In Appendix B.5, which displays the output during all experiments, it is interesting to notice that the sensor that changes its temperature more rapidly, S2, is always the sensor that also changes the output more rapidly.

After the thermal chamber program ends, the door of the thermal chamber is opened. In all sensors, it was verified a sudden increase in output. In sensor 2, represented in Fig 5.24, this increase was one more time, more severe. The gradient increase in this sensor during the first 20 seconds after open the door was, in some cases, three times superior to putting the weight. During that same period, the temperature drooped approximately 15ºC.

Each time a paper was shaking near the display, the temperature decreases, as expected. The effect of air flowing decreases while the assembly cools down, which means that the output variation are related with cooling and not with vibrations. These variations were, in the first instances, comparable to the ones associated with the weights tests.

What is odd to observe is that when the door of the chamber was opened, the temperature drooped rapidly, and the outputs of the sensors increased. On the other side, when the airflow was promoted, the temperature in the sensor also decreased, as it was expected, but the output decreases.

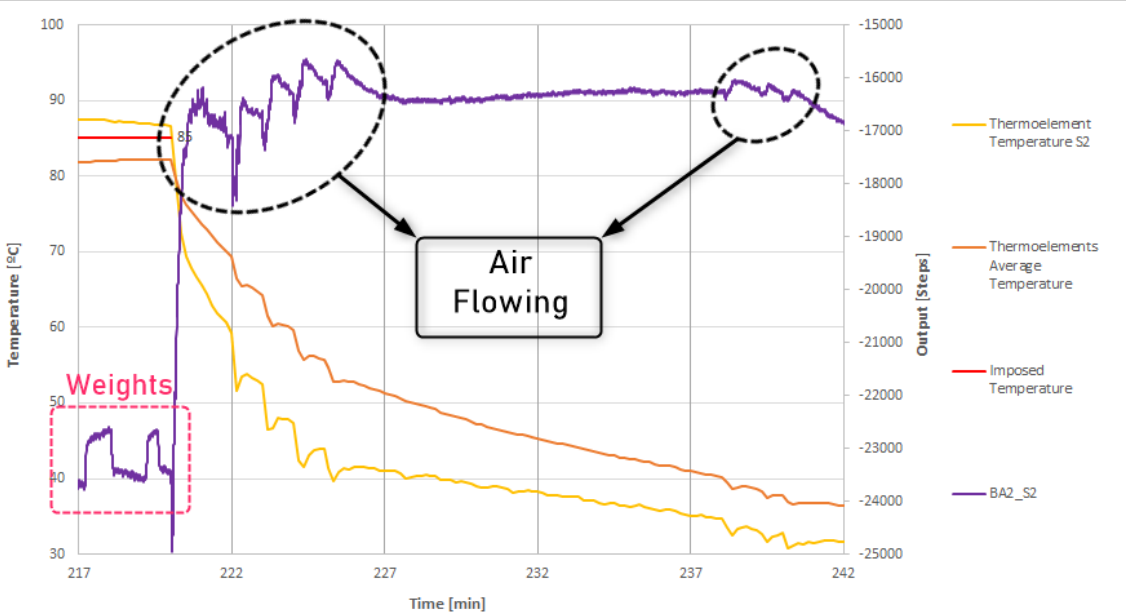

Figure 5.24: Air flow in BA2

Additionally, a comparison between the data obtained with the assembly testing and with the developed bending apparatus is presented in Fig 5.25. To obtain this chart, as interpolation over the assembly data was performed. Therefore, there is an error related with that approximation. When comparing different setups and sensor positions the absolute values are not relevant. Therefore, the results are presented in relation to the first temperature value in order to evaluate the tendencies. It is interesting to observe that the general tendency remained. The sensibility is usually the lowest at 80ºC and the highest at 24ºC.

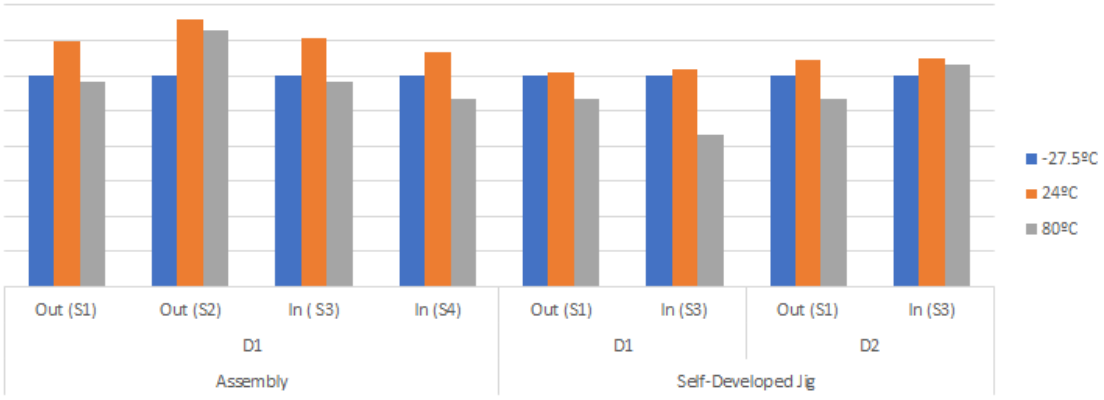

Figure 5.25: Assembly setp vs Developed bending apparatus

The results of the weight tests of experiments BA1, BA2 and AA are presented in Fig 5.26, Fig 5.27, and Fig 5.28.

These values are directly proportional to the sensibility. It is possible to observe that

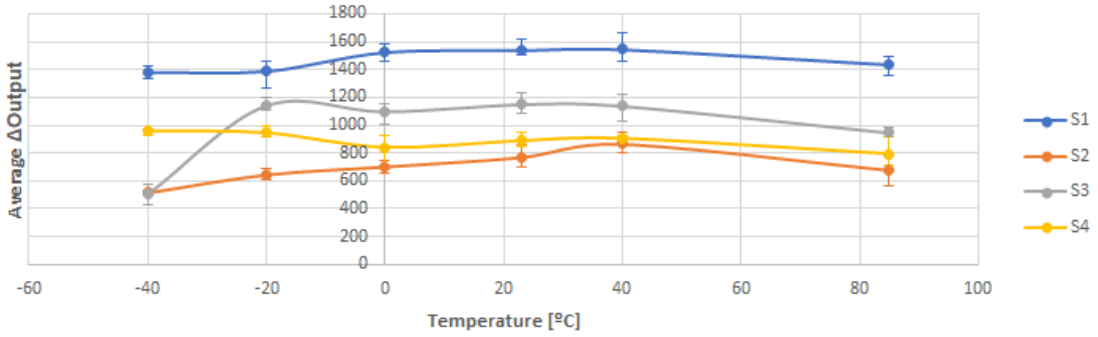

Figure 5.26: Average output variation in the first experiment before aging (BA1)

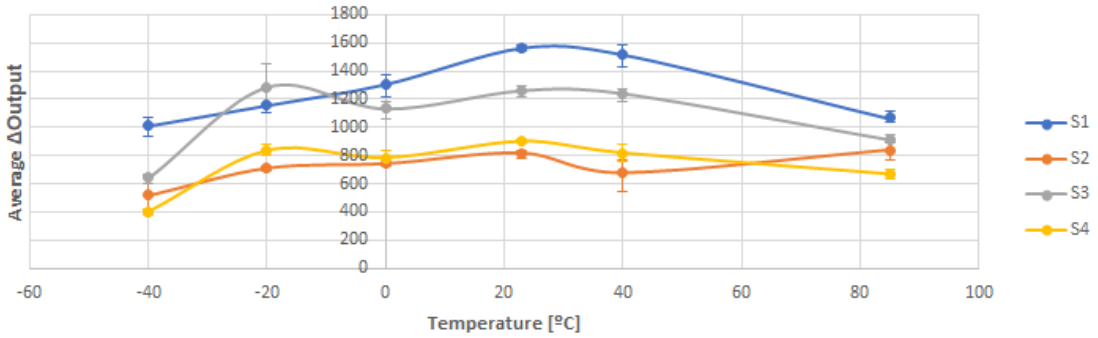

Figure 5.27: Average output variation in the second experiment before aging (BA2)

the sensibility is changing in temperature differently for each sensor. For example, in S3 during BA1, the sensibility between -40 and 40ºC increased 80%.

A2

A2 intends to analyse the effect of aging in the assembly, taking into account that inside the thermal chamber all parts remaining screwed. Focusing only on the before aging charts, in Fig 5.26, Fig 5.27, it is observed that the tendencies for each experiment are similar but not as equal as they would be expected. It is possible that the not optimized screwing order contributed to additional tensions in the FSEs, which were relieved during the initial experiments.

If we observe then the AA's chart in Fig 5.27 by eye, it appears that the after aging experiment has more similarities with the graph of the experience 2 than the two experiences realized before aging has with each other.

To perform this comparison fairly, the "distance" between matrices was calculated using two methods:

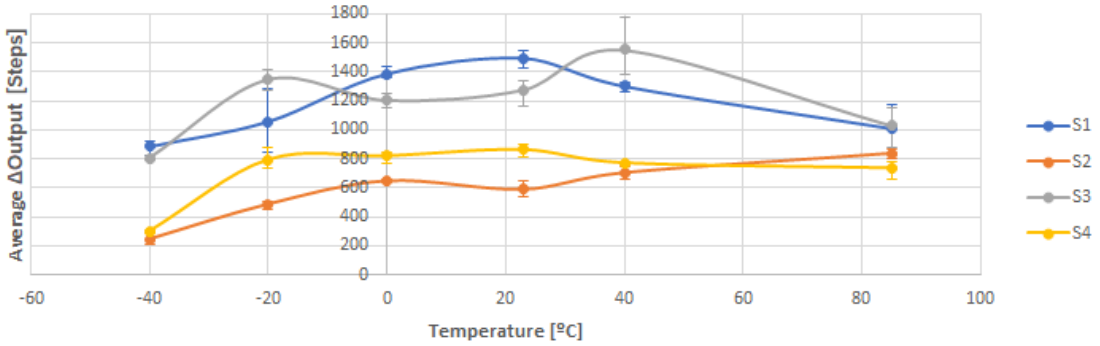

Figure 5.28: Average output variation in the experiment after aging (AA)

$$\mathrm{d}_1(\mathbf{A},\mathbf{B}) = \sum_{i=1}^{n}\sum_{j=1}^{n}|a_{ij}-b_{ij}|$$

$$\mathrm{d}_2(\mathbf{A},\mathbf{B}) = \sqrt{\sum_{i=1}^{n}\sum_{j=1}^{n}(a_{ij}-b_{ij})^2}$$

Where **A** and **B** are two matrices with dimensions n×n. The second method, d_2, was used to test the appearance of outliers.

The calculated distances are presented in Table 5.2.

Table 5.1: Distances between matrices with the Average output for each sensor and temperature

Value	BA1 vs BA2	BA2 vs AA	BA1 vs AA
d_1	3260	2557	4974
d_2	926	662	1276

It is visible that, for both methods, the distance between matrices BA1 and BA2 is larger than the distance between matrices BA2 and AA.

It was already explained that placing the 2 weights simultaneously might induce an error when comparing with other experiences. For that reason, it was decided to perform the distance calculations between matrices containing only the last measurement.

The calculated distances are presented in Table 5.2.

Table 5.2: Distances between the matrices with the last measurement for each sensor and temperature

Value	BA1 vs BA2	BA2 vs AA	BA1 vs AA
d_1	3871	2840	2840
d_2	1050	660	1153

Once again, the results show that aging had a more negligible effect than something that happened between the before aging experiments. One of the possible explanations could be tension relieved between experiments 1 and 2, namely in the screws that allowed the PCB, spring, or both to slide slightly.

In relation to BA2, the measurements of AA varied an average of 16.5 %. S2 presented the most significant variations. If the data from this sensor is deleted, then the average variation between BA2 and AA would have been 9.6 %. Some malfunction may have appeared in sensor S2 since it is also the sensor where the temperature effects are harsher.

Despite the analysis of weight detection done so far, if we observe Appendix B.6, it is visible that the output temperature-related variation patterns are more identical between experiments BA1 and BA2 than between BA2 and AA. Furthermore, it is interesting to observe that, even though the aging modified significantly the way the absolute output varies with temperature during the experiments, it didn't change the sensibility of the weight readouts in the same order of magnitude.

The complete graphs of output during the 3 experiments are presented in Appendix B.5.

5.4 Calibration

Studies' Results

C1

After reviewing the screwing driver parameters, 100% units were between limits. It is possible that the seating of the screw was not being detected properly. The ranking of the screwing sequences, which was determined through the previously presented score, is shown in Table 5.3.

Table 5.3: Ranking of the screwing sequences

Sequence Ranking	Score	$\hat{Out}$	$\hat{\sigma}$
C	0.23	1	0.77
A	0.13	0.95	0.82
F	0.04	0.92	0.88
E	-0.06	0.94	1

Sequence C) presented the highest averaged output and the lowest standard variation, so it was the best option. Between sequences E) and F), the second was expected to present a higher standard deviation. Once again it is highlighted that the these experiments should be done in the future with more samples.

C2

Additionally, a study focused on the re-definition of the force-sensing calibration test's upper and lower limits was performed to ensure process capability and product robustness.

Since there is only a small amount of data available for statistical analysis of each screwing order, and all the assembled samples resulted in force-sensing capable products, the measurements of the 16 samples were analyzed as a single batch.

As expected by the previous experiments, the middle sensors differ significantly in output from the outer ones during the calibration process, essentially due to the different stiffness in their configuration. This can be observed in the chart of Fig 5.29.

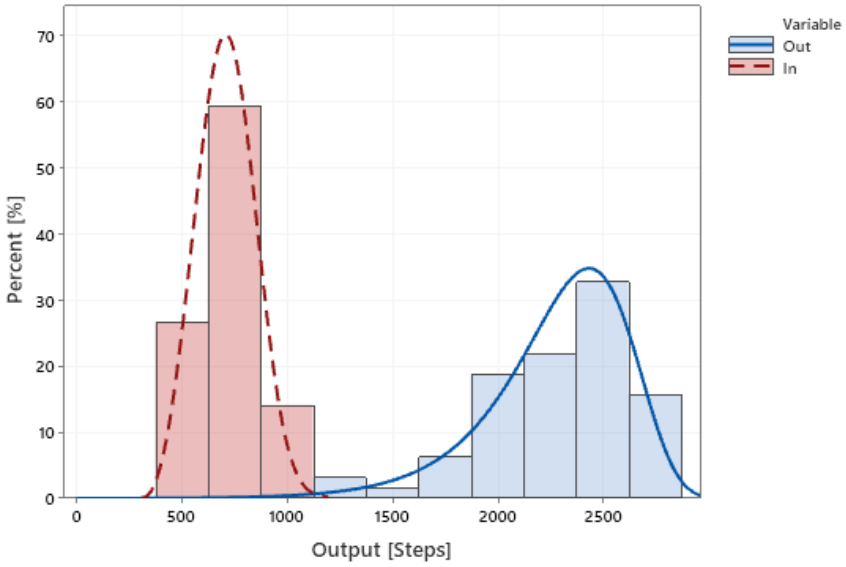

Figure 5.29: Difference in output between the inside and outer positions

For this reason alone, this investigation considered two separate analyses to determine two sets of limits for each type of sensor.

Starting with the inside sensors and using the 4 screwing sequences as a reference, we can observe in Fig 5.30 that it follows a normal distribution, as demonstrated on the normality test by the p-value>0.05.

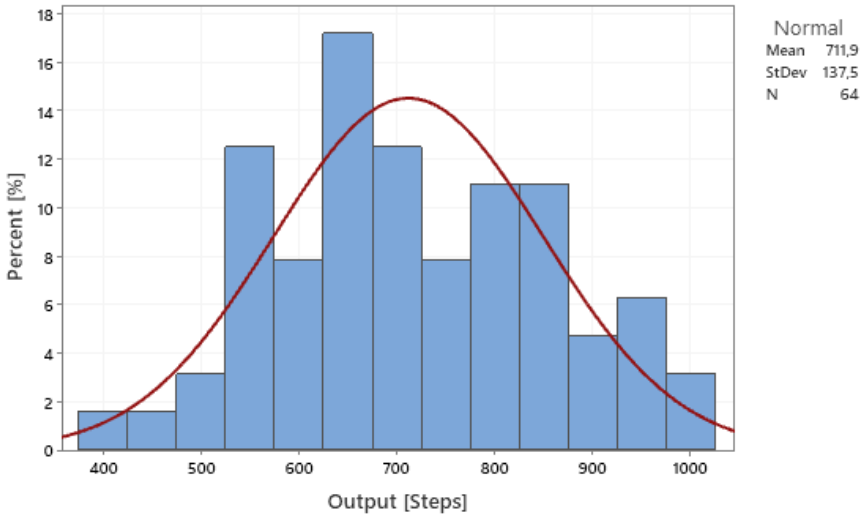

(a) Fitting plot (normal distribution)

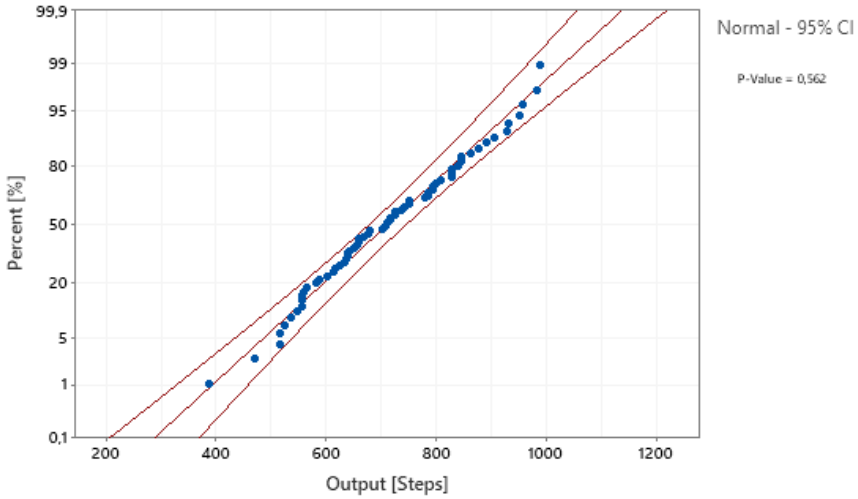

(b) Probability plot

Figure 5.30: Inside position plots

Since the measurements are normally distributed, it is possible to analytically define upper and lower bound limits based on the process performance index concept of process performance (Ppk).

Defining and achieving a minimum value of 1.33 Ppk will ensure that this process is capable (with a yield of 99.99%), as visible in table 5.4, and ready to production, according to the automotive industry standards.

Table 5.4: Process performance in percent

P_{PK}	Outputs within specifications
0.5	86.8%
0.8	98.4%
1.0	99.7%
1.2	99.97%
1.33	99.99%

Using the formulas presented in Chapter 2, it is possible to calculate the following values.

$$\begin{aligned} \text{PpU} &= \frac{(\text{USL} - X)}{3\sigma} \\ 1.33 &= \frac{(\text{USL} - 711.9)}{3 \times 137.5} \\ \text{USL} &= 1261 \end{aligned}$$

$$\begin{aligned} \text{PpL} &= \frac{(X - \text{LSL})}{3\sigma} \\ 1.33 &= \frac{(711.9 - \text{LSL})}{3 \times 137.5} \\ \text{LSL} &= 163 \end{aligned}$$

Using the statistical software Minitab to evaluate the calculated limits, it was possible to confirm that the current process has a performance of Ppk 1.33 has intended to. The result is presented in Fig 5.31

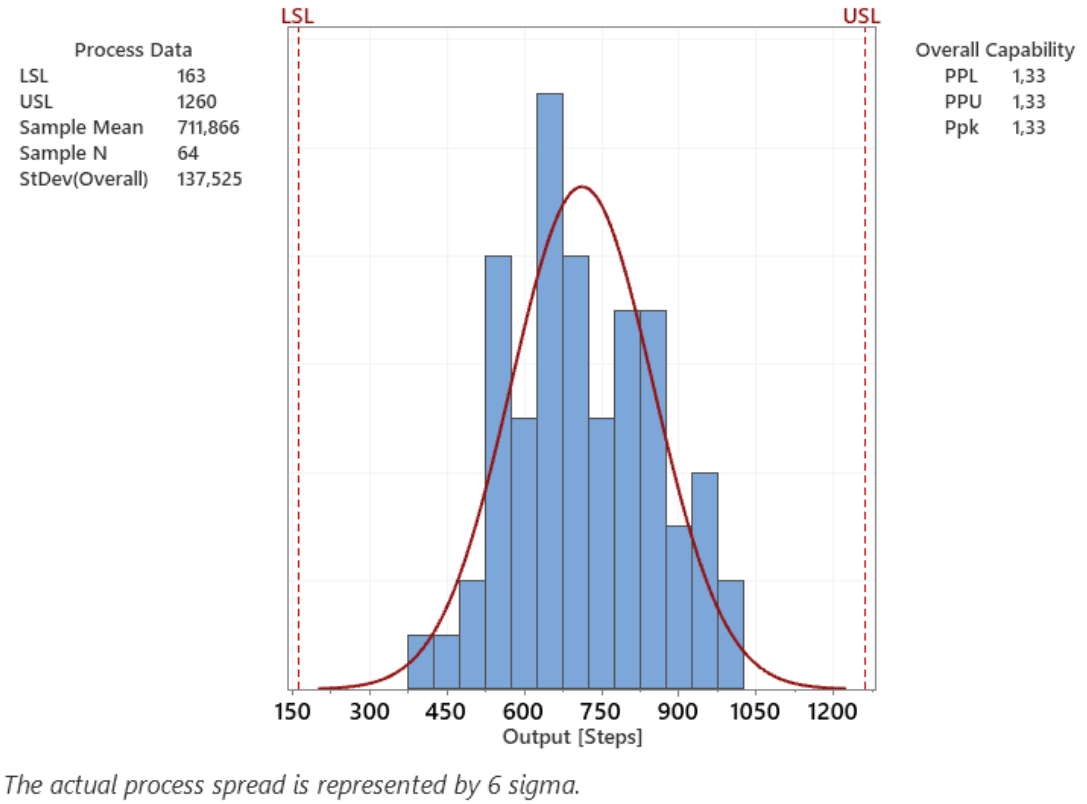

Figure 5.31: Inside position: process capability report

Analogously, the outer sensors were tests to verify the process' normality.

The histogram in Fig 5.32 and the p-value < 0.05 show that the process is right skewed and not symmetric, and should be better described by a non-normal distribution.

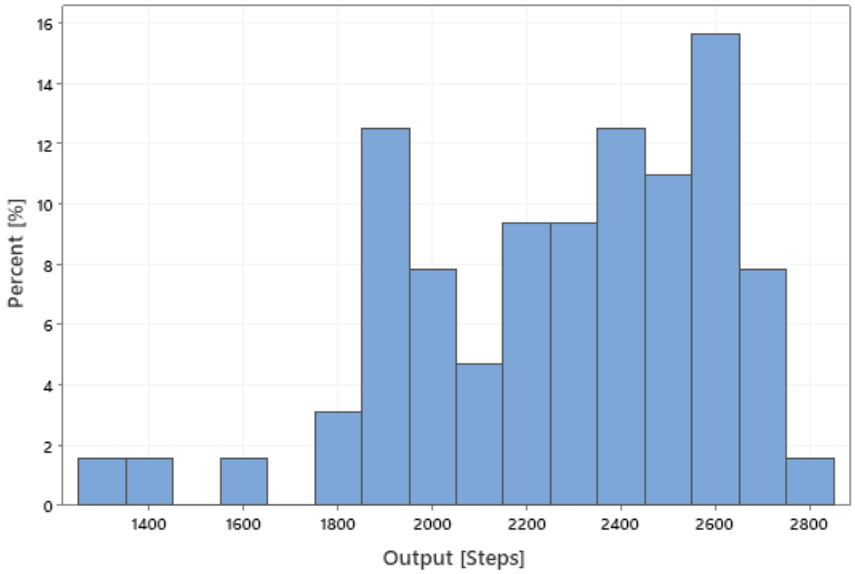

(a) Fitting plot (normal distribution)

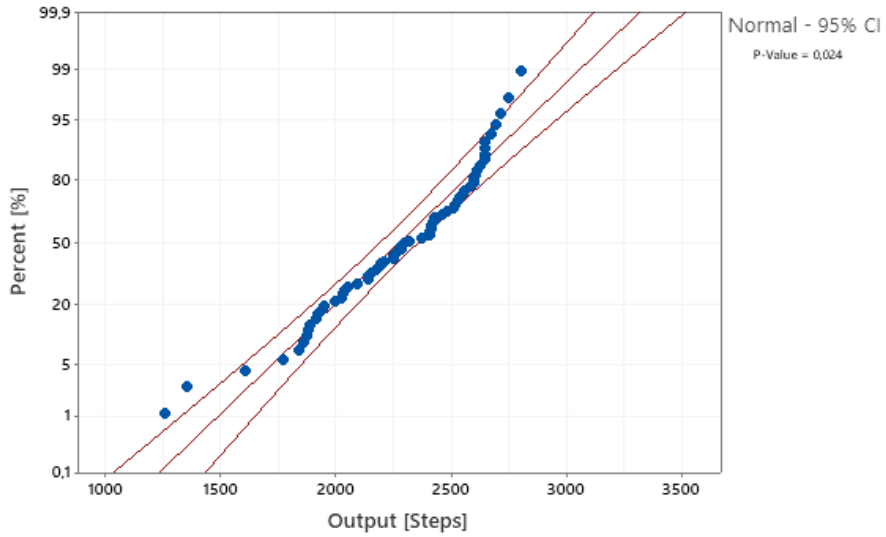

(b) Fitting plot (normal distribution)

Figure 5.32: Outer positions plots

One of the most popular distributions used in engineering, science, and economy fields is the Weibull distribution - consisting of a scale and shape parameter.

The Weibull fitted distribution best describes the data collected from our process, as presented in Fig 5.33.

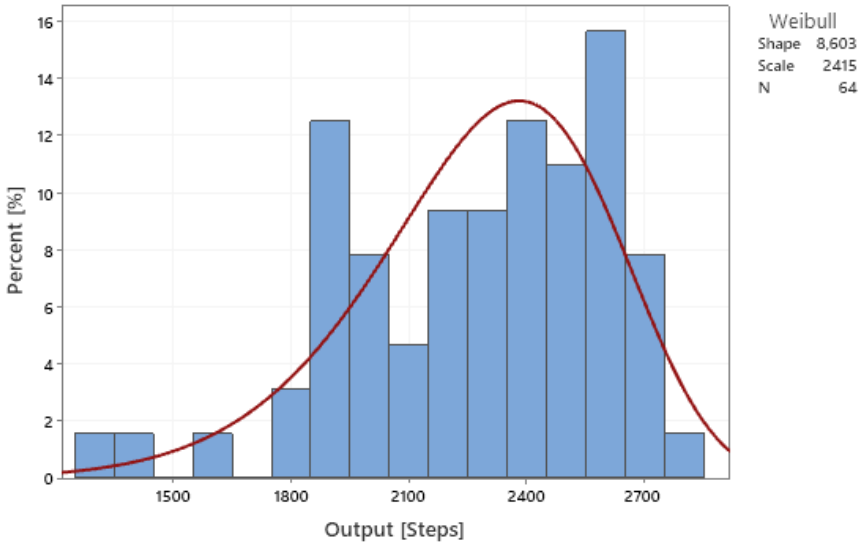

(a) Fitting plot (normal distribution)

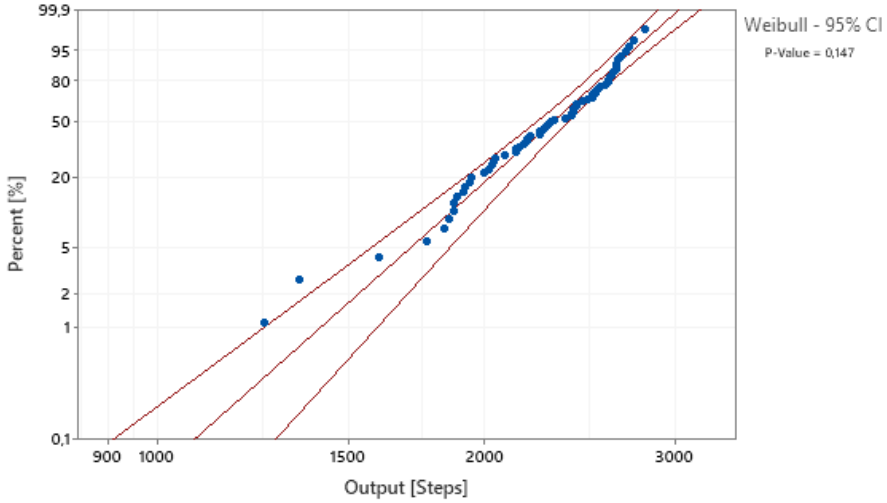

(b) Fitting plot (normal distribution)

Figure 5.33: Ppk values and calculation

Unfortunately, capability indices cannot be estimated the same way for normal and non-normal data because their distributions are different. For example, the shape of our Outer sensors distribution is non-symmetric, and the distribution coverage of a non-normal distribution cannot be represented by the number of standard deviations (a parameter unique to the normal distribution).

To define USL and LSL limits based on process performance, a different approach was taken.

A process yield of 99,99% was set as target, representing an equivalent 1.33 Ppk in a normal distributed process, and the upper and lower bounds were determined in order

to ensure this population coverage on our distribution. Minitab calculated the limits visualized in Fig 5.34.

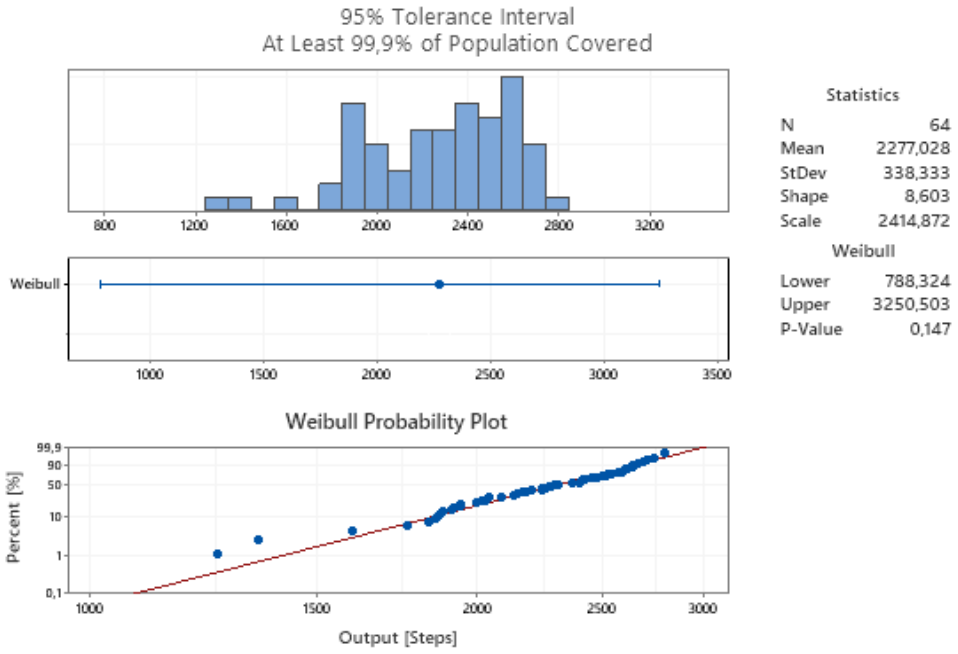

Figure 5.34: Coverage limits using Weibull

Running a process capability to study on our data, using the previously determined 99,99% population coverage limits (not representative of a Ppk of 1.33) as a starting point for our LSL and USL, it was possible to decide on process performance.

To achieve the desired Ppk, these USL and LSL values were iteractively tweaked until they converged to 1.33. The LSL was set at 725 and the USL at 3168, as exemplified in Fig 5.35.

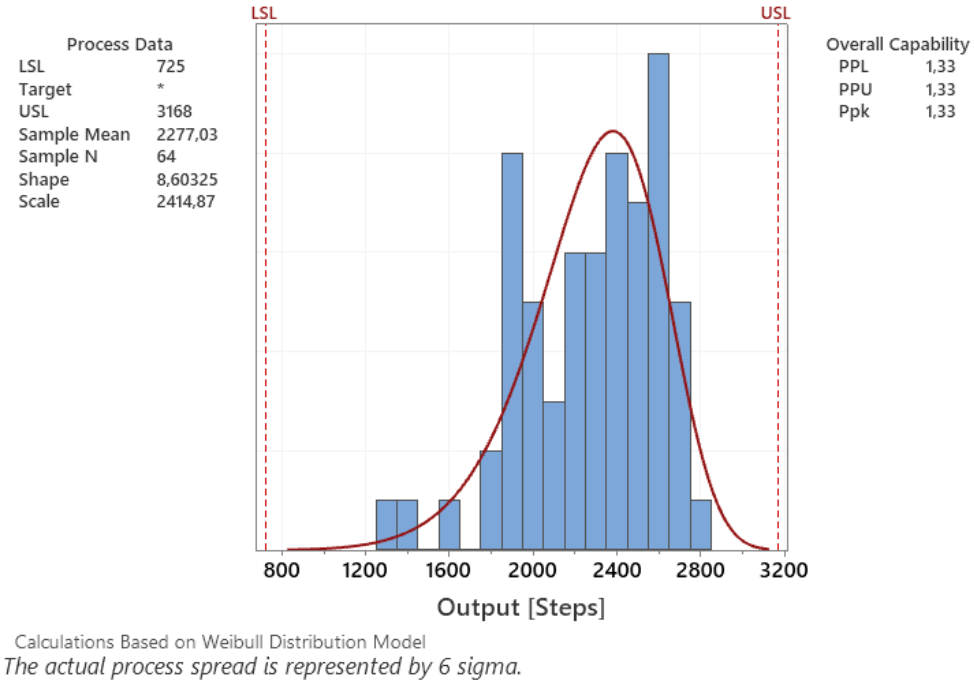

Figure 5.35: Definition of new process limits with Weibul distribution

This investigation made it possible to define process limits based on normal and non-normal available data acquired from the actual process statistically and scientifically, ensuring process capability and product robustness.

Ideally, bigger sample sizes and different batch productions would be evaluated, something to be done as future work.

5.5 Summary

This Chapter explores the results obtained from the various performed experiments. Beginning with the tensile machine testing, then with the developed bending apparatus, assembly testing, and calibration, the results are present and analyzed. The testing categories and experiments are the same and presented in the same order as in Chapter 4. This Chapter also proceeds with the conclusions and the future work perspectives.

Chapter 6

Conclusions and Future Works

Working with a mechanical development team from Bosch, this project was a proof of concept over a new system intended to measure the force applied in an automobile display. Regarding all the aspects that might influence the performance of the force sensing system, the project mainly focused on its aging, temperature variation and air flow, and screwing sequence. For that, the study about the sensors' output and, in some cases, the stiffness of some components was conducted.

6.1 Final Conclusions

The aging effect was studied in the tensile machine and with assembly tests. The results from the first testing method were not as precise as the ones obtained with the second, and, for that reason, they were not taken into account. Nevertheless, they were helpful to point out some possible issues in the operation of the force sensing system, for instance, the potential variation in the gauge positioning and spring stiffness related to tolerancing and PCB's warpage.

In the assembly testings, the aging did not influence the increase in output more than other factors, such as possible tensions relieved during experiments. In the end, the main conclusion was that despite the aging had significantly affected the way the absolute output varied with temperature, it didn't change the system's sensitivity in the same order of magnitude.

The temperature and air flow were studied with the developed bending apparatus and assembly tests. Either testing the force sensing elements (FSE) individually with the apparatus or in the assembly, a similar sensitivity variation tendency for temperatures of -27.5, 24, and 80^{o}C was observed. During step temperature tests with the assembly, it was observed that the sensibility varied differently for each sensor, but always between 13 and 95 % of maximum increase. In the same experiments, it was observed that the temperature largely influenced the absolute value of the sensors. Even if the force is calculated by a differential increase of output, the temperature can influence the readouts, mainly in slow light touches. For software compensation purposes, it is pointed that the output variations due to temperature followed patterns that might be unpredictable due to apparent complexity. The air flowing affected the absolute output by promoting the cooling. This information might be relevant in the case the system will include an active cooling system in the display.

The calibration process presented several results out of specification, including some incoherent values. The screwing parameters were corrected, and the calibration of 16

samples was carried out, resulting in 100% of samples inside specifications. During the calibration process, four screwing sequences were tested. Afterward, they were ranked from best to worst, according to the obtained sensitivities, namely its absolute values and dispersion between sensors. In the end, through process capability analysis, new specification limits for the calibration process were suggested.

During the performed experiments, knowledge not directly related with the objectives was gathered. One example was information about the mechanical behavior of the FSE or how to possibly reduce the variation in system's sensitivity.

6.2 Future Working Perspectives

The suggested future works, related with the project developed in this dissertation, are:

- The screwing sequences were tested with 16 samples, which does not allow a reliable statistical analysis. Therefore, new screwing sequences should be tested in the following sample manufacturing phases, with the increased sample size;
- Minimize the influence of airflow by applying some coating on the strain gauges;
- Perform experiments with thermally compensated strain gauges;
- Optimize the tolerance design for each component to minimize sensitivity and stiffness variation;
- Test the effect of vibrations and mechanical fatigue in the system;
- Development of an AI-based algorithm to correctly measure the force applied.

References

[1] Ki-Hyuk Seol, Seungjun Park, Seok-Jeong Song, and Hyoungsik Nam. Finger and stylus discrimination scheme based on capacitive touch screen panel and support vector machine classifier. *Japanese Journal of Applied Physics*, 58(7):074501, jun 2019. doi: 10.7567/1347-4065/ab2672.

[2] Seung-Hwan Lee, Jae-Sung An, Seong-Kwan Hong, and Oh-Kyong Kwon. A highly linear and accurate fork-shaped electrode pattern for large-sized capacitive touch screen panels. *IEEE Sensors Journal*, 18(15):6345–6351, 2018. doi: 10.1109/JSEN.2018.2836340.

[3] Gary Barrett and Ryomei Omote. Projected-capacitive touch technology. *Information Display*, 26(3):16–21, 2010.

[4] Timothy Hoye and Joseph Kozak. Touch screens: A pressing technology. In *Tenth Annual Freshman Engineering Sustainability in the New Millennium Conference April*, volume 10, 2010.

[5] Tech Insights. https://www.techinsights.com/blog/beyond-apples-force3d-touch-synaptics-key. 2021-04.

[6] Moceheb Lazam Shuwandy, B.B. Zaidan, A.A. Zaidan, A.S. Albahri, A.H. Alamoodi, O.S. Albahri, and Mamoun Alazab. mhealth authentication approach based 3d touchscreen and microphone sensors for real-time remote healthcare monitoring system: Comprehensive review, open issues and methodological aspects. *Computer Science Review*, 38:100300, 2020. ISSN 1574-0137. doi: https://doi.org/10.1016/j.cosrev.2020.100300.

[7] David S. Hermann. The case is building for automotive displays. 26th:1–6, July 2019. doi: 10.23919/AM-FPD.2019.8830589.

[8] Force Sensing Provides Flexibility and Reliability. https://www.mouser.com/pdfDocs/force-sensing-provides-flexibility-and-reliability.pdf. 2021-07.

[9] Mitsuo Adachi. Chances and challenges for automotive displays. pages 1–4, 2018. doi: 10.23919/AM-FPD.2018.8437379.

[10] David S Hermann. Automotive displays-trends, opportunities and challenges. In *2018 25th International Workshop on Active-Matrix Flatpanel Displays and Devices (AM-FPD)*, pages 1–6. IEEE, 2018.

[11] Bosch in Portugal. https://www.bosch.pt/en/. 2021-03.

[12] Environment - Bosch. https://www.bosch.com/company/sustainability/environment/. 2021-04-03.

[13] Sustainability Report - Bosch. https://assets.bosch.com/bosch-sustainability-report-2019-factbook.pdf. 2021-04.

[14] Shixuan Yang and Nanshu Lu. Gauge factor and stretchability of silicon-on-polymer strain gauges. *Sensors*, 13(7):8577–8594, 2013. ISSN 1424-8220. doi: 10.3390/s130708577.

[15] An lesson about Strain Gauges, howpublished = https://me363.byu.edu/strain$_g auges.pdf, note = 2021 - 08$.

[16] Karl Hoffmann. *Applying the Wheatstone bridge circuit*. HBM Germany, 1974.

[17] T.H.G. Megson. Chapter 13 - deflection of beams. In T.H.G. Megson, editor, *Structural and Stress Analysis (Third Edition)*, pages 337–388. Butterworth-Heinemann, Boston, third edition edition, 2014. ISBN 978-0-08-099936-4. doi: https://doi.org/10.1016/B978-0-08-099936-4.00013-9.

[18] ToolsTalk MT. https://www.flexibleassembly.com/Atlas-Copco-ToolsTalk-MT-Configuration-Manual.pdf= 2021-08.

[19] 6 Sigma - Process Capability, howpublished = https://sixsigmastudyguide.com/process-capability-cp-cpk/, note = 2021-08.

[20] Anthony patera, daniel frey, and nicholas hadjiconstantinou. 2.086 numerical computation for mechanical engineers. fall 2012. massachusetts institute of technology: Mit opencourseware, https://ocw.mit.edu.

[21] Haydon Kerk Pittman. https://www.haydonkerkpittman.com/learningzone/faq/linear-actuators-stepper-motors = 2021-08.

Appendix A

Developed Bending Apparatus

A.1 Exploded View

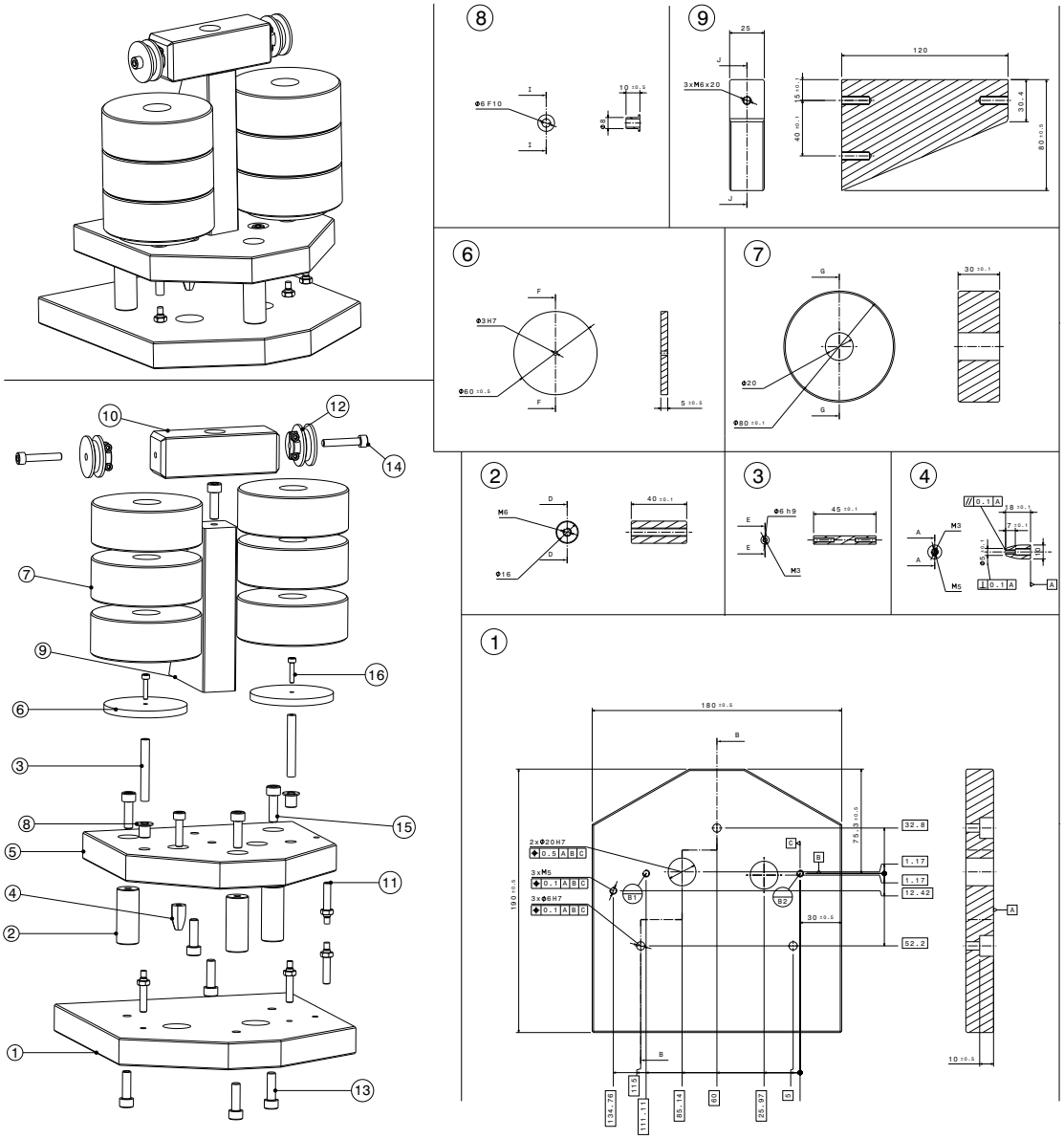

Figure A.1: Exploded view - part 1/2

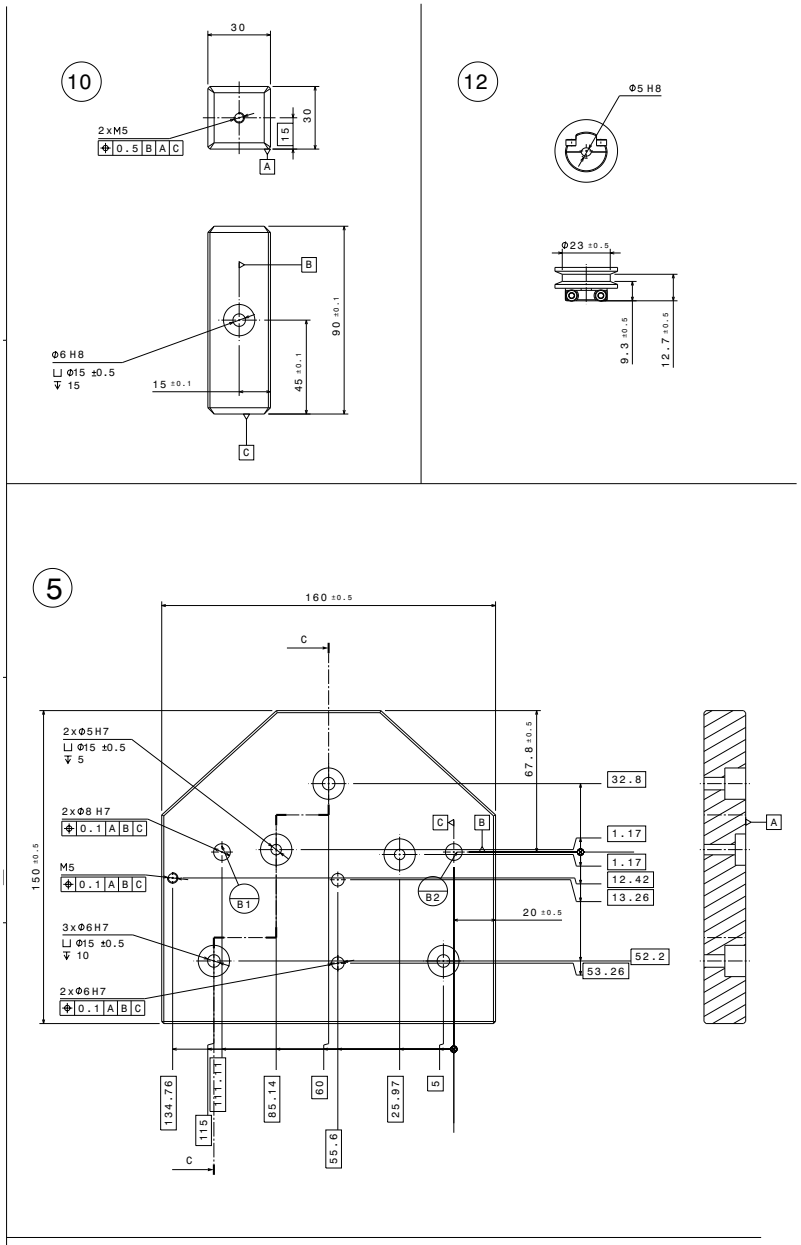

Number	Quat.	Designation	Suplier	Part Number	Material
1	1	Lower Plate	Self-Made	/	Aluminium
2	3	Support Pillar	Self-Made	/	Steel
			MISUMI	DSF16-40-M6-HN	/
3	2	Precision Rods (45mm) and h9	Self-Made	/	Steel
			MISUMI	RGOS6-45	/
4	2	Carrier Simulation	Self-Made	/	Steel
5	1	Top Plate	Self-Made	/	Aluminium
6	2	Weight Support	Self-Made	/	Aluminium
7	6	Weight	Self-Made	/	Steel or eq. (d>7g/cm3)
			MISUMI	RDOS80-30	/
8	2	Self-lubricating bushings with flange	MISUMI (or IGUS)	XFM-0608-10	/
9	1	Triangular Block	Self-Made	/	Aluminium
10	1	Quadrangular Block	Self-Made	/	Aluminium
11	4	Stoppers	MISUMI	PUSS5-25	/
12	2	Pulley	MISUMI	MBRDC28-2.5-5	/
13	9	M6 for Fixing Pillars and Blocks	MISUMI	CSH-ST-M6-20	/
14	2	M5 for Fixing Pulley	MISUMI	CSH-ST-M5-28	/
15	2	M5 for Fixing Simulate Carriers	MISUMI	CSH-ST-M5-20	/
16	2	M3 for Fixing Weight Supports	MISUMI	CSH-STN-M3-15	/

Figure A.2: Exploded view - part 2/2

A.2 Results of FSE 6 and 9 tested with Developed Bending Apparatus

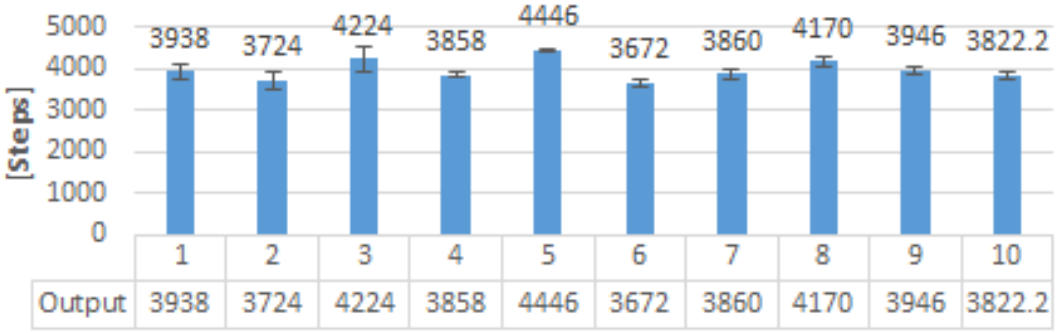

Figure A.3: FSE number 9, S1

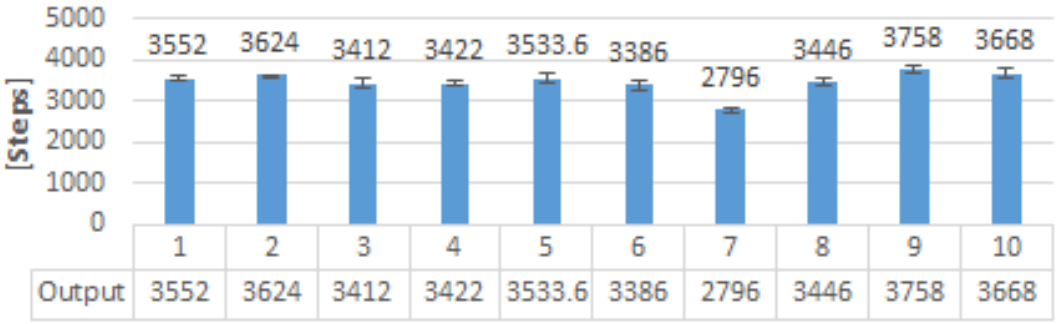

Figure A.4: FSE number 9, S3

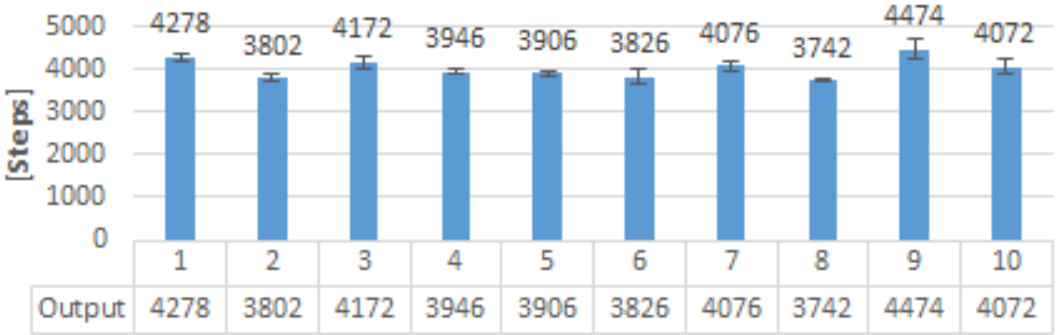

Figure A.5: FSE number 6, S1

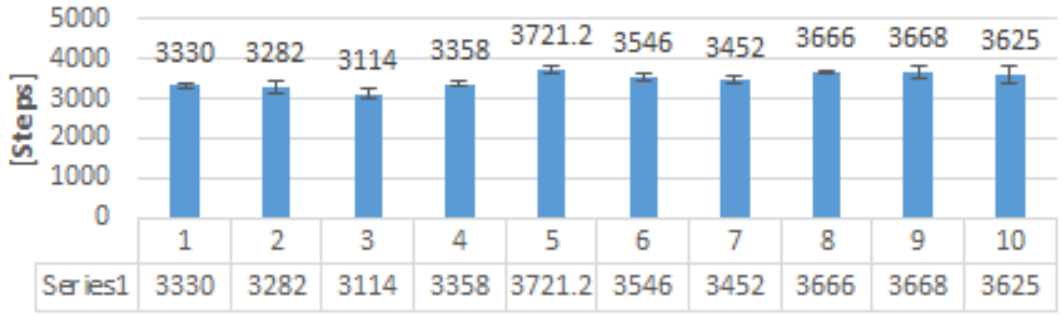

Figure A.6: FSE number 6, S3

A.3 Output Measurement Methods

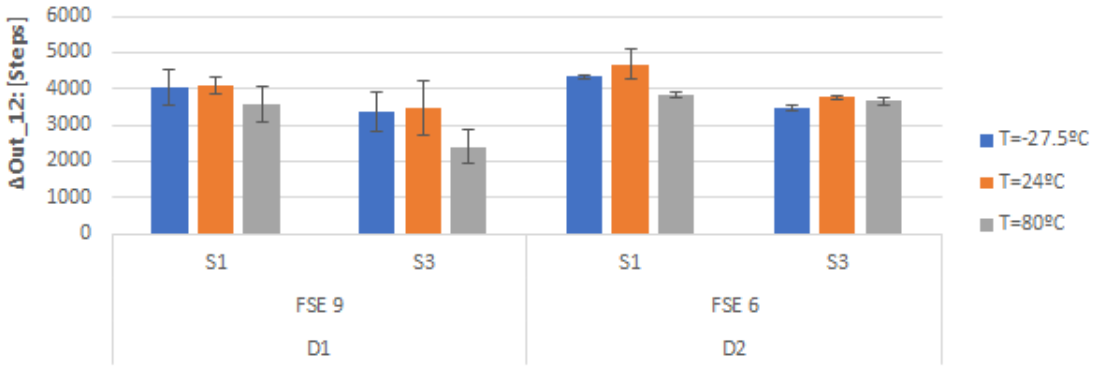

Figure A.7: DBA3: ΔOut_{12}

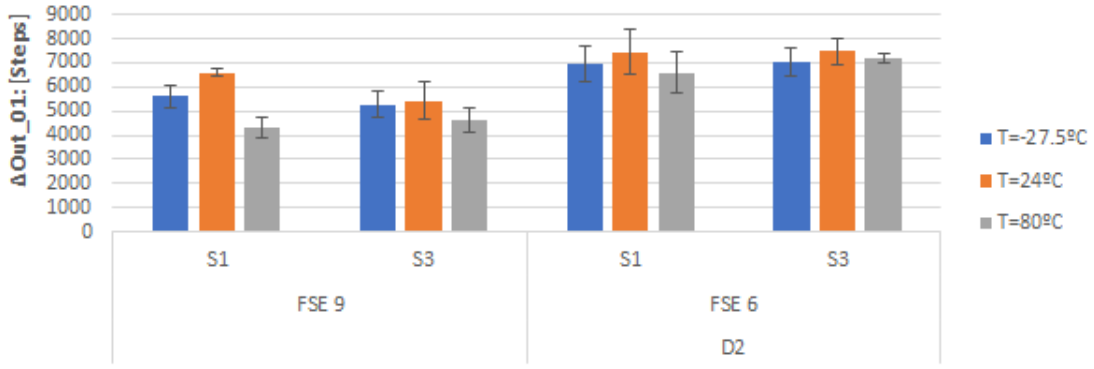

Figure A.8: DBA3: ΔOut_{01}

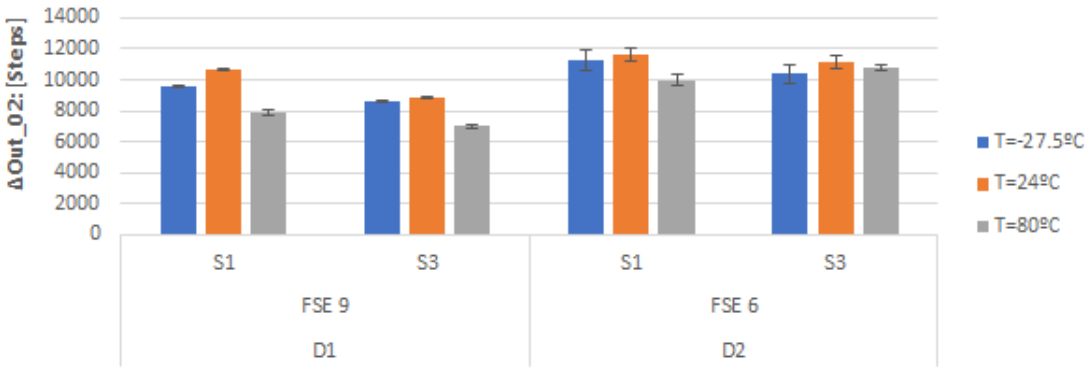

Figure A.9: DBA3: ΔOut_{02}

Appendix B

Assembly

B.1 Time Schedule of the Experiments with the Assembly

Full test				
Start Time	End Time	Duration	Imposed temperature (ºC)	Test
00:00:00	00:15:00	00:15:00	23	Wait
00:15:00	00:20:00	00:05:00	23	Test_Weigts
00:20:00	00:55:00	00:35:00	-20	Wait
00:55:00	01:00:00	00:05:00	-20	Test_Weigts
01:00:00	01:35:00	00:35:00	-40	Wait
01:35:00	01:40:00	00:05:00	-40	Test_Weigts
01:40:00	02:15:00	00:35:00	0	Wait
02:15:00	02:20:00	00:05:00	0	Test_Weigts
02:20:00	02:55:00	00:35:00	40	Wait
02:55:00	03:00:00	00:05:00	40	Test_Weigts
03:00:00	03:35:00	00:35:00	85	Wait
03:35:00	03:40:00	00:05:00	85	Test_Weigts
03:40:00	03:40:00	00:00:00	85	Open Door
03:40:00	03:42:00	00:02:00	Door chamber opened	Wait
03:42:00	03:42:15	00:00:15		Force air to flow
03:42:15	03:43:00	00:00:45		Wait
03:43:00	03:43:15	00:00:15		Force air to flow
03:43:15	03:44:00	00:00:45		Wait
03:44:00	03:44:15	00:00:15		Force air to flow
03:44:15	03:45:00	00:00:45		Wait
03:45:00	03:45:15	00:00:15		Force air to flow
03:45:15	03:46:00	00:00:45		Wait
03:46:00	03:46:15	00:00:15		Force air to flow
03:46:15	03:47:00	00:00:45		
03:47:00	03:58:00	00:00:45		Wait
03:58:00	03:58:15	00:00:15		Force air to flow
03:58:15	03:59:00	00:00:45		Wait
03:59:00	03:59:15	00:00:15		Force air to flow
03:59:15	04:00:00	00:00:45		Wait
04:00:00	04:00:15	00:00:15		Force air to flow
04:00:15	...	...		Cool at T_amb

B.2 Test with weights

Table B.1: Test with weights schedule

Test_Weights (5min)	
Start Time	Action
00:00:00	Measurement X1
00:00:00	Put weight 1
00:00:30	Put weight 2
00:00:30	Measurement Y1
00:01:00	Remove weight 1
00:01:30	Remove weight 2
00:01:30	Measurement X2
00:02:00	Put weight 2
00:02:30	Put weight 1
00:02:30	Measurement Y2
00:03:00	Remove weight 2
00:03:30	Remove weight 1
00:03:30	Measurement X3
00:04:00	Put weights simultaniously
00:04:30	Measurement Y3
00:04:30	Remove weights simultaniously
00:05:00	End

$$Average\Delta Output = \frac{1}{3}\sum_{i=1}^{3}\left(measurement_{Yi} - measurement_{Xi}\right) \tag{B.1}$$

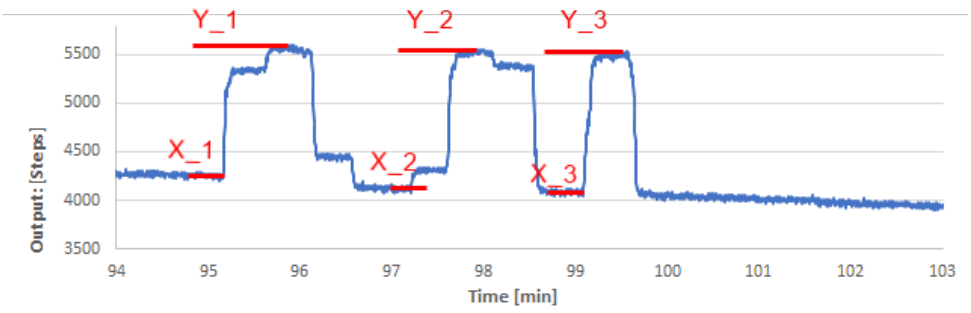

Figure B.1: Example of the measurements in a random sensor

B.3 Test with weights - Complete results

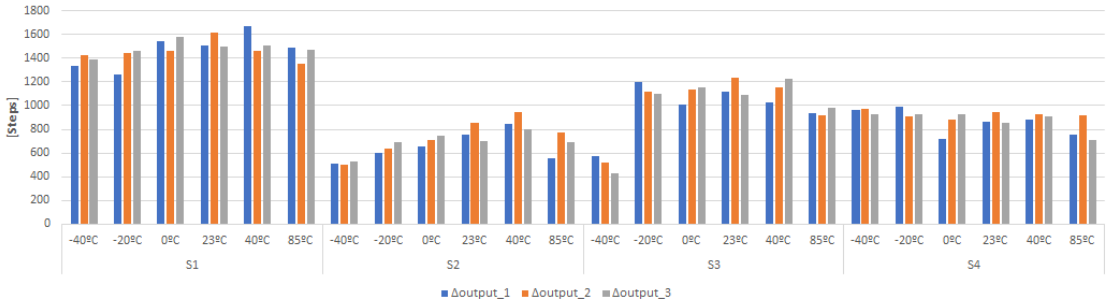

Figure B.2: BA1 - All measurements

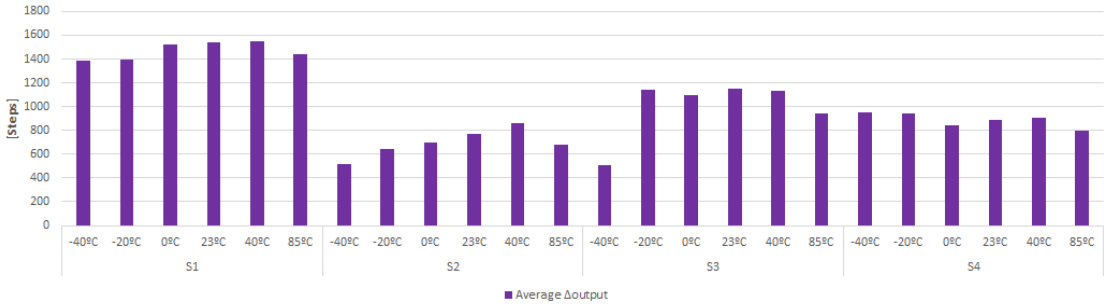

Figure B.3: BA1 - Average

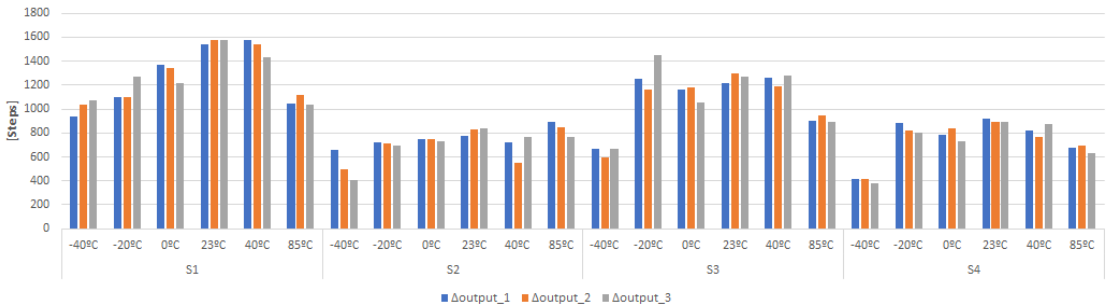

Figure B.4: BA2 - All measurements

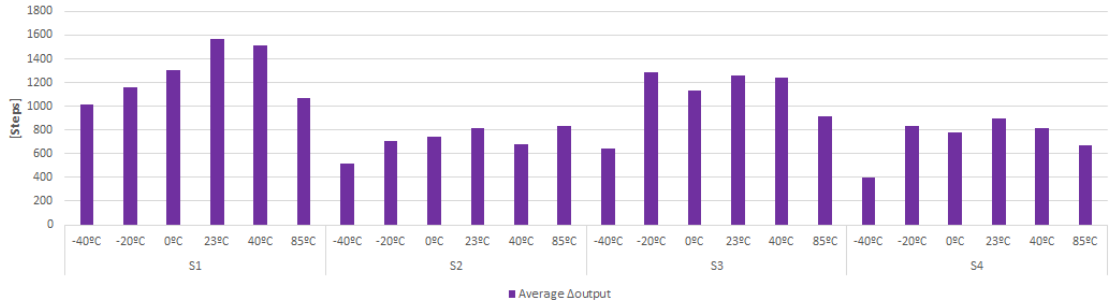

Figure B.5: BA2 - Average

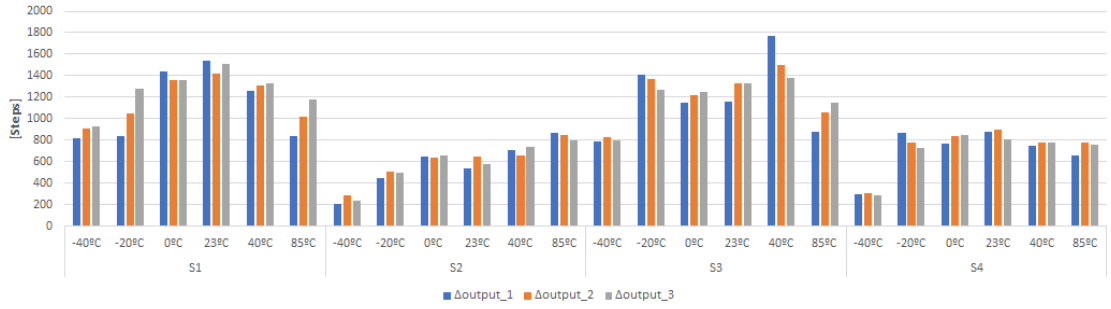

Figure B.6: AA - All measurements

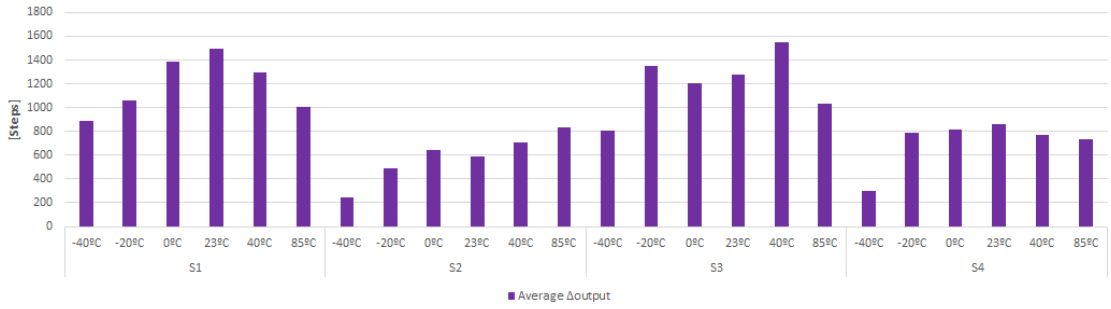

Figure B.7: AA - Average

B.4 Thermocouples temperature

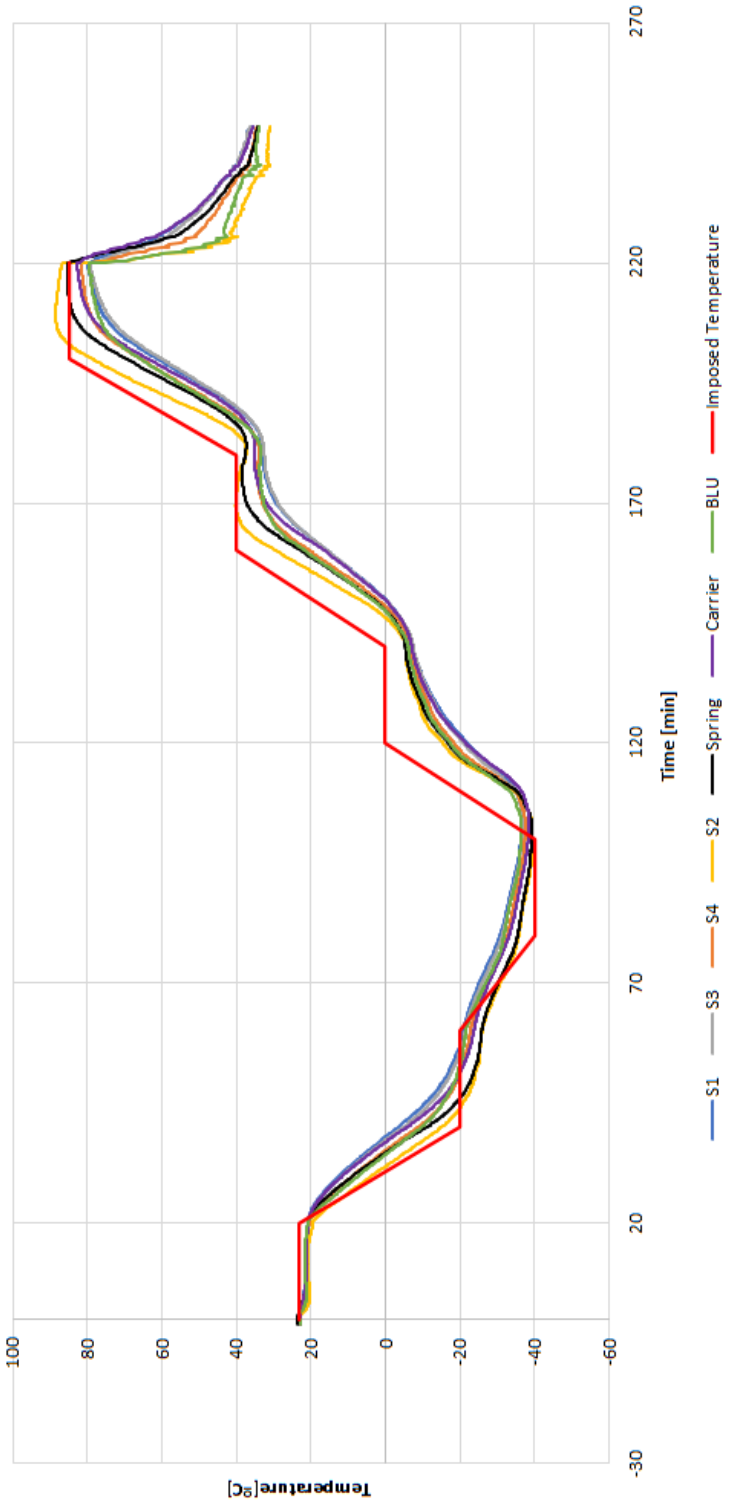

B.5 Output variation during experiments

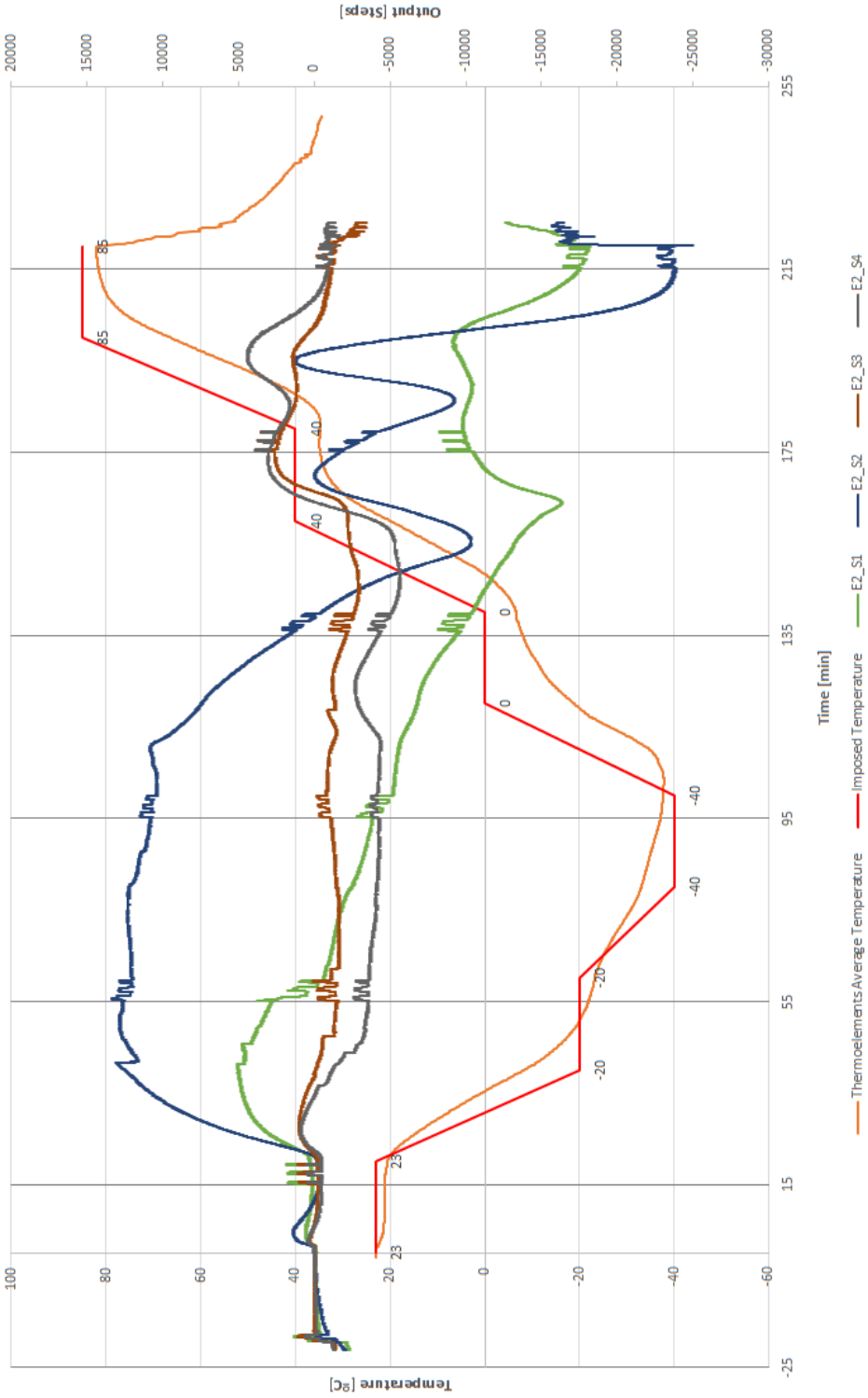

Figure B.8: Output variation during experiment BA1

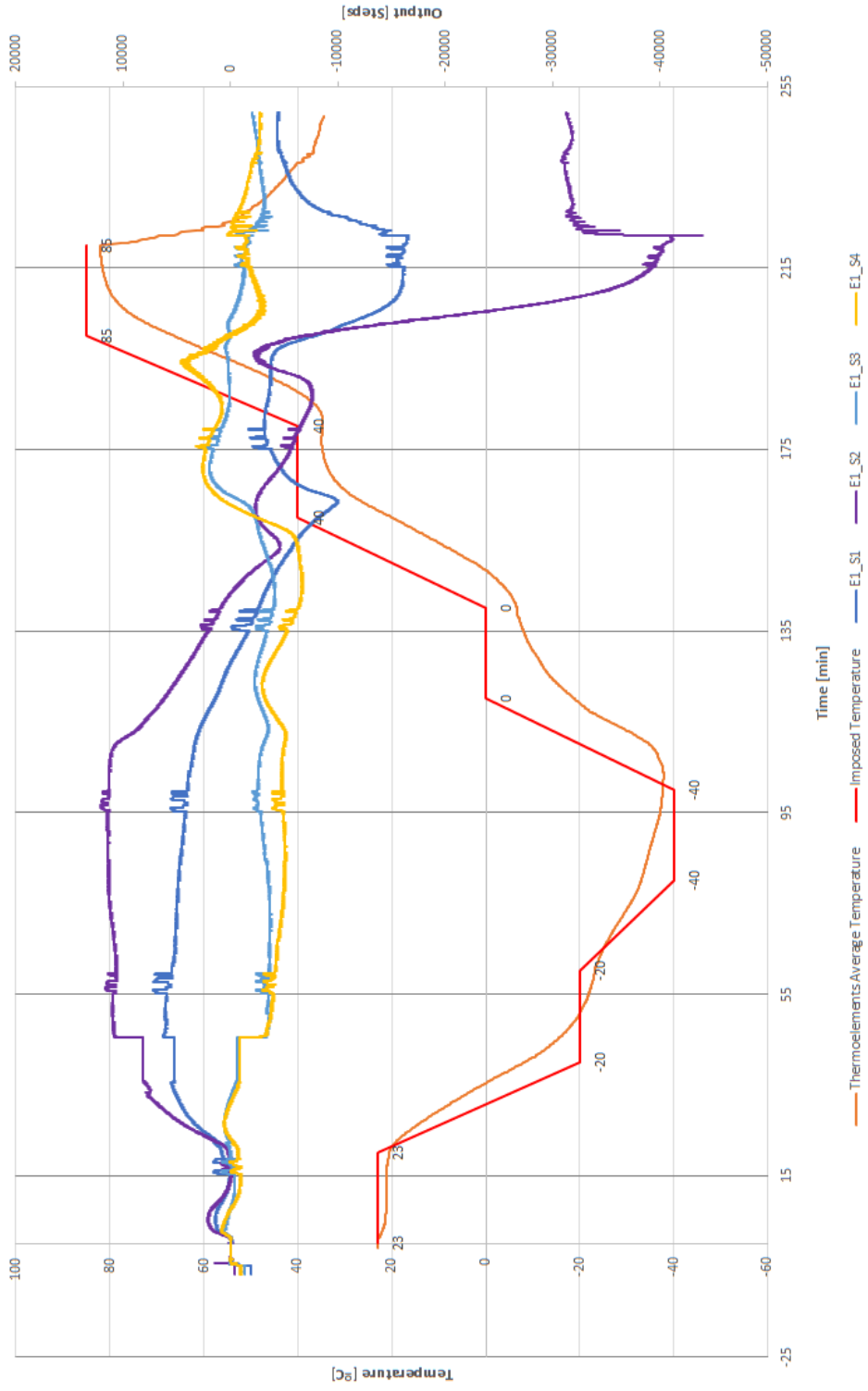

Figure B.9: Output variation during experiment BA2

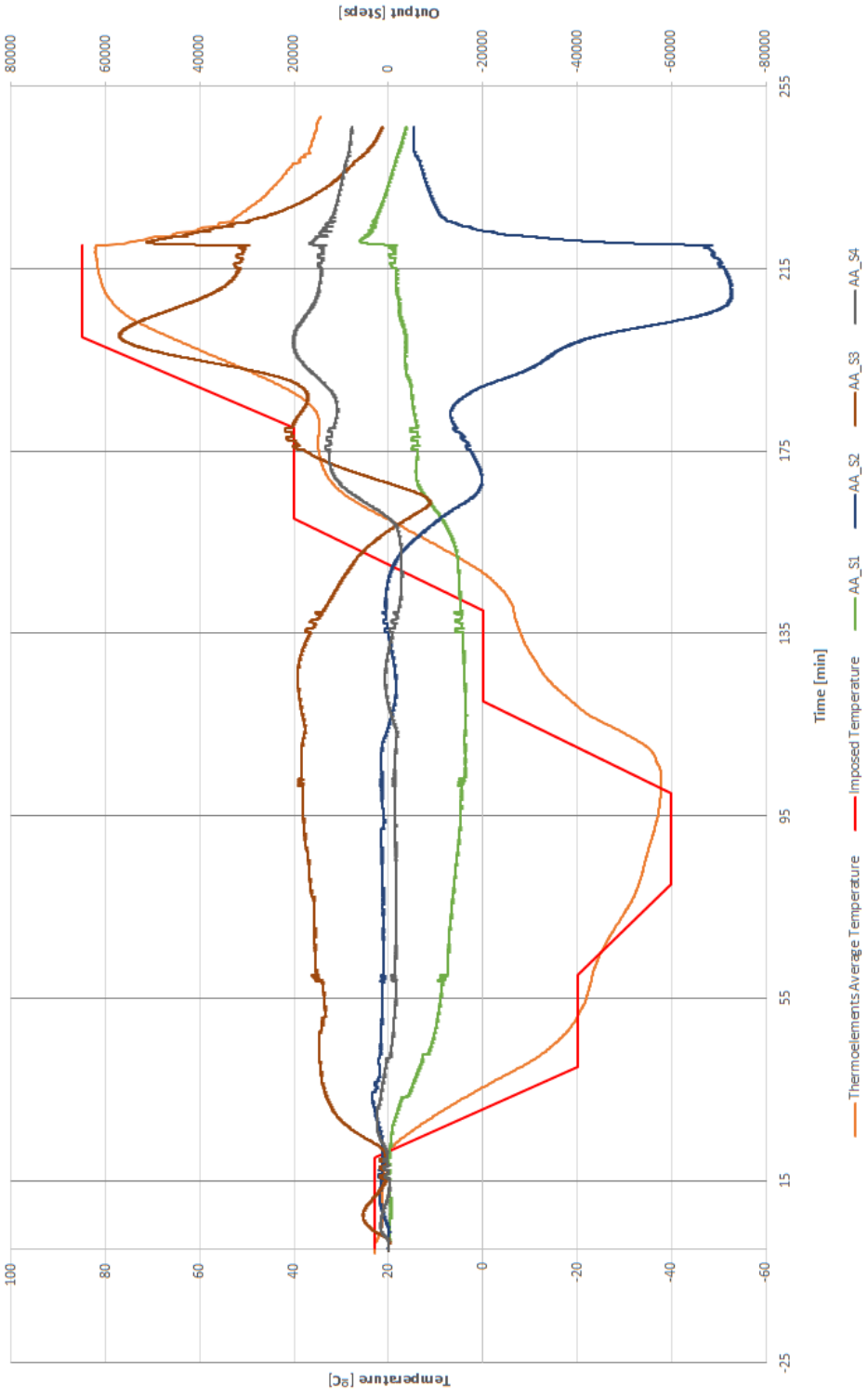

Figure B.10: Output variation during experiment AA

B.6 Output variation in each sensor

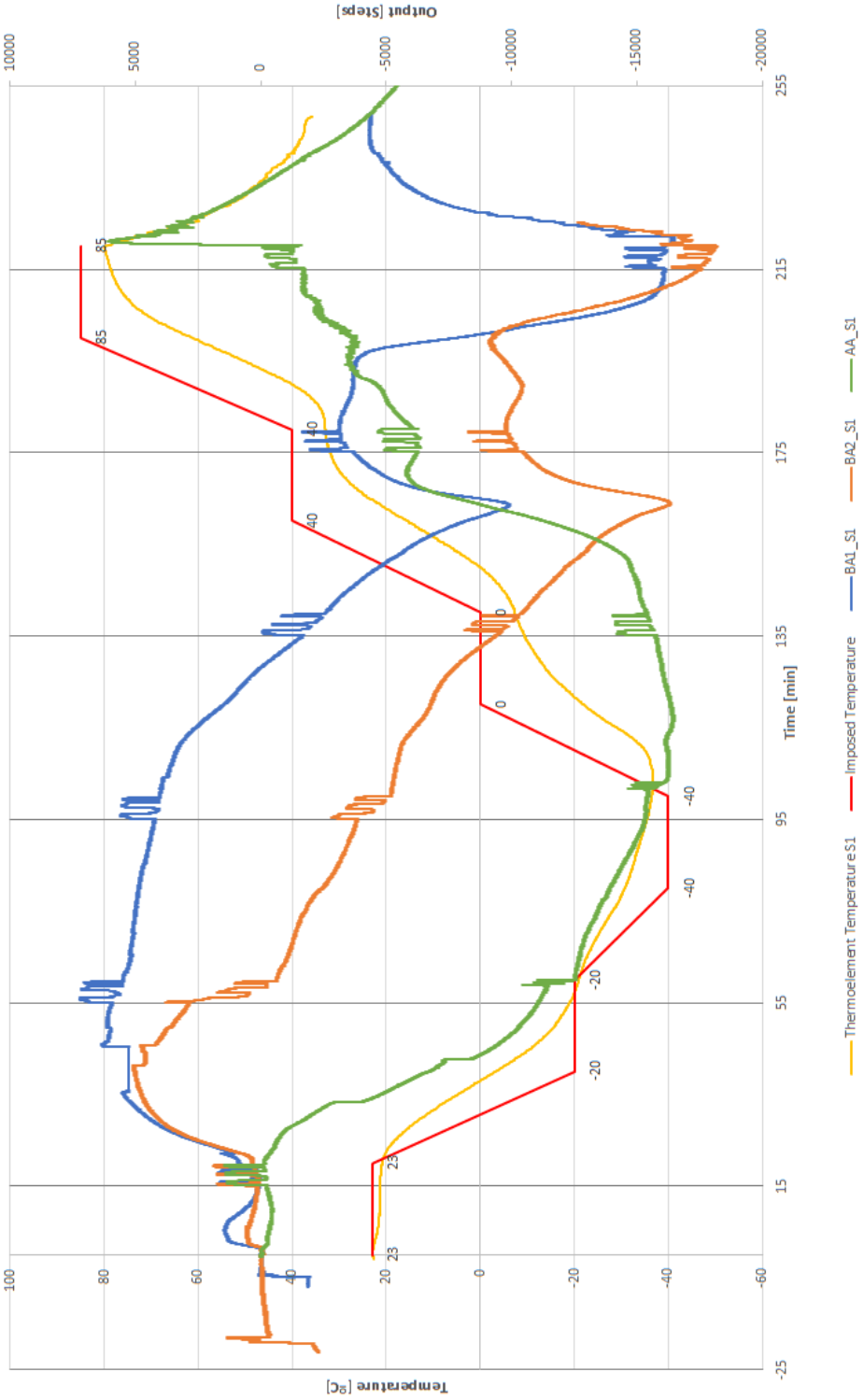

Figure B.11: Output variation in S1

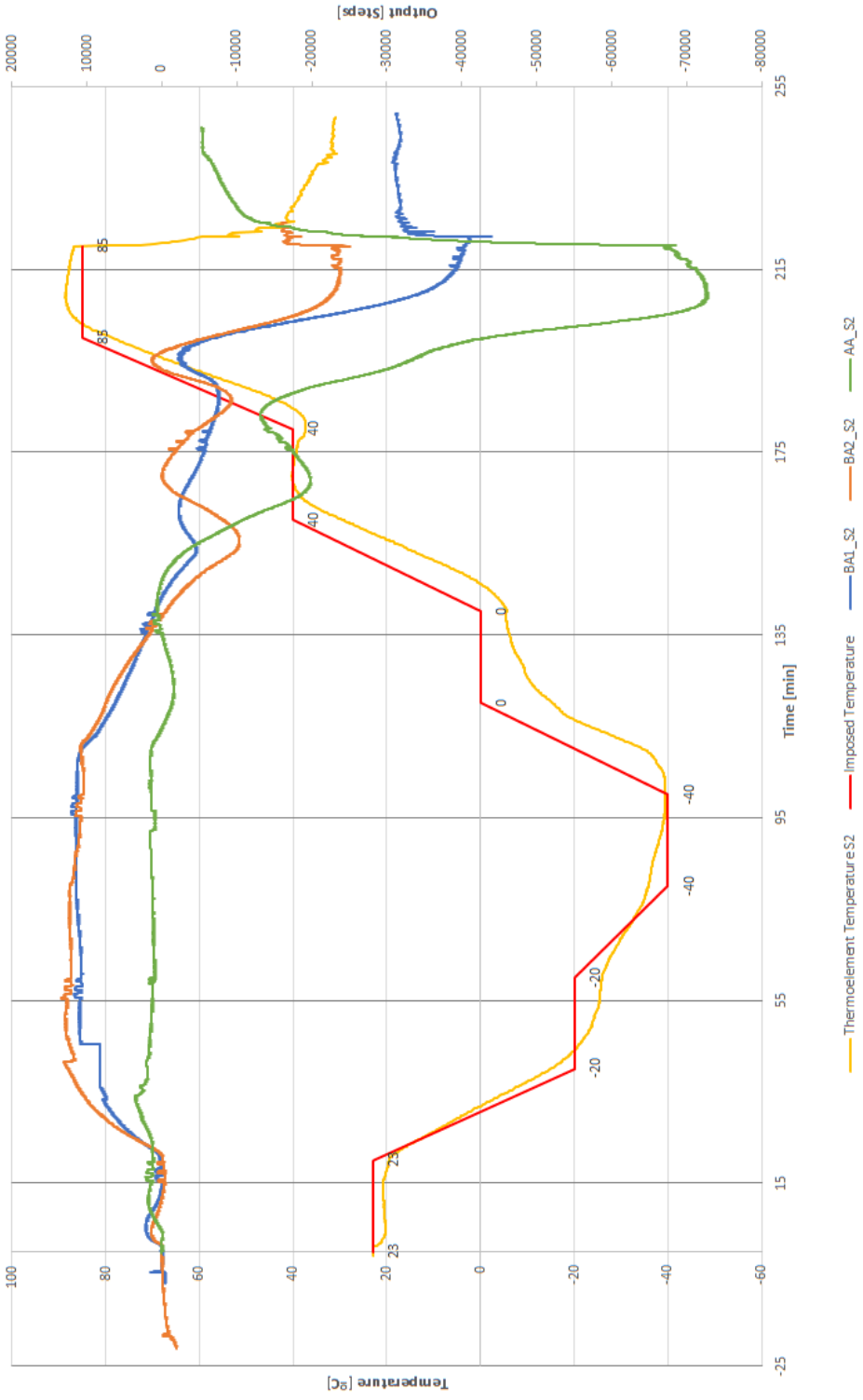

Figure B.12: Output variation in S2

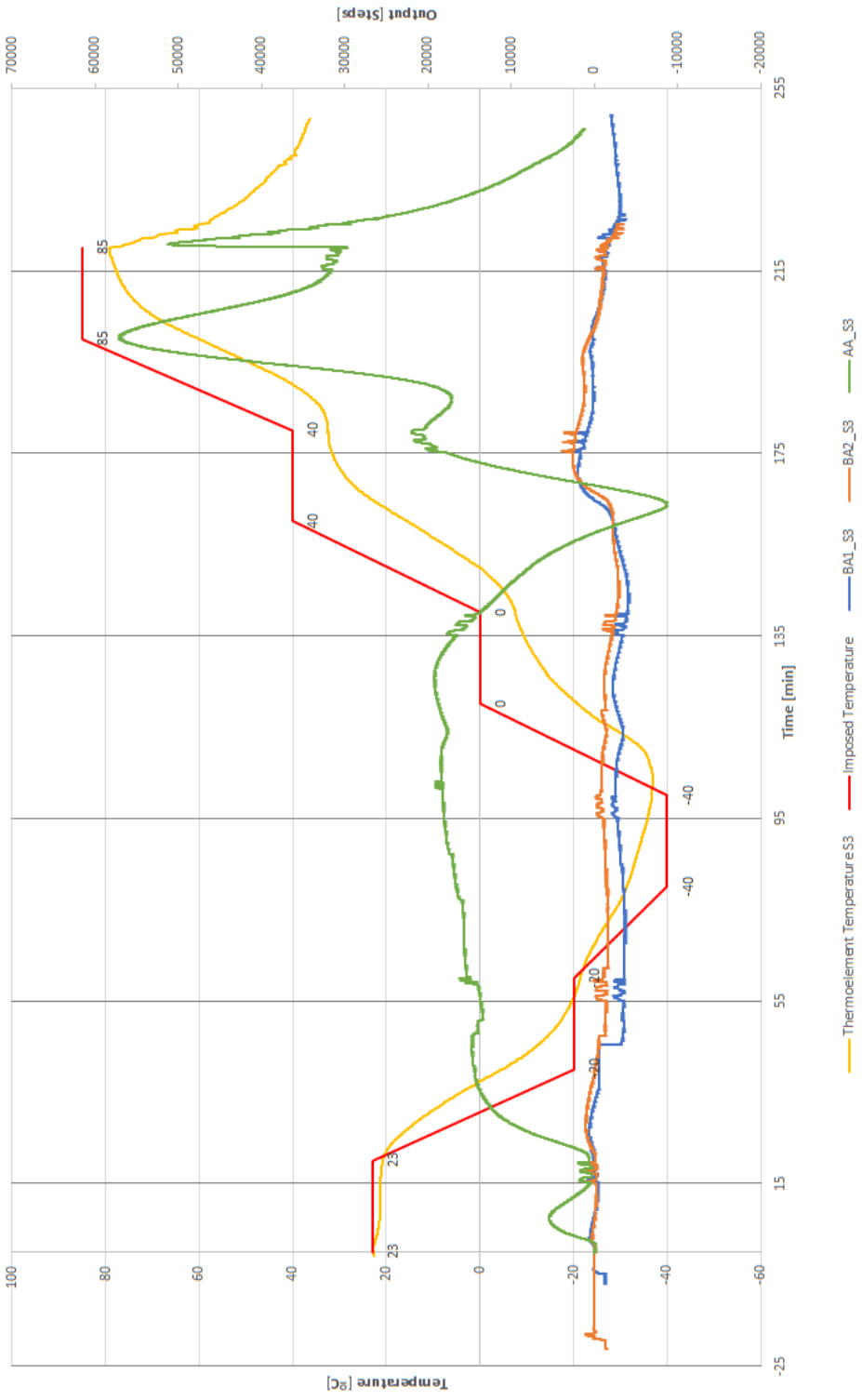

Figure B.13: Output variation in S3

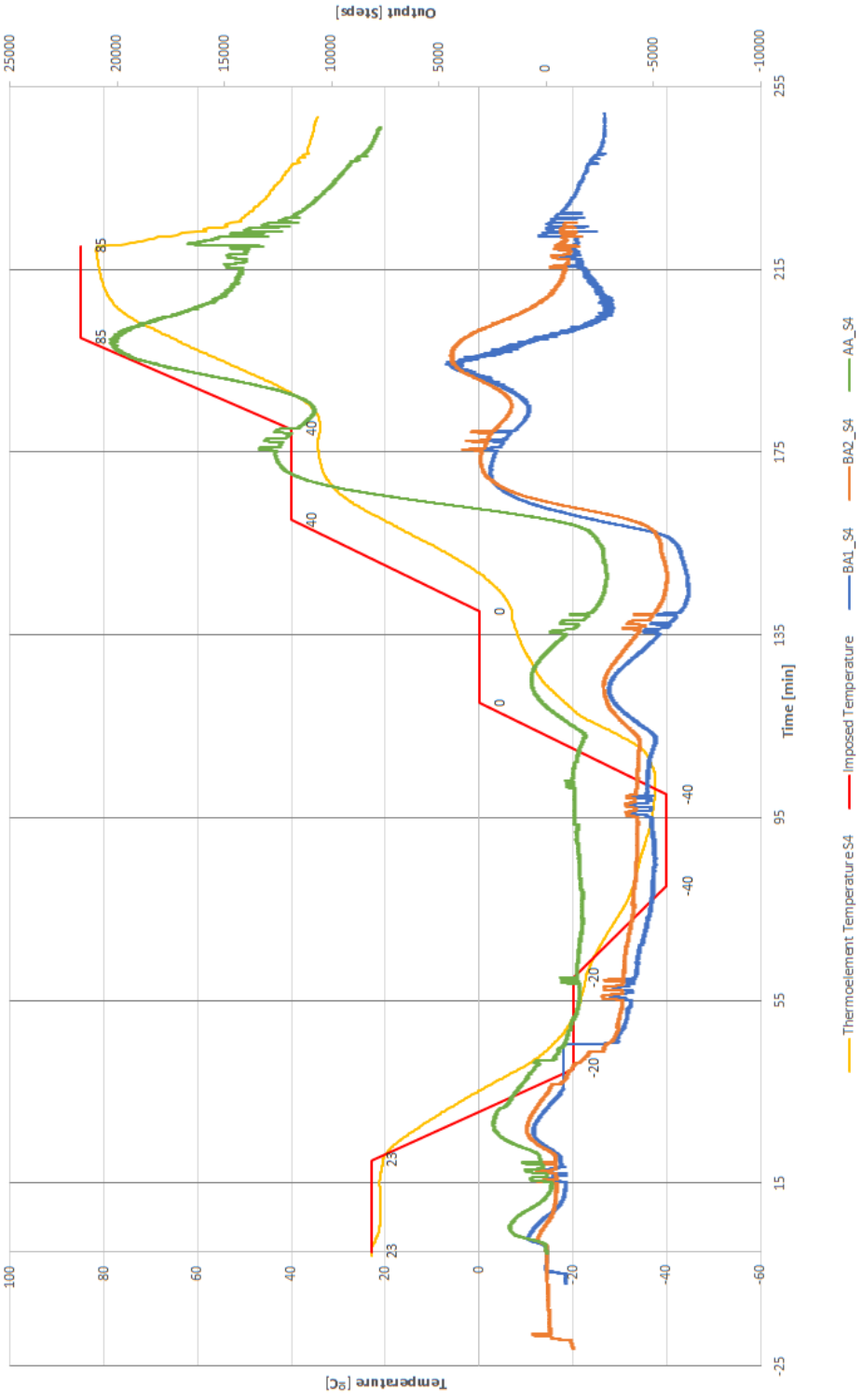

Figure B.14: Output variation in S4

Appendix C

Screwing

C.1 Screwing Sequences

Designation	Order	Features
A)	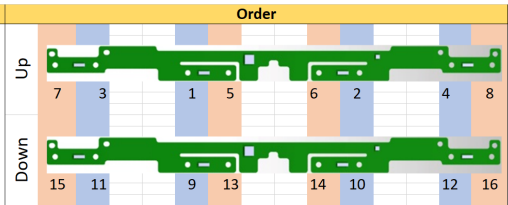	Upper FSE first
B)	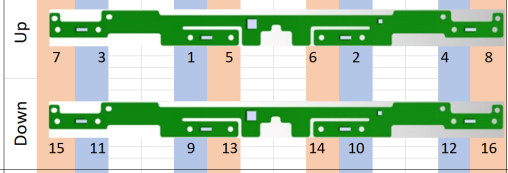	A) with spacers
C)	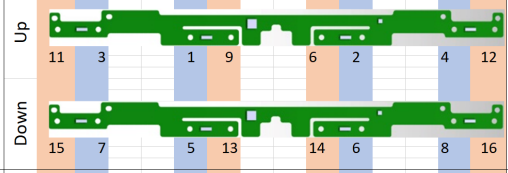	Screws of the carrier first
D)		C) with pre-screwing of the upper FSE in the carrier
E)	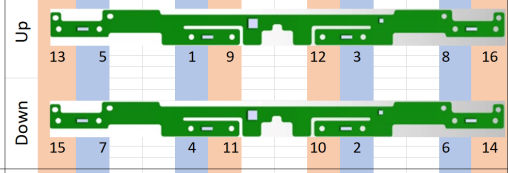	Small cross
F)	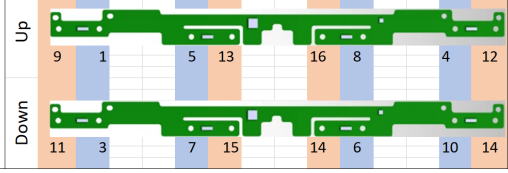	Big cross

C.2 Screwing Results

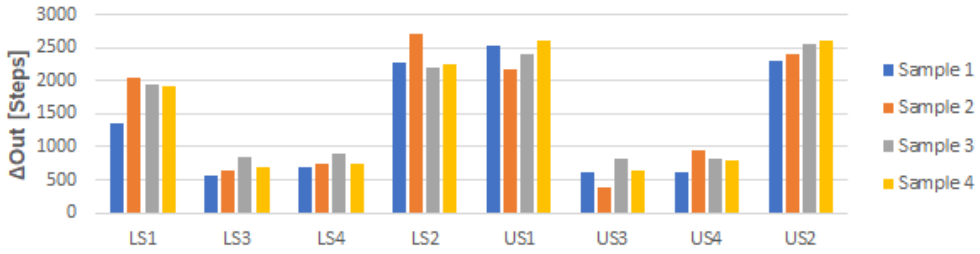

Figure C.1: Results of screwing sequence A

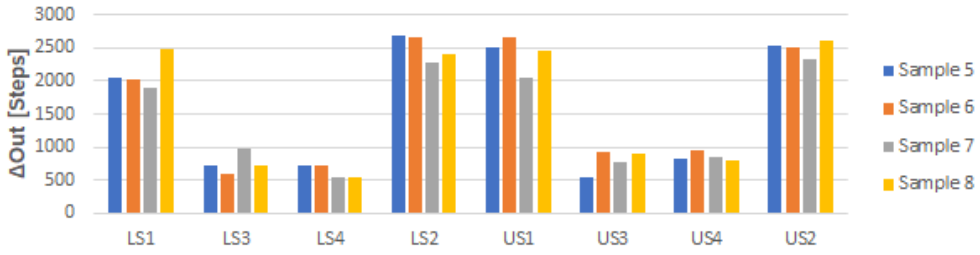

Figure C.2: Results of screwing sequence C

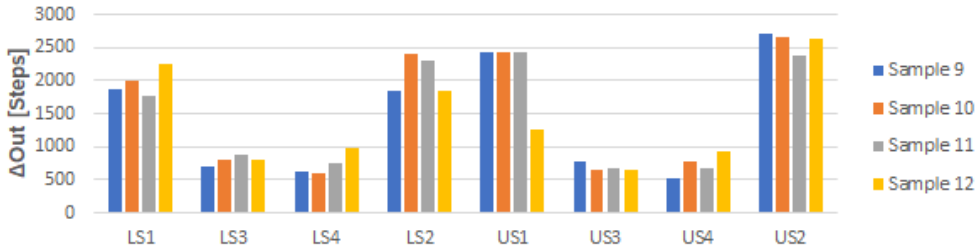

Figure C.3: Results of screwing sequence E

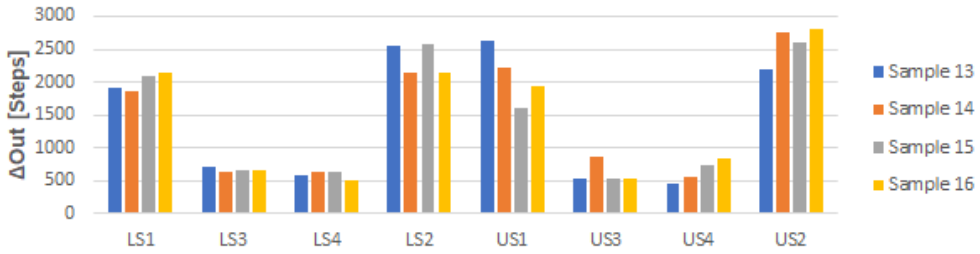

Figure C.4: Results of screwing sequence F